Plains volcanism in Tharsis region on Mars: Ages and Rheology of Eruption Products

Vulkanismus plání v oblasti Tharsis na Marsu: Stáří a reologické vlastnosti vyvřelých hornin

A DISSERTATION

SUBMITTED FOR THE

THE MASTER OF SCIENCE DEGREE IN GEOLOGY

by

Bc. Petr Brož

Supervisors:
Mgr. Prokop Závada, PhD.
and Doc. RNDr. František Holub, CSc.

Charles University in Prague, Faculty of Science,
Institute of Petrology and Structural Geology

Plains volcanism in Tharsis region on Mars: Ages and Rheology of Eruption Products

Remote sensing data show clusters of low shield volcanoes in *Tharsis* volcanic province on Mars (Hauber et al., 2009). These low shield volcanoes and associated landforms are comparable with terrestrial plain-style volcanic products (Plescia, 1981) as defined by Greeley (1982) in the Snake River Plain in Idaho, which represents an intermediate style of volcanic activity ranging between flood basalts and the Hawaiian shields.

While a number of recent studies addressed some aspects of low shield volcanoes, in particular their morphology, morphometry, and lava rheology, no systematic study including the chronology for the entire region of *Tharsis* is available so far. The goal of this work is to determine relative and absolute ages of low shield volcanoes and surrounding lava flows and their basic rheological properties.

We used crater size-frequency distribution method (CSFD) developed by Hartman and Neukum (2001) and Ivanov (2001) for determination of absolute dating of the surface. For calculation of the rheological properties of the lava, we used methods established by Hiesinger et al. (2007). It is known that the low shield volcanoes on Mars consist of basaltic lavas that had low viscosities during their effusion, which can be attributed either due to the high effusion rates, high temperatures of erupting lava or low content of Si coupled with high content of Fe-Mg components in the melt.

Detailed morphometric study of selected volcanic landforms was carried out using *Context Camera* (CTX) pictures with resolution around 5-6 meters per pixel. This study comprised 61 low shield volcanoes selected in the entire volcanic province of *Tharsis*, 10 lava flows that poured out from the low shield volcanoes and also lava flows with sources in the surrounding plains. For the volcanoes, we established absolute ages and their volumes. Lava flows are characterized by yield strength, effusion rates and viscosities of erupted lavas. We used several techniques to measure the lava flow thickness (Hiesinger et al., 2007; De Hon, 1974, Smith et al., 2001). We found, that the high resolution topographic data from *Mars Orbiter Laser Altimeter* (MOLA) onboard *Mars Global Surveyor* are sufficient for this kind of analysis.

The results confirmed, that volcanic activity forming low shield volcanoes in the *Tharsis* was active intermittently through the long geological history of Mars up to recent times. Most of the observed clusters formed about 50 to 130 Ma ago corresponding to Late Amazonian with few cases of significantly older ages in the regions of *Tempe Terra* (about 370 – 1000 Ma, middle Amazonian) and *Syria Planum* (about 1340 – 2880 Ma, early to middle Amazonian). The extent of the older volcanic activity may have been much larger,

considering the fact that older volcanic products can be hidden under the younger volcanic deposits.

The results about rheological properties of investigated lavas are in agreement with previous investigations of Martian lava flows and also with their terrestrial analogues. Measured lava flows reveal rheological parameters comparable to basaltic (or partly andesitic) lavas forming the Hawaiian low shield volcanoes, lunar mare domes or lava flows on Venus. We found that lava flows pouring out from vents on top of low shield volcanoes and from fissure vents in the surrounding plains have the same properties, which can reflect their common magmatic source.

Vulkanismus plání v oblasti Tharsis na Marsu: Stáří a reologické vlastnosti vyvřelých hornin.

Dálkový průzkum Marsu ukázal skupiny nízkých štítových sopek v oblasti vulkanické provincie *Tharsis* na Marsu (Hauber et al., 2009). Tyto nízké štítové sopky a doprovodné vulkanické útvary odpovídají jejich pozemským ekvivalentům spojeným s vulkanismem plání, který popsal americký geolog Greely (1982) ve Snake River Plain v Idaho (USA) jako přechodný typ mezi výlevným vulkanismem bazaltů a Havajským typem erupcí.

Množství současných výzkumů se zabývalo některými vlastnostmi nízkých štítových sopek, zejména jejich morfologií, morfometriií a vlastnostmi vyvřelé lávy. Komplexním výzkumem historie nízkých štítových sopek se ale zatím žádná práce nezabývala. Cílem naší práce bylo určit relativní a absolutní stáří nízkých štítových sopek a současně určit základní reologické vlastnosti lávových proudů v širším okolí zájmové oblasti. Hlavním cílem bylo zjistit, jestli existuje nějaká genetická spojitost mezi jednotlivými skupinami sopek v oblasti *Tharsis*, a jak jsou jednotlivé sopky staré.

Pro určení absolutního stáří jednotlivých jednotek jsme použili metodu založenou na počítání četnosti impaktních kráterů a jejich velikostí vyvinutou Hartmanem a Neukumem (2001) a Ivanovem (2001) a pro reologické vlastnosti jsme použili metodu úspěšně použitou například v práci Hiesingera a kol. (2007). Je známo, že nízké štítové sopky jsou tvořeny hlavně bazaltickými horninami s nízkou viskozitou, která mohla být způsobena vysokou rychlostí erupce, vysokou teplotou, či nízkým obsahem Si a zároveň vysokým obsahem Fe-Mg v extrudované tavenině.

Celkově jsme zmapovali 61 sopek napříč celou oblastí *Tharsis* za pomoci snímků z *Context Camera* (CTX) s rozlišením mezi 5 až 6 metry na pixel a 10 lávových proudů, které vytekly z kráterů štítových sopek nebo z jiného zdroje na přilehlých okolních pláních. Pro sopky jsme určili jejich absolutní a relativní věk a jejich objem, pro lávové proudy mez roztékavosti (yield strength), rychlost erupcí a viskozitu. Jelikož reologie lávy je primárně závislá na tloušťce lávového proudu (Hiesinger et al., 2007), použili jsme několik rozdílných technik pro její určení (Hiesinger et al., 2007; De Hon, 1974, Smith et al., 2001). Zjistili jsme, že topografická data pořízená přístrojem *Mars Orbiter Laser Altimeter* (MOLA) na palubě *Mars Global Surveyor* mají dostatečné rozlišení pro tento typ studie.

Výsledky ukázaly, že vulkanismus formující nízké štítové sopky v *Tharsis* byl v Marsovské historii dlouhodobý a že byl aktivní v geologicky nedávné době. Věky většiny zkoumaných skupin sopek spadají mezi 50 až 130 milióny let, což odpovídá pozdnímu Amazonianu, s několika případy starších věků jako

například skupina sopek v oblasti *Tempe Terra* (370 až 1000 miliónu let, střední Amazonian) a *Syria Planum* (okolo 1340 až 2880 milióny let, spodní až střední Amazonian). Rozsah staršího vulkanismu může být mnohem větší vzhledem ke skutečnosti, že pozorování a použité techniky umožňuje zkoumat pouze nejmladší projevy vulkanismu.

Výsledky reologického měření jsou ve shodě s předchozími publikovanými pracemi ohledně lávových proudů na Marsu a taktéž s pozorováními pozemských proudů. Vypočítané vlastnosti marsovských láv odpovídají bazaltovým (a místy andezitovým) lávám, které tvoří Havajské sopky na Zemi, extruzívní dómy v měsíčních mořích a lávovým proudům na Venuši. Dále jsme zjistili, že vlastnosti lávových proudů vycházející z kráterů na vrcholcích nízkých štítových sopek jsou srovnatelné s lávami, které vyvěraly z puklin na okolních pláních. To může znamenat, že lávy z obou dílčích oblastí měly stejný magmatický zdroj.

Declaration

Author declares that the presented Master's thesis is an original work. This thesis contains no material published elsewhere or extracted in whole or in part from a thesis by which I have qualified for or been awarded another degree or diploma. No other person's work has been used without due acknowledgment in the main text of the thesis. This thesis summarizes findings established on the basis of satellite data obtained from planetary probes the *Mars Reconnaissance Orbiter* and the *Mars Global Surveyor* and processed at *Deutschen Zentrums für Luft- und Raumfahrt* (DLR). Cooperation the German authorities, namely with Ernst Hauber and Felix Jagert is acknowledged.

Data included in this thesis were obtained on the basis of collaboration with Felix Jagert.

In Písek, 15th of April, 2010

……
Petr Brož

Acknowledgement

Author wants to thank to everybody, who gave him support and help during the writing of this master thesis.

The help of Ernst Hauber, leader of our research team, and Felix Jagert, my colleague from Bochum University is acknowledged. Prokop Závada from Academy of Sciences of the Czech Republic provided scientific corrections and is thanked for patience with language corrections. Thanks belong to the DLR team, especially Angelika Hoffmeister and Marita Wählish, and *Freie University* team, namely Thomas Kneissl, Thomas Platz, Greg Michael and they leader Gerhard Neukum.

Master thesis would never have emerged without financial support of ERASMUS mobility program for students, which partly covered my costs during stay through April to September 2009 in Berlin, Germany.

Equally important was the support of my family and friends while writing the thesis. Without their prodding and support, I would have long ago lost faith that this thesis would be finished.

Petr Brož

Contents

1. Resumé

The major aim of this diploma thesis is to constrain the absolute ages of low shield volcanoes in *Tharsis* region on Mars, basic rheological properties of surrounding lava flows and relative ages of the lava flow units on the basis of their structural position. Different lava flows were measured for calculation of their rheological properties using their shape parameters and compared with lava flows connected with low shield volcanoes and with plain-style volcanoes on Mars. Ages of over 61 independent low shield volcanoes in *Tharsis* region were determined. Dimensions of 10 lava flows were measured for their rheological properties. Our work was based on detailed evaluation of Mars' surface satellite images taken by *Context Camera* (CTX) on board of *Mars Reconnaissance Orbiter* (MRO) with resolution around 5-6 meters/pixel and elevation measurements taken by *Mars Orbiter Laser Altimeter* (MOLA) on board of *Mars Global Surveyor* (MGS). We also used *High Resolution Stereo Camera* (HRSC) data in several cases. This work was done in cooperation with *Deutsches Zentrum für Luft- und Raumfahrt* (DLR) Berlin with my colleagues Ernst Hauber (DLR) and Felix Jagert (*Ruhr-Universität Bochum, Germany*) during my six-months-stay in Berlin in the year 2009 that was supported by *ERASMUS* program foundation.

This work consists of two parts. First part is devoted to evaluation of chronology for low shield volcanoes in *Tharsis* region, second part deals with measurements of basic rheological properties of lava flows connected with plain-style volcanism. Regarding the chronology, we used production rate function of impact craters which was developed by Hartman and Neukum (2001) and special software designed by team of authors from *Freie Universität Berlin* for *ArcGIS* interface named *CraterTools* and *CraterStats* for plotting craters frequency. This method gave us a tool to estimate absolute ages of many surface landforms based on frequency of impact craters and their sizes. We found that volcanic activity on Mars was a long-lasting and complex process.

We used remote sensing data for calculating volumes of the low shield volcanoes from their dimensions and shapes and for measurement of the morphological parameters of the lava flows. Second part of the work attempts to estimate basic rheological properties of these flows, namely the yield strength, plastic viscosity and effusion rates and speculate about the chemistry of the investigated lava units. Products of plain-style volcanism and low shield volcanoes were also compared on the basis of the determined rheological properties of lava. Our results are also compared with other studies about Martian lava flows

Various satellite-borne instruments orbiting the Mars provide a powerful tool for understanding processes which formed this planet. Besides the significant morphological effect of Martian volcanism, degassing of erupted lava probably formed the atmosphere of Mars and influenced the composition of the recent

chemistry of surficial material. For the sake of future estimation of the gas volume possibly released during extrusion of the lavas, we attempted to establish the volume of low shield volcanoes and lava flows. The evolution of *Tharsis* volcanic province, characteristic with large plains covered with lava flows was likely accompanied by release of enormous volumes of volatiles including water vapor and carbon dioxide. The gas products maybe allowed existence of liquid water on the Mars surface for some unspecified time interval.

2. Mars – the Red planet

Mars is the fourth planet from the Sun and after the Mercury it is the second smallest planet in the Solar system. Mars belongs together with Mercury, Venus and Earth to terrestrial planets, which are typical with hard rocky surface covering hot melted mantle surrounding small liquid or solid core. Its orbital distance from the Sun is ca. 227.92 millions kilometres and it orbits once in ca. 687 days. Martian day, called Sol, is 24 h 37 min. long.

Mars is different in comparison with Earth in many ways. Regarding the size, Mars has equatorial diameter 6,792.4 km in contrast to 12,756.27 km for Earth, it is therefore about two times smaller than Earth. The volume of Mars is 0.64185×10^{24} kg (around 11% of Earth mass) and its average density is 3,934 kg/m^3 (Earth 5,515 kg/m^3). For this reason the gravitational acceleration on the surface is only 3.71 m/s^2. Mars has dense atmosphere with atmospheric pressure of 6.35 mbar measured on Viking 1 landing site and consists of CO_2 (95.32%), N_2 (2.7%) and Ar (1.6%), O_2 (0.13%), CO (0.08%) and H_20 (210 ppm) (Barlov, 2008). For summary about basic properties of Mars see Table 2.1.

Planet	Mars	Earth
Equatorial radius [km]	6,792.40	12,756
Polar radius [km]	6,752.40	12,713.60
Volume [10^{24} kg]	0,642	5,874
Surface area [km^2]	144 mil.	510 mil.
Mean density [kg/m^3]	3,934	5,515
Equatorial surface gravity [m/s^2]	3.711	9.78
Surface pressure [mbar]	6.9	1,014

Table 2.1: Basic comparison between Mars and Earth.

Mars has differentiated inner structure like Earth: crust, mantle and small core. An isostatic calculation of crust load indicates that the crust is between 32 to 62 km thick and overlies a melted mantle about 1,700 to 2,100 km thick (Wieczorek and Zuber, 2004; Zuber, 2001). In the middle of the planet is a small core of unknown composition with radius around 1,300 to 1,700 km. There is no evidence about the presence of

strong magnetic field around planet, but some measurements suggest, that the magnetic field was present in the early history of Mars because of remanent magnetization of crustal rocks (Spohn et al., 1998). The most prominent Martian topography feature, called the crustal dichotomy boundary, is the topographic step of 1 to 3 km between the northern and southern hemisphere. This boundary irregularly follows the equator and separates older southern highlands from relatively flat younger northern plains. It has to be older than 4 billion years and its origin is still enigmatic (e.g. Kiefer, 2008; Marinova et al., 2008).

2.1. Volcanism

Volcanism is a process characterized by transport of molten material from inner parts of planets to their surfaces. On Mars, similarly to the Earth and Moon, the main part of volcanism is typical with basaltic lavas. This is explained by similar composition of all terrestrial planets in the solar system, which formed by planetary accretion from protosolar nebula by mutual collisions of chondritic meteorites, because basalt is the liquid product of partial melting of chondritic meteorites. The resulting solid basalt consists of calcium-rich pyroxene, plagioclase and less than 20 percent of other minerals like olivine, amphibole or feldspathoids (Carr, 2006). This composition is in agreement with remote sensing data observations, which indicate mafic minerals such as pyroxene and olivine due to strong Fe^{2+} absorptions in spectral reflectance measurements (Greeley and Schneid, 1991). Geochemical models, observations *in situ* and some meteorites derived from Mars also confirm that the Martian surface is composed mainly by basaltic rocks on a global scale like basalt or andezite (e.g. Greeley and Spudis, 1981).

Basalt is typical with gray to black colour and fine-grained texture reflecting rapid undercooling of the basalt lava on the surface. Direct evidence about the composition of Martian crust comes from basaltic meteorites expelled from the surface of Mars. Their origin was reliably identified on the basis of similarity between gas compositions in their vesicles with composition of Martian atmosphere measured by satellite-borne instruments. These meteorites are mostly basaltic cumulates, which means that they formed by the accumulation of crystals that segregated from the basaltic melt (McSween, 1999). Another evidence supporting basaltic composition of the erupted lavas is the identification of columnar jointing of solidified lava flows (Milazzo et al., 2009), characteristic for basaltic lava flows on Earth.

Typical basalt consists of the following oxides: SiO_2 (50 wt %), Al_2O_3 (15 wt %), CaO (12 wt %) and circa equal amounts of FeO and MgO (10 wt %). The major parameter used for discriminating of the genetically different types of basalts is the content of alkali bearing oxides, namely Na_2O and K_2O. The basalt magma erupting on Earth typically has temperatures ranging between 1000 and 1300°C and contains only small amount of volatiles (0.2 to 2 wt %) formed mainly by H_2O and CO_2 (Sigurdsson et al., 1999).

Besides melt and crystals, the magma also contains dissolved volatiles which form bubbles at decreasing pressure close to the surface. Volatiles can finally escape to the atmosphere from the coalescing bubbles at the surface of extruded magma. Total amount of volatiles escaping from the extruded basalts on Earth ranges from 0.2 to 2 wt% (Sigurdsson et al., 1999), and their exsolution occurs at relatively shallow depths of usually <2 km (Wilson and Head; 1983). The total amount of volatiles dissolved in magma depends mainly on pressure, temperature and magma composition (Sigurdsson et al., 1999). The expansion of the exsolved gasses and increased content of gas-bearing bubbles increases buoyancy of the magma, which increases magma ascent velocity (Wilson and Head, 1983). Since Martian magmas were probably volatile-poor (Wilson and Head, 1994), their eruption style was therefore rather effusive than explosive. The presence of abundant CO_2 and H_2O (as ice in polar region) on Mars argues for extensive planetary degassing via eruptions (Wilson and Head, 1983). In addition, calculations indicate that the expanding volatiles under Martian conditions (low atmospheric pressure and gravity and even with low volatile contents of magma (~0.03 wt. %) are susceptible to fragment the erupting magma to produce plinian explosive eruptions and pyroclastic deposits (Head and Wilson, 1998).

The composition of lava emitted from a volcanic center reflects both the composition of its source as well as a myriad of dynamic phenomena that characterize its generation, segregation, ascent, and eruption (Sigurdsson et al., 1999). Because of different gravity, structure and density of the Martian crust, and lower atmospheric pressure on Mars in contrast to conditions on Earth, the processes of magmatic differentiation and possible amount of volatiles released from the magma are unknown (Wilson and Head, 1994). Magma in the mantle rises primarily due to buoyancy in form of diapirs. The ascent in the crust can be either diapiric or through dykes. The differences in gravitational acceleration between Earth and Mars cause that the buoyant forces acting on the magma are smaller for Mars. In contrast, the intrinsic properties of the magmas (e.g. the viscosity and yield strength) on Earth and Mars are similar (Carr, 2006). These properties are reflected in the shapes of solidified lava flows and can be conveniently constrained by morphometric measurements (Hiesinger et al., 2007) using the remote sensing data based on images in visible range from space probes.

The composition of rising magma is not stable in time; it changes during its ascent to the surface due the assimilation and differentiation. Therefore, different kinds of magmatic rocks can be expelled from a single vent on a longer time scale of volcanic activity. The fact, that Mars is composed only from basaltic rocks, suggests that in contrast to Earth, the processes of crustal differentiation and assimilation on Mars were insignificant.

Eruption style is controlled by a combination of factors such as magma composition and eruption

temperature and volatile content in the erupting magma. While temperature and composition are the major factors controlling viscosity of the erupting lava, volatile content influences eruption velocity from the vent. Besides these factors, eruption style is also controlled by tectonic settings and external global physical parameters like atmospheric pressure and gravity (Wilson and Head, 1983). Eruption of lava is either explosive or effusive. For Mars in contrast to Earth, effusions of basaltic lavas can spread laterally on larger areas. Wilson and Head (1994) estimate that lavas extruding on Mars should be typically 6 times longer and thinner than equivalent terrestrial flows. Due to different condition (e.g. gravity, crust thickness) between Mars and Earth, it was suggested, that magma chambers on Mars are deeper and that magma on Mars likely ascends through thicker dykes than on Earth (Carr, 2006). Volcanoes form at places, where the dykes are vent on the surface.

Volcanoes are classified by their morphology, size, shape, arrangement of their vents and their genetical characteristics. Their morphologic properties are results of many complex and often interrelated parameters, which characterize typical eruption styles (Greeley and Spudis, 1981). Most of the volcanoes on Mars are similar to the terrestrial shield volcanoes on Earth, which reveal dip angles of their slopes below 10° and the central summit of a cone-shaped volcano dominated by a collapse caldera. Terrestrial shield volcanoes are composed mainly by basaltic rocks, which extrude from the vents and form lava flows by gravitation on the surface (Carr, 2006).

2.2. Volcanism on Mars

Before 1960s there was only little information about morphology of Martian surface. From telescopic observations before space probe times, it was known that Mars is probably characterized by rocky surface with two lighter spots in pole areas interpreted as ice sheets. In the late 1960s two NASA missions *Mariner 6* and *7* took first pictures which indicated that Mars is a dead world much like the Moon rather than the Earth with liquid water and strong erosion. On the other hand the early probes definitely confirmed Mars as a terrestrial planet with hard rocky surface. Situation changed in 1971 when the next American probe *Mariner 9* was inserted on the orbit around Mars and remained there for 349 days during which it collected 7,329 pictures (Jaumann, 2006). First images from *Mariner 9* revealed that the atmosphere of the whole planet is stirred by planetary dust storm. Only four dark spots with central craters on the top popped above the global dust storm clouds. These were later identified as peaks of volcanic calderas at the top of huge shield volcanoes (Carr, 2006). Later images revealed that substantial parts of Mars are covered by volcanic material (Greeley and Spudis, 1981). It was the first proof, that active volcanism existed on the Martian surface in the past and this discovery inspired the first hypothesis regarding the evolution and chemistry of Martian atmosphere (Carr, 2006).

Newer pictures and continuous research brought additional pieces of information into the complex mosaic of volcanic history on Mars (Carr, 2006) (see Figure 2.1). It was found that the extensive volcanic products are non-uniformly distributed and include a wide variety of volcanic landforms (Werner, 2009). This strong morphological variability, like for different volcanic regions on Earth, is probably associated with different eruption styles. Shield volcanoes, cinder cones, tholi, paterae, lava flows pouring out from vents and lava tubes were recognized on Mars. Greeley and Schneid (1991) suggested that around 46% of Martian surface is covered by volcanic material and that these areas could be classified as individual volcanic units. Most exposed areas were recognised like plains and plateaus, with abundant volcanic material. In these areas, they estimated the thicknesses of volcanic units using partly buried impact craters based on the De Hon method to be in average from 170 m in Late Noachian to 320 m in Middle Amazonian.

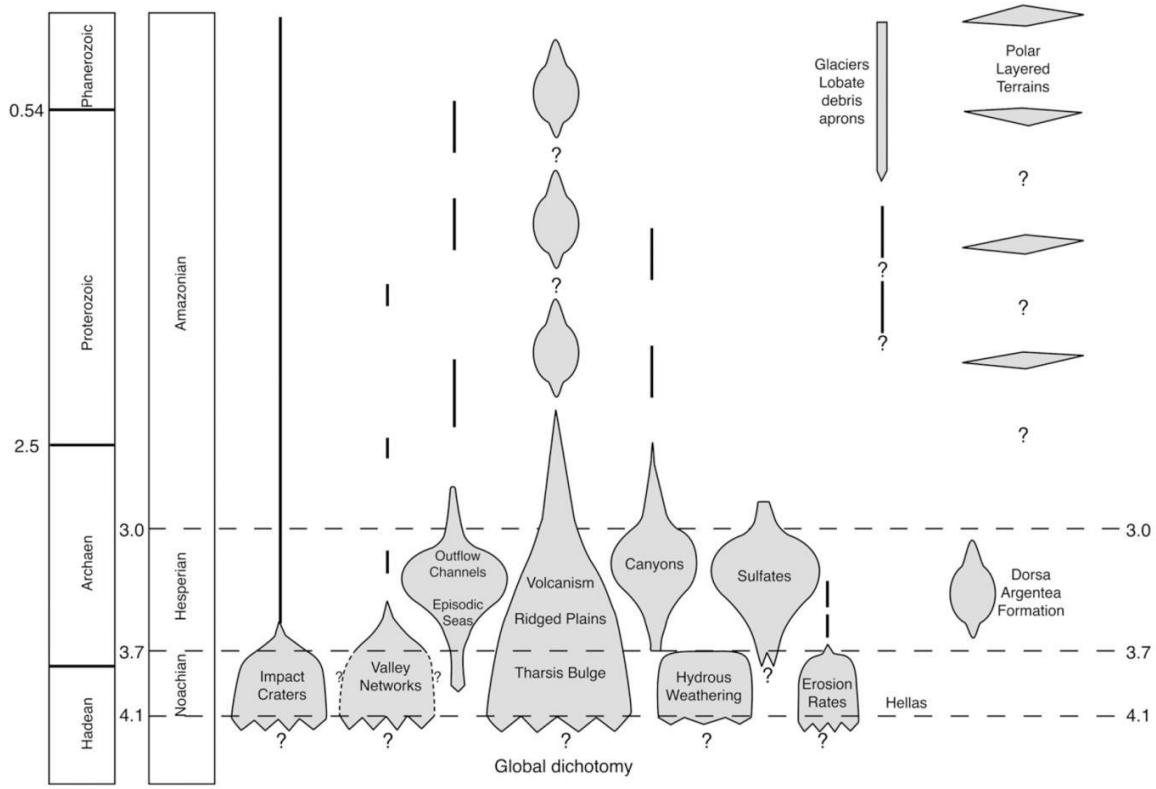

Figure 2.1: Interpretation of Martian evolution in time and comparison with similar major time subdivisions for Earth. Relative contribution of different processes that formed the Martian surface are indicated (Carr and Head, 2009).

In contrast to Earth, there are no signs about the possible plate tectonic activity on Mars for at least the last ~4 Ga. The surface is probably formed by a single and stable tectonic plate. This is supported by the fact that the volcanic activity forming the enormous volcanoes like *Elysium Mons* or *Olympus Mons* had to remain focused into one place for a long time (Wilson and Head, 1983). The magma chambers feeding these volcanoes were likely much larger than any on Earth, which is reflected by the size of the calderas and also the finding that the individual eruptions were much more voluminous and were separated by long intervals

between each eruption (Carr, 2006). It is possible, that magma chambers were not filled with molten material during the entire time of the volcanic activity, which lasted billions of years, but were supplied episodically with new magma (Carr, 2006).

Greeley and Schneid (1991) estimated the total volume of extrusive and intrusive magma generated on Mars over the last 3.8 billion years as 654 x 10^6 km^3 (with average velocity of magma production of 0.17 km^3/yr). The calculated mean ascent rates on Mars are few orders of magnitude smaller than on Earth (26 to 34 km^3/yr) or on Venus (less than 20 km^3/yr) but are higher than magma ascent rates for the Moon (0.025 km^3/yr).

Photogeological observation of Martian surface revealed two main types of volcanic landforms: a) the central volcanoes that resulted from continued and prolonged eruption from a central point source vent including shield volcanoes, steep-sides domes, radially textured low-profile volcanoes in heavy cratered terrain called highland *patera* interpreted as ash shields (Greeley and Spudis, 1981), and a typical volcano *Alba Patera* and b) large variety of small landforms, such as cinder cones. Remaining areas are volcanic plains situated mainly around central volcanoes. These are typical with presence of mare ridges and flow lobes (finger-like structure of the frontal part of a lava flow), are the most useful. Greeley and Spudis (1981) used the division of volcanic provinces into few subdivisions: a) simple flows, broad, smooth to straight plains containing numerous mare-type ridges but no flow lobes b) complex flows composed by overlapping flow lobes interpreted to be thin, multiply-cooling units c) plains without any common landforms and associated with large volcanic centers and d) volcanic plains later strongly modelled by erosion.

2.3. Volcanic provinces on Mars

It is obvious that the origin of Mars surface was strongly modelled by some kind of volcanic activity. At early stages of the Mars geological history, the surface of Mars was formed by a magmatic ocean enveloping the entire planet. As this vast hot ocean slowly cooled down, newly formed crust was heavily bombarded by asteroids and comets. Such collisions are reflected by abundant impact craters on the recent surface. Patches of smoother Martian surface characterize several volcanic provinces that originated by eruption of magma controlled by regional tectonic or local deformational features (Werner, 2009). Crater counting in these areas suggests that the volcanic activity started in Noachian period (less than 3.7 Ga) and continued to the Late Amazonian (200 to 100 Ma) in the *Tharsis* region (Werner, 2009). Besides the two main prominent volcanic provinces, the *Tharsis* region and *Elysium* volcanic province, there are few other regions (see Figure 2.2 for more details) revealing clear signs of previous volcanic activity, such as the old volcanoes *Tyrrhena Patera* and *Hadriaca Patera* on the southern hemisphere. However, *Tyrrhena* and *Hadriaca Patera* display completely different morphology and shapes in contrast to other volcanoes on Mars. These volcanoes are

associated with explosive volcanism probably related to phreatomagmatic activity and ash flow deposits (Williams et al., 2007; Williams et al., 2008; Werner, 2009).

The largest volcanic province on Mars, which is also typical with the biggest volcanoes and the most extensive lava plains, is the *Tharsis* region. *Tharsis* region is characterized by anomalously high elevations centered just south of the equator at 265°E (Carr, 2006). The volcanic products of the entire province form a large morphological bulge rising around 10 kilometres above the surrounding plains and 5,000 km wide. The volcanism in this area probably started in the early history of Mars 3.8 billion years ago and continued until recent times (Carr, 2006). The huge volcanoes popping up from the broad morphological bulge are the *Olympus Mons*, *Alba Patera* and *Tharsis Montes* (*Ascraeus Mons*, *Pavonis Mons*, *Arsia Mons*). Besides these enormous volcanoes, a large number of smaller volcanoes, but still significantly bigger that common volcanoes on Earth, are also present. However, the majority of the *Tharsis* region volcanic province and the surrounding plains is characterized by hundreds of non-uniformly distributed **low shield volcanoes** (Greeley, 1982). The latter features reveal diameter of only several tens of kilometres and height of several hundred meters with flank slope around 0.5° (Greeley, 1982, Hauber et al., 2009).

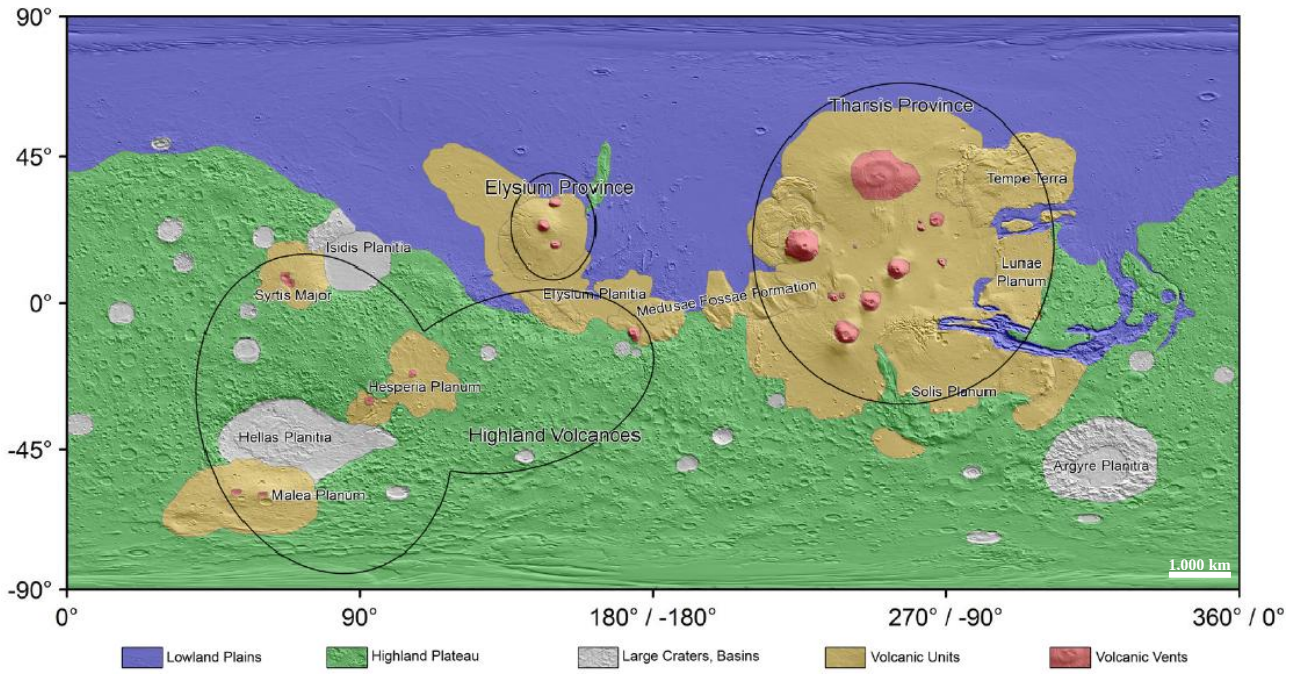

Figure 2.2: Locations of major volcanic regions on Mars. Two prominent regions, *Elysium* Province and *Tharsis* Province, are marked with black circles. Area of volcanic activity on the southern hemisphere, representing the old surface, is generally referred to as "Highland Volcanoes" (Werner, 2005). Positions of low shield volcanoes are not depicted on this image. Idealized dichotomy boundary corresponds to boundary between Lowland Plains (blue) and Highland Plateau (green).

2.3.1. Elysium Volcanic Province

Elysium volcanic province is the second-largest volcanic region on Mars. It is located on the northern hemisphere in the lowlands near the equator. It spans over 2,000 km and forms a 5 km high elevation (Carr, 2006; Werner, 2009). It represents the youngest volcanic area, which is characterized by long lava flows fed by vents and shield volcanoes that range in size but their shapes are comparable to those in the Tharsis region. The long-lived volcanic activity in the *Elysium volcanic province* lasted from 3.7 Ga to about 3.5 Ga years ago (Werner, 2009). The morphology of the province is dominated by three main shield volcanoes: *Elysium Mons*, *Albor Tholus* and *Hecates Tholus*. The biggest *Elysium Mons*, is a shield volcano rising 14 km above the surrounding lava plains with a diameter of around 240 km. Top of the volcano is formed by a simple caldera crater, which is 100 meters deep and 14 km wide. Several lava flows radiating from the central dome extended as far as 1,000 km to the southeast of the central summit. In addition, numerous younger lava flows erupted from several fissures pits and parasitic craters around the caldera (Carr, 2006).

Apollinaris Patera is another huge volcano located south-east from the *Elysium Mons* and north from the dichotomy boundary (Werner; 2009). Similarly to the large volcanoes in *Tharsis*, large volcanoes in *Elysium volcanic province* are classified as cones constructed episodically from basaltic lavas forming multiple lava flows and the composite volcanoes are possibly constructed by interbedded lava and pyroclastic material (Werner, 2009), which is typical for stratovolcanoes on Earth.

The *Elysium* volcanic province is similar to *Tharsis* region in shape, morphological landforms and probable chemical composition. It rises above the surrounding plains about 500 km north from the dichotomy boundary at *Elysium Planiti* (see Figure 2.2). The volcanic products in *Elysium Planitia* sourced from the underlying old fracture system *Cerberus Fossae*, The neighbouring lowland areas are covered by long lava flows that sometimes connect with local small volcanic landforms distributed randomly in the region (Burr, 2005; Werner et al.; 2003, Murray et al.; 2005, Jaeger et al.; 2007). Low shield volcanoes that built up above the fissures in Elysium volcanic province are similar to low shield volcanoes in the Tharsis region. A shape measurement of low shield volcanoes in this area was made by Vaucher et al. (2009).

2.3.2. Tharsis volcanic province

The *Tharsis* region is the biggest volcanic province on Mars (Figure 2.3). It is situated on the northern hemisphere near the equatorial area and forms the most expressive landscape on Mars. The weight of the volcanic products forming the extensive morphological bulge of the *Tharsis* volcanic province induced deformation of the lithosphere (Philips et al., 2001) and caused faulting across over half of the planet

surface. Chronology data based on crater counting and stratigraphy suggests that volcanism in *Tharsis* started in the early history of the planet before 3.8 billion years ago and continued until recent times (200-100 Ma) (Carr, 2006; Werner; 2009). This is in agreement with radiometric dating of Martian meteorites found on Earth which revealed similar ages (see Nyquist et al., 2001; Werner, 2009).

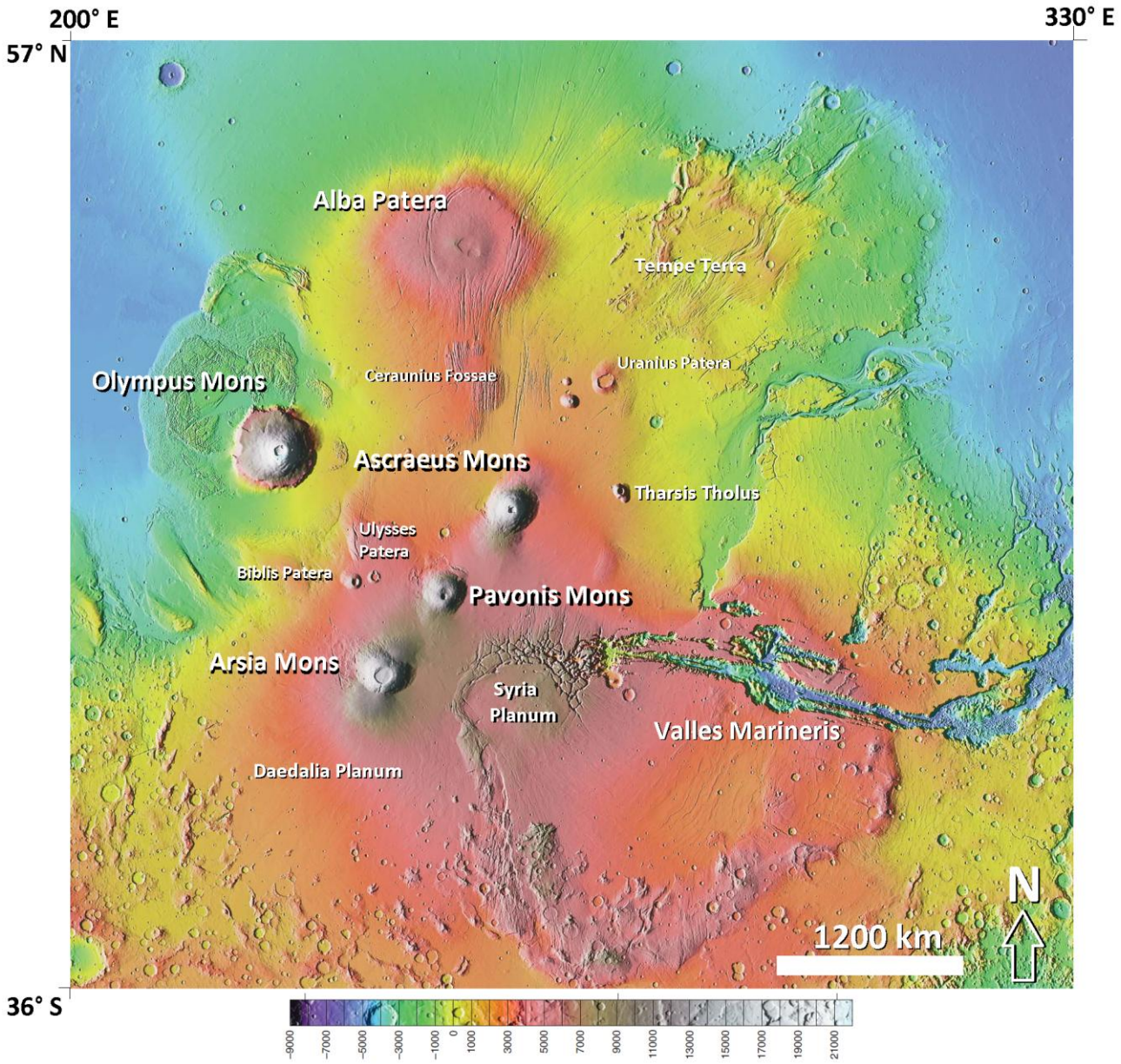

Figure 2.3: Detail of *Tharsis* volcanic region with main morphological features.

The morphological bulge consists of a wide range of different units and distinct volcanic landforms. In the southern part of the *Tharsis region* is *Syria Planum* with numerous low volcanic mounds that have about 20 km in diameter. These small positive landforms were classified as *low shield volcanoes*. In northern direction from *Syria Planum*, a group of three large volcanoes, called *Tharsis Montes* are aligned in the southwest-northeast direction, rise 10 km above the surrounding terrain and are spaced at 500 km from each

other. From south to north, the volcanoes are called *Arsia Mons*, *Pavonis Mons* and *Ascraeus Mons*. The tallest volcano in the solar system, *Olympus Mons,* is situated just off the northwest flank of the morphological bulge. *Alba Patera,* an old shield volcano, terminates the *Tharsis* on the north. The north-eastern region of *Tharsis* is called *Tempe Terra* and represents an old and strongly fractured crust locally superposed by younger volcanic units including low shield volcanoes. *Lunae Planum* is closing *Tharsis* in eastern direction. There are several small volcanoes (but still around the size of Hawaiian Big Island) which are also aligned in the SW-NE trending line. This line corresponds to a major tectonic lineament of the planet and its origin remains obscure (Carr, 2006).

The *Tharsis* and *Elysium volcanic province* are long-lived volcanic regions. There are many hypotheses explaining origin of the morphological anomaly encompassing both these volcanic regions. Microgravity maps and topographical measurements together with structural analysis of the tectonic lineaments inspired few models explaining the origin of *Tharsis*. The hypotheses include the mantle (super)plume (Harder and Christensen, 1996), isostatic uplift (Sleep and Phillips, 1979), magmatic underplating of material derived from subcrustal erosion of the northern lowlands (Wise et al., 1979) or volcanic construction (e.g., Solomon and Head, 1982). The two most widely accepted models are "the plume" or "volcanic construction" of *Tharsis*. For the plume model, a longtime volcanic activity would be required. This hypothesis was rejected recently as insufficient to explain the current geoid and topography (Zhong, 2002). A more accepted hypothesis today is the origin of *Tharsis* by volcanism (Zhong and Roberts, 2003).

The northernmost volcano of *Tharsis* family is *Alba Patera,* an old atypical shield volcano with a base diameter of around 1,100 km that rises around 6 km above the surrounding plains. *Alba Patera* has, like other shield volcanoes on Mars, a complex caldera on its top with around 120 km in diameter. The flank slope of the volcano is only around 1° (Werner, 2009). Around periphery of *the Alba Patera,* two grabens extend in north-south direction and curve around the periphery of the volcano: *Alba Fossae* on the western and *Tantalus Fossae* on the eastern flank. Both graben systems curve to the north-western direction just north from the volcano. The age determination surprisingly suggests relatively young ages of some parts of *Alba Patera* (Neukum and Hiller, 1981). Werner (2009) measured at least four episodes of volcanic activity of northern part of *Tharsis* bulge at about 3.4 Ga, 2 Ga, 800 Ma and young age around 250 Ma ago.

In the southern part of *Alba Patera*, there is another graben system, named *Ceraunius Fossae*. It follows the same trend as the fracture systems of *Alba* and *Tantalus Fossae* and also reveals similar morphological features. *Ceraunius Fossae* is partly buried in its middle part by younger lava flows that poured out from low shield volcanoes.

The westernmost volcano of *Tharsis* is *Olympus Mons* (Figure 2.4). It is the biggest known mountain in the Solar system rising 22 km above plains with a basal diameter of about 600 to 800 km measured from the edges of the scarp surrounding the main edifice. The slopes of this volcano dip at about 5° but near the marginal scarp, it increases up to 30°. The total volume of *Olympus Mons* is around 2.4×10^6 km^3, which is 2 or 3 times larger than other *Tharsis* volcanoes or the entire Hawaii-Emperor chain (Carr, 2006). Because of the enormous load of the whole volcanic material, the lithosphere bent and subsided to the mantle. The central part of the volcano comprises a complex caldera that formed by at least 6 independent episodes of caldera collapse (Mouginis-Mark, 1981). It has 72 × 91 km across and is up to 3.2 km deep. The crater counting age estimates suggest that all the caldera collapses occurred from 200 to 100 Ma. The calderas are thus associated with the youngest volcanic activity on *Olympus Mons*. Prominent caldera collapses were accompanied by resurfacing events (new lava eruptions along the caldera fractures) which partly buried an older surface (Mougis-Mark, 1981). The age in this range is in good agreement with age determination for flanks of *Olympus Mons* measured by Hartmann (1999) and Hartmann and Neukum (2001).

Broad elevations with rough surface and crescent-shaped outer boundary in the northern and western part of the aureole around *Olympus Mons* probably formed by historical gravity-induced failures of this volcano (Carr, 2006). The eastern part of this aureole is partly buried by younger volcanic material which is associated with plain-style volcanism.

The distinctive group of three volcanoes *Tharsis Montes, Ascraeus Mons*, *Pavonis Mons* together with *Arsia Mons* are classified as shield volcanoes with multiply collapsed calderas on their tops (e.g. Pike, 1978; Scott and Tanaka, 1986). Head and Wilson (1998) argue that there are strong theoretical and observational arguments suggesting that these are in fact composite volcanoes (stratovolcanoes). All these volcanoes have a long and complex history of volcanic eruptions, crater counting suggests that their main growth event happened about 3.55 Ga but their activitity continued episodically in many other following events (Werner; 2009).

The caldera of *Arsia Mons* volcano is destroyed by numerous small collapses on its northeastern and southwestern part. Small pits mark a rift-like structure disrupting the volcano flanks in SW-NE direction. Large volume of magma vented from these pits on the surface. The rift-like structure is tracable also the central crater of the caldera, where it is associated with low positive landforms, likely representing a family of low shield volcanoes. In contrast, there are no low shield volcanoes around the main volcanic body of *Arsia Mons* (Hauber et al., 2009). From eastern apron of *Pavonis Mons,* lava flows poured out to the surrounding plains. These lava flows were later partly or completely buried by eruption products of low shield volcanoes and lava flows that erupted from low shield volcanoes in the south to east of *Arsia Mons*

(Hauber et al., 2009). Only few more shield volcanoes are found around the *Ascreus Mons* volcano. These are located in the eastern and northwestern direction from this landmark (Hauber et al., 2009).

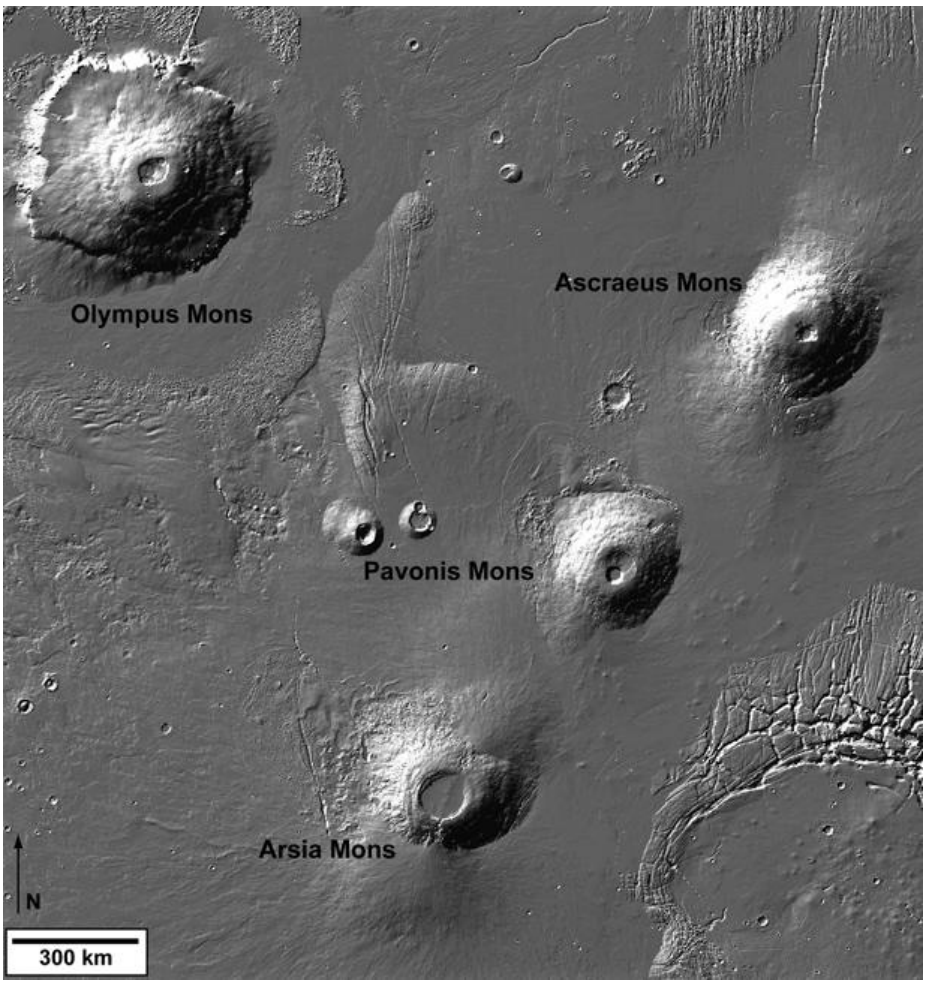

Figure 2.4: Largest volcanoes in *Tharsis region*. *Syria Planum* is visible with low shield volcanoes in lower right corner. A cluster of volcanoes, east from *Pavonis Mons* is also visible. Image based on MOLA measurement, source: http://i.space.com/images/071017-mars-tharsis-02.jpg.

2.4. Plain-style volcanism

The relatively flat plains around the volcanoes in the volcanic provinces are formed by lava flows that poured out from various sources (see Figure 2.5). The source vents are often difficult or impossible to recognize, but it is clear that some of the flows originated from linear fissures (Greeley and Spudis, 1981). The plain-style volcanic regions can be divided into two broad categories. In the first category, the volcanic features are common and are only rarely marked by low compressional sinuous ridges called the "wrinkle ridges"[1] (Carr, 2006). In the second category of the plain-style regions, the relative abundance of volcanic

[1] Wrinkle ridges are tectonic features often sinuous ridge on a lunar mare created when the basaltic lava first cooled and contracted.

products is low and most of them are marked by the "wrinkle ridge" morphology. The first group is mainly associated with volcanic provinces like *Tharsis* (or *Elysium*) (Carr, 2006). This environment is the major point of interest for this diploma work. The plain-lava flows of the first category were derived from low shield volcanoes and from numerous vents above the fracture systems transecting the whole *Tharsis* region. Such regions are probably formed by several overlapping lava flow units. All plains in the northwestern areas of *Tharsis* are lava flow plains, similarly to *Syria Planum* in the southern part of *Tharsis* (Carr, 2006). There are two different types of the lava flows in the lava plains: sheet lava flows and tube-fed flows, where the lava flow units were confined within barriers or ridges of solidified lava that can completely envelope the mobile interior of the lava flow (Carr, 2006). This kind of volcanic activity is similar to plain-style volcanism as defined in the Snake River Plain on Earth (Greeley, 1982).

Plain-style volcanism, defined by American geologist Ronald Greeley (1982) in the Snake River plain in Idaho, represents an intermediate volcanic style between the "flood basalts" and the "Hawaiian style" of volcanic activity with large shield volcanoes. Typical volcanic landforms in plain-style volcanic areas are multiple lava flow units which erupted primarily from point sources, low shield volcanoes and lateral transport of magma (lava) through channels or lava tunnels (Figure 2.5). The plain-style volcanism is also typical with voluminous overlapping flows and vents spatially associated with rift zones bounded by vertical fractures in the crust (Greeley, 1982). In plain-style volcanism, the lava flows dominate over small cones and low shield volcanoes.

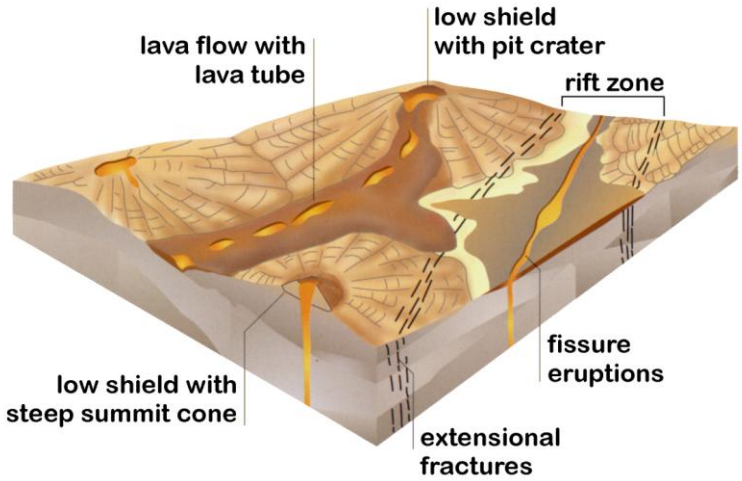

Figure 2.5: Illustration of plain-style volcanism by Greeley (1982) based on Snake River Plain volcanic area in Idaho, USA. The block diagram depicts lava flows venting from craters of low shield volcanoes or fissures of the rift zone. Mainly basaltic lava is transported laterally through the lava channels, tunnels or spreads radially from the place of fissure eruptions. This illustration of plain-style volcanism closely resembles some volcanic regions observed on Mars.

Low shield volcanoes are small volcanic landforms that form by radial diffluence of erupted lava. In the case of Snake River plain, lava flows are between 1 to 5 meters thick and formed by *pahoehoe* as well as *aa* lava. The older volcanic features are typically partly or completely buried by newer lava or pyroclastic material (Greeley, 1982).

Lava tubes longer than 20 km are common in many volcanic regions on Earth. Similar structures were recognized also on Moon and Mars, where they are hundreds of kilometres long (Greeley, 1982).

Viking probes took images of Mars surface with resolution which allowed recognizing widespread volcanic features in *Tharsis* and *Elysium* volcanic landforms and first morphometric analyses (Plescia, 1981 and Hodges and Moore, 1994). The Viking images revealed volcanic features typical for plain-style volcanism activity as defined on Earth (Greeley 1982). A comprehensive comparative study between *Snake River Plain* and volcanic province *Tempe Terra* on Mars based on Viking images was made by Plescia in 1981.

Schumacher and Breuer (2007) suggest that plain-style volcanism might represent a relatively recent type of Martian volcanism caused by a zone of partial melting in atypically warm mantle underneath a thickened crust, rather than within a mantle plume.

2.4.1. Low shield volcanoes

Low shield volcanoes are positive broad landforms that develop by episodic magma eruptions and diffluence of low viscosity magma from the central vent or fissure. A conical body builds up by extrusion of numerous subsequently emplaced lava flows that overlap each other. The base of low shield volcanoes has typically few tens of kilometres in diameter, elevation less than few hundred meters (maximum 400 m) and dip of the flanks below 3° for Earth and below 0.5° for Martian conditions (Greeley, 1982; Hauber et al., 2009). Most of the low shield volcanoes have summit pit craters and steeper slopes encompassing the summit areas, which result from late-stage and low-volume *aa* lava eruptions (Greeley, 1982). On Earth, low shield volcanoes are typical for the *Snake River Plain* in Idaho, *Iceland* and *Hawaii* volcanic regions (Greeley, 1982).

Images collected by Viking Orbiter offered only cursory informations about shapes of smaller volcanic features with basal diameter of few tens of kilometers that rise typically only few hundred meters above the surrounding elevation datum. These forms have extremely shallow flank slopes of less than 0.5°, which is the major reason why they were almost invisible in the Viking images (Hauber et al., 2009). Until new data

from MOLA was obtained, their morphometric analysis was not possible. Most studies using the MOLA image datasets focused on larger features, while few studies were devoted to low shield volcanoes (Sakimoto et al., 2003; Hauber; 2007, Baptista et al. 2009). Low shield volcanoes are abundant in the *Elysium Volcanic Province* and randomly distributed in *Tharsis* region, the most extensive volcanic province on Mars. Other studies reported small conical landforms also in other parts of Mars, e.g. in northern polar region (Garvin et al., 2000a; Sakimoto et al., 2001), but these were not confirmed later as low shield volcanoes on the basis of their morphometric properties and their volcanic origin is being investigated (Warner and Farmer, 2008; Kneissl and Neukum, 2008).

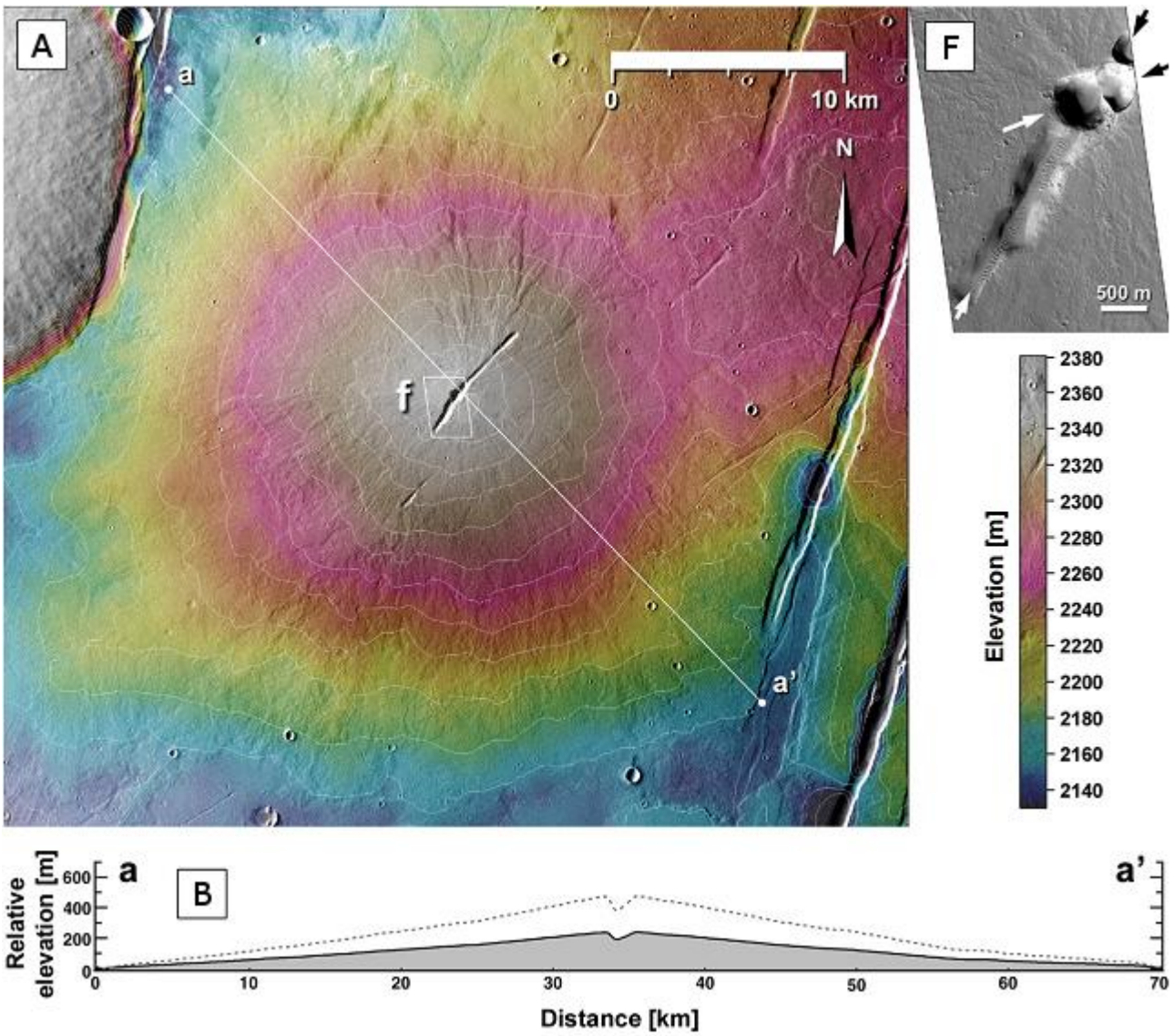

Figure 2.6: A) Topographic image of typical low shield volcano southeast of *Jovis Tholus* (HRSC image mosaic mergedwith colour-coded MOLA DEM; contour line interval 20 m; center of shield at 17.87°N/243.55°E) with profile (B) marked as *a* and *a´*. Note the low topographic profile and large basal spread characteristic for the low shield volcano. (F) is detail of summit crater marked on image (A). From Hauber et al. (2009).

Low shield volcanoes on Mars were first described by Plescia (1981) in a comparative study between the *Tempe Terra* region and Snake River Plain in Idaho, USA. Sakimoto (2008) reported identification of more than 500 individual low shield volcanoes on the entire Mars surface. However, Hauber et al. (2009) were not able to identify most of these landforms reported by Sakimoto (2008) outside *Elysium* and *Tharsis* regions either in MOLA shaded DEM (Digital Elevation Model) nor in the image data. Shaded MOLA DEM revealed low shield volcanoes only in *Elysium* and *Tharsis* regions (Hauber et al., 2009). Other small volcanic features outside these regions were therefore excluded from the low shield volcano group.

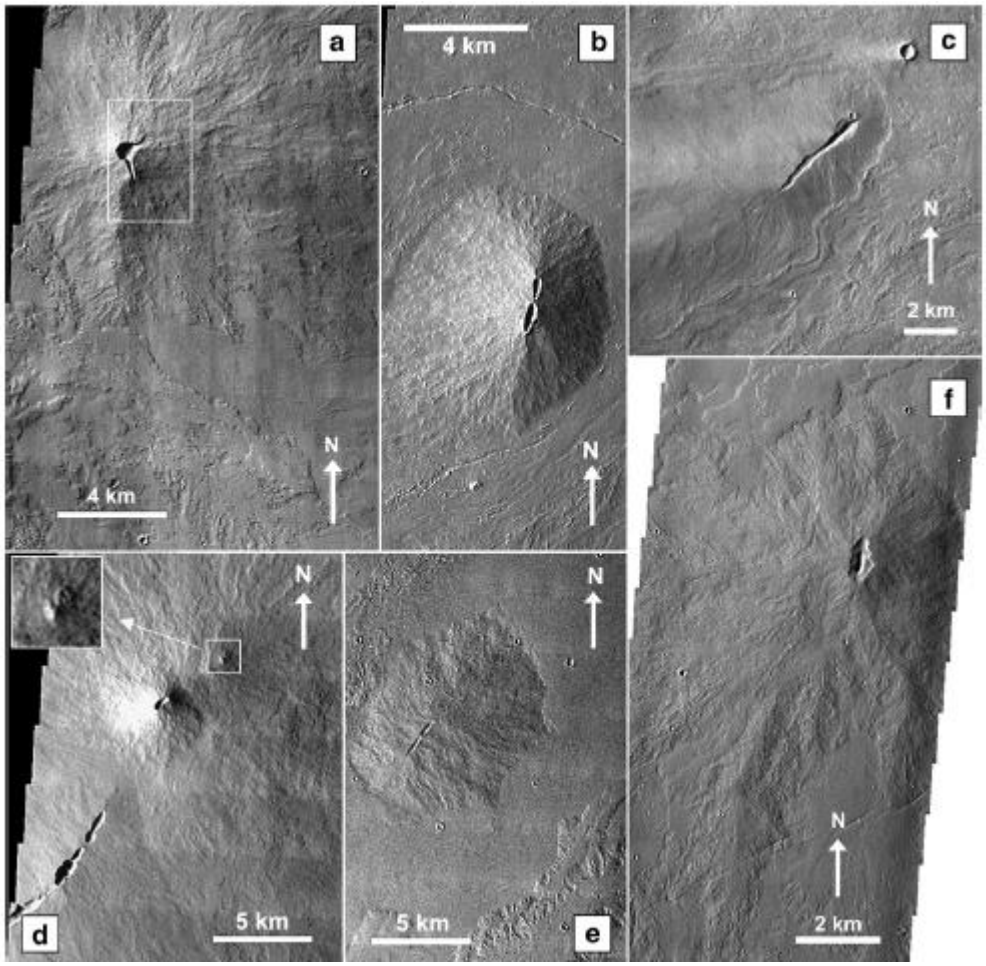

Figure 2.7: Examples of low shield volcanoes visible in Themis-VIS images in Tharsis region on Mars. Volcanoes have wide range of shapes and summit vents. From Hauber et al., 2009.

Low shield volcanoes typically form clusters (see Figure 2.8) and only rarely occur as isolated features. The clusters comprise from tens up to hundreds of individual shield volcanoes. Dense clusters with overlapping relationships mark the *Tempe Terra* (Plescia, 1981) or *Syria Planum* (Schupack and Sakimoto, 2006; Baptista et al., 2009) in the *Tharsis* region. Clustering of low shields, earlier described by Hauber (2009), was confirmed by our observations. Other low shield volcano clusters in *Tharsis* are situated south and east of *Pavonis Mons*, around *Ascraeus Mons*, on the caldera floor of *Arsia Mons*, southeast of *Olympus*

Mons and in the *Ceraunius Fossae* region (Hauber et al., 2009).

Hauber et al. (2009) described low shield volcanoes as landforms with flank slopes ranging from 0.5 to 2° (see Figure 2.6). However, most of them have slope angles smaller than <1° based on MOLA measurements. Typical height of shields revealed by MOLA data is only several hundred meters (maximum around 400 m), which corresponds to previous studies (Hodges, 1980). High resolution MOLA data allowed to precisely delineate the boundaries of the low shields and revealed low shield diameters of 60 to 80 kilometres with relatively wide spread (Brož, 2008). In contrast, older works indicated much smaller basal diameters, only between 2 to 10 kilometres (Moore and Hodges, 1980) due to hardly recognizable transition between low shields and surrounding plain on the albedo[2] and shading in older images. In addition, MOLA allows measurements of summit caldera depths for few cases. For example, Hauber et al. (2009) established caldera depths to few tens of meters.

Topography data and images suggest that flanks of low shield volcanoes are formed by overlapping lava flows that radiate outward from the central shield summit. Topographic profiles across some low shield volcanoes show almost ideal symmetry with constant slopes on both sides (Hauber et al., 2009). Some low shield volcanoes reveal a clear break in their slope angle with slightly steeper angles for the summit part than for the distal part of the low shields. This break is typical for most of the terrestrial shields volcanoes. Shapes of the low shield volcanoes on Mars in plan view are not ideally circular, but elongated, which is controlled by the regional tectonic settings. For example, most of the shields in *Tempe Terra* have their long axes distributed in the NE direction (Hauber et al., 2009).

Hauber et al. (2009) also attempted to establish the volumes and basal areas of individual low shield volcanoes using the gridded digital elevation model (DEM) based on MOLA data and simplified conical geometry of a volcanic shield (Davidson and De Silva, 2000), because most of the volcanoes have circular or slightly elliptical shape in plain view. Measured basal areas of low shield volcanoes of several hundred to about 2000 km^2 suggest volumes in range from 1 km^3 to 200 km^3. This is more than for shields in Mexico (Hasenaka, 1994) but still much less than for the Hawaiian volcanoes (from 10,000 to 70,000 km^3).

Flank slopes are much smaller on Martian shields (of less 1°) than on low shield volcanoes described on Earth. For example, Icelandic low shield volcanoes have generally slopes around 2.7°. Examples of basaltic volcanic provinces on Earth with low shield volcanoes displaying slopes of less than 1° are rare (Hauber et al., 2009).

[2] Ability of reflecting light.

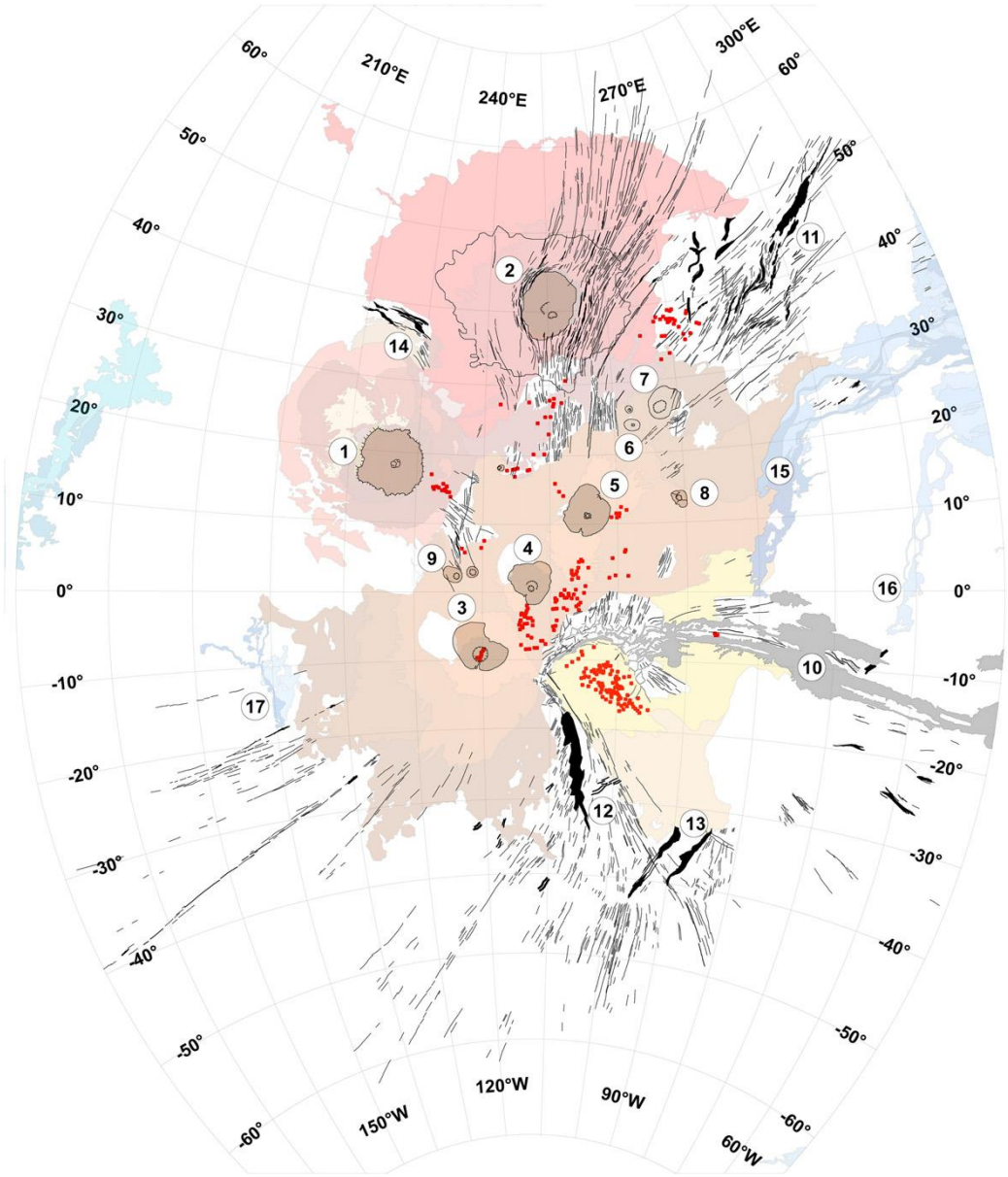

Figure 2.8: Positions of low shield volcanoes (red dots) in *Tharsis* region by Hauber et al. 2009. These are mainly situated in clusters widely spread through the entire region. Shades of red and violet indicate volcanic plains. Numbers indicate the prominent landforms: *Olympus Mons* (1), *Alba Patera* (2), *Arsia Mons* (3), *Pavonis Mons* (4), *Ascraeus Mons* (5), *Ceraunius Tholus* (6), *Ulysses Patera* (7), *Tharsis Tholus* (8), *Biblis Patera* (9), *Valles Marineris* (10), *Tempe Fossae* (11), *Thaumasia Riftzonen* (12, 13), *Acheron Fossae* (14), *Kasei Vallis* (15), *Maja Valles* (16) and *Mangala Vallis* (17).

Hauber et al. (2009) found out that more than 80% of low shield volcanoes have a small summit crater or linear fissure vent. Shapes of the vents are circular or elliptical and relatively small in comparison with the basal diameter of volcano. The elongation direction of craters or fissures also typicaly follows the underlying tectonic trends. Diameters of summit craters range from few hundred meters up to few kilometers. The summit areas of young volcanoes reveal overlapping radial lava flows that vented from the craters. These subtle morphologies are however not seen in older regions like *Tempe Terr*a or *Syria Planum* due to erosion and disruption by impact craters. Flanks of summit craters and linear fissures range from

>45° to steep angles (Hauber et al., 2009). In some instances, linear distribution of the summit craters following the regional tectonic fractures was clearly discernible. This was also observed on Kilauea on Earth where summit craters are often elongated in the direction of the associated volcanic rift zone (Okubo and Martel, 1989).

Fissure vents are typical for plain-style volcanism and are common on Martian surface. Fissure vents form above dikes feeding the lava flows (Hauber et al., 2009 and references therein).

Low shield volcanoes are mainly associated with two types of lava flows that vented from the central summit craters: simple, narrow lava flows and broad sheet flows (Walker, 1972). Differences between these two lava forms are difficult to identify even with the MOLA images, due to superposition of the surface by eolian deposits or due to lava flow overlapping relationships. Narrow lava flows are typically longer than 10 kilometres and only 1 to 3 kilometres wide. Considering the shallow slope angles of their basal channels, the latter lava flows had to have low viscosities, which suggests their basaltic to basaltic-andesitic compositions (Hauber et al., 2009).

2.5. Stratigraphy

2.5.1. The crater counts techniques

Impact craters are formed by random impacts of bodies on the surfaces of terrestrial planets. Their density gives a planetologist a tool for estimation of the absolute age for the area of interest.

The age determination method based on crater density on the surface of terrestrial planets is based on mathematical analysis technique, which was developed in 1960s and 1970s by Crater Analysis Techniques Working Group (Arvidson, 1979). It is based on the relation between crater-size frequency distributuion (CSFD) and relative ages of planetary surfaces. The method was originally developed for the Moon, from where geological samples were brought by Apollo module and other space probes. Specimens from the Moon were dated by radioisotopic methods and correlated with density of impact craters at the sampling sites. This offered a unique opportunity to correlate the crater frequency and absolute ages of geological units bombarded by meteorites. The result of this analysis was a cumulative production function curve showing ratio of impact craters to investigated surface area. This curve was later recalibrated for Martian conditions (Ivanov, 2001). This was possible considering the similar conditions throughout the early inner solar system (Neukum et al., 2001). However, Mars was more geologically active than the Moon, so it has to be kept in mind that especially small features (e.g. impact craters) on the Martian surface are slowly eroded.

On the other hand, relatively young surfaces, representing for example the surficial parts of lava flows are ideal for dating with crater counts statistics, since normal craters have been lost due to erosion (Hartman, 2001).

Neukum et al. (2001) and Ivanov (2001) used crater counts to estimate ages of Martian surfaces and combined the results with studies of Martian meteorites to establish a rough chronology of Martian history. Locally high crater densities on Mars or radiometric dating of Martian meteorite ALH84001 suggest that some parts of Mars are about 4.5 Ga old and represent the oldest surfaces corresponding to deeply eroded primordial crust. Although erosion destroyed small craters on Martian surface, these are still visible on Phobos (Hartman and Neukum, 2001), a Martian satellite. Hartman and Neukum (2001) used crater counts to date the Martian epochs previously defined by Tanaka in 1986 (see Figure 2.9); Noachian Period before about 3.5 Ga, the Hesperian-Amazonian boundary at about 2.9 to 3.3 Ga ago, Late Amazonian Epoch, which lasted from 300 to 600 Ma ago. In addition, some lava flows revealed very young ages of about 10 Ma (Hartman and Neukum, 2001).

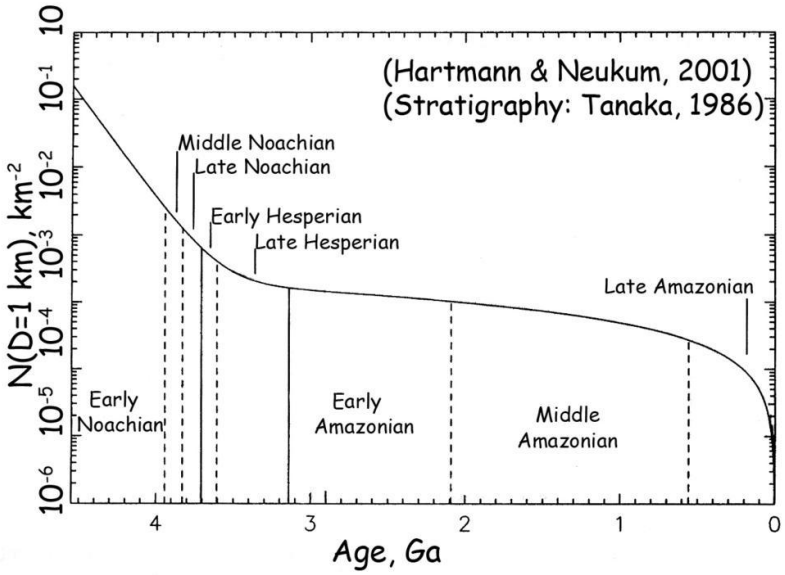

Figure 2.9: Chronology curve developed by Neukum and Ivanov (2001) using stratigraphy defined by Tanaka (1986) for Mars.

It is clear that crater count technique has several fundamental limitations because it is statistical method based on researcher's interpretation. First limitation is connected with interpretation and mapping of impact crater structures by the researcher. Hartman et al. (1981) suggested that the comparison of impact structure tracing results within same units made by different workers varies at 10% around the correct age. Second shortcoming of the method arises from subjective establishment of stratigraphic unit boundaries. However, in our case, the latter limitation had only small negative effect, because low shield volcano boundaries were easily recognisable. Third, population of craters allows establishing only the youngest age of the topmost

exposed layer on the surface. The statistical nature of the method requires covering larger areas in order to achieve reliable datasets. To extend the crater count to include craters with larger diameters, this demand may conflict with the limited area of small geological units like individual lava flows (Hartman, 2001). All these limitations together are susceptible to alter the final result by a factor of about 1.2 to 1.3; corresponding to error of 5-20% in resulting ages (Hartman et al., 2001; Lissauer et al., 1988).

2.5.2. Ages of Mars volcanic activity

Volcanism on Mars is an old phenomenon and it probable originated shortly after the time of planet formation from collisions of planetisimals in the Solar system (see Figure 2.10). All big volcanic features were built up to their present size in the early Martian history 3.6 Ga and their initial activity dates back to 4 Ga ago (Werner, 2009). Recently extensive volcanic units are situated in different parts of Mars. Mars is exceptional in the group of terrestrial planets, because its morphology records the distinct events of volcanic eruptions. In contrast, Mercury and Moon were frozen shortly after their formation and Venus and Earth are still being remodeled by erosion processes.

The present study investigates low shield volcanoes which are distributed mainly in two volcanic provinces, the *Elysium* and *Tharsis* volcanic regions. Large volcano *Elysium Mons* in *Elysium* volcanic region formed 3.7 Ga ago and its reached maximum size 3.5 Ga ago, but still continued with volcanic activity between 3.4 to 3.3 Ga. The caldera on the top of volcano revealed ages of 3.5 Ga with later resurfacing in 1.6 Ga of unclear non-volcanic origin (Werner, 2009).

Volcanic activity in the *Tharsis* region is more continuous trough time than in the *Elysium* volcanic province. Although the CSFD suggests that the main large shield volcanoes in *Tharsis* formed 3.55 Ga ago when the huge shield volcanoes in the region reached their final size, the latter volcanoes also reveal younger volcanic eruptions dating back to 500 to 100 Ma (Werner, 2009).

It contrast to Earth, volcanic activity on Mars was rather episodical than continuous through time. The major divide of the volcanic history on Mars (Werner, 2009) which marks the transition from vigorous activity associated with the major volcanoes (*Elysium Mons*, *Tharsis Montes* and *Olympus Mons*) and the volcanic activity that postdates the large volcanoes. The first vigorous volcanism of the first episode can be attributed to the cessation of the magnetic dynamo (before 3.9 Ga) which was probably followed by a large plume activity which formed volcanic centers *Tharsis* and *Elysium.* This epoch ended around 3.6 Ga, but plains-forming activity ended even earlier 3.7 Ga (Werner, 2009). After this major event, there were only episodic volcanic activity events of unknown reason and source of melted material. Greeley and Spudis

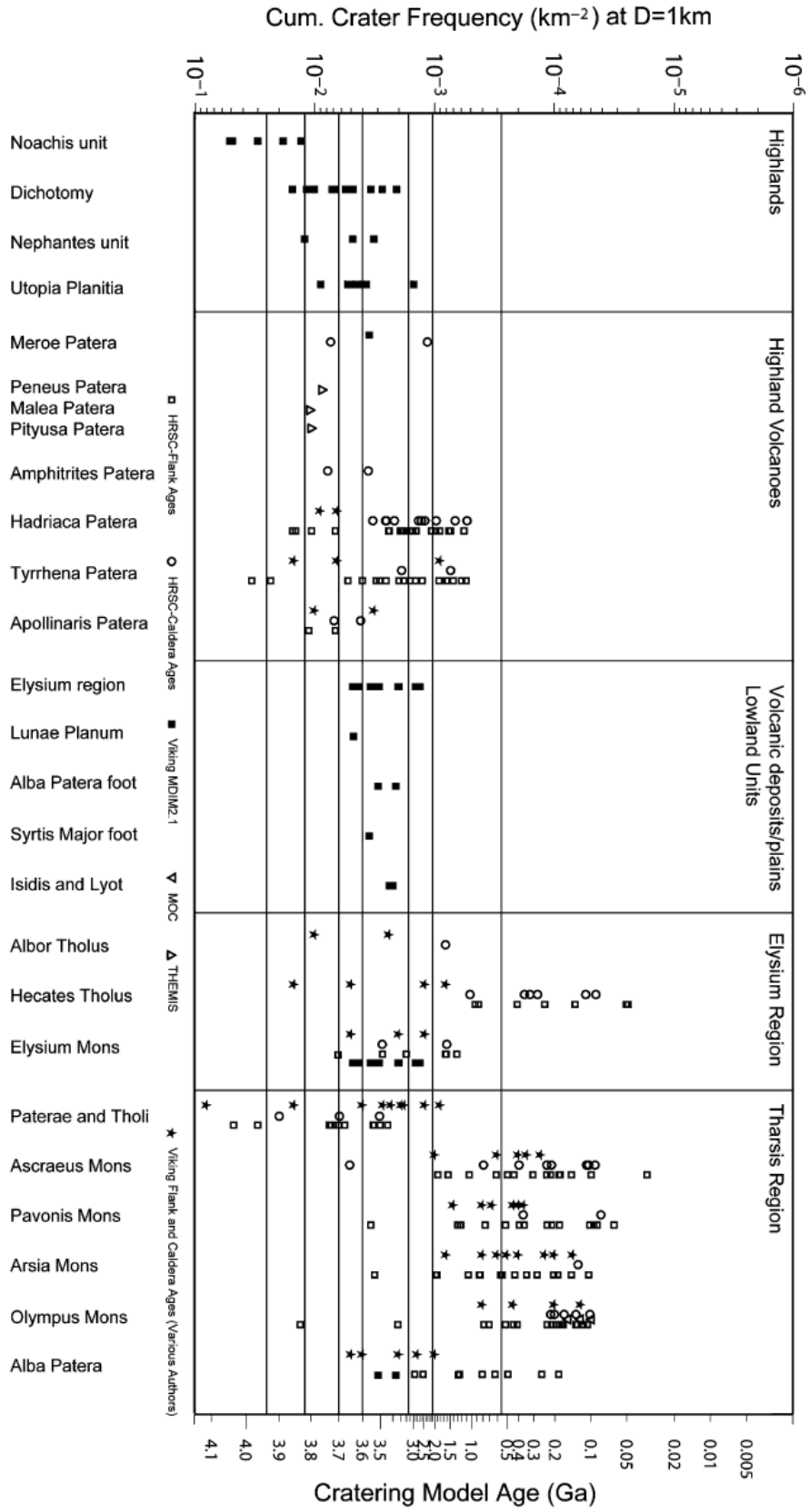

Figure 2.10: Summarization of volcanoes ages on Mars and some prominent volcanic plains (empty and filled squares). Left scale shows crater cumulative frequencies, scale on the right refers to model ages using cratering chronology model by Hartman and Neukum (2001). From Werner (2009).

(1981) suggested that the uplift of *Tharsis* and *Elysium* regions may have triggered release of large-scale catastrophic water floods carving large channels into the volcanic landscape. Continued uplift and lithospheric thinning contributed to magma formation by decompression melting in the mantle to feed the large volcanoes and surrounding extensive lava plains with more magma, but the volcanic activity slowly diminished.

2.6. Rheology

Lack of samples from Mars and other bodies in the solar system preclude direct rheological estimates of the lavas on the basis of their composition. Therefore, the planetary scientists attempted to relate lava flow physical properties on the basis of the morphology of lava extrusions (McColley and Head, 2004; Warner and Gregg, 2003; Hulme, 1976; Hiesinger et al., 2007; Vaucher et al., 2009). The final morphology of hot lava in lava flows is determined by the rheology of the lava marked by the yield strength and the plastic viscosity (Wilson and Head, 1983). One of the first morphometric studies made was based on terrestrial lava flows (Walker, 1973). Walker (1983) found that the gross chemistry of lava is affected by flow dimensions, and that the effusion rate controls the length of lava flows. The higher the eruption rates, the longer are the lava flows (Walker, 1973; Greeley and Spudis, 1981). Investigation of the *Mare Imbrium* region on the Moon revealed that lava flows exist on flanks with very gentle gradients around 0.1°. Moore and Schaber (1975) concluded that lavas on slopes with low gradients behave like Bingham fluids, for which the yield strength is an important parameter that can be calculated from the geometry of the flows (Hulme, 1974). The plastic viscosity of a Bingham fluid at relatively higher shear rates can be obtained from Jeffrey´s equation relating the viscosity of a flow to the lava effusion rate and lava flow dimensions (Hiesinger et al., 2007, and references therein).

The above outlined method has the potential to provide valuable geological and geochemical data based only on photogeologic interpretation (Greeley and Spudis, 1981). The utilization of remotely sensed data for estimation of the rheological properties of the lava flows is based on few general assumptions (e.g. Hiesinger et al., 2007).

a) Flow dimensions are related to the rheological properties of the flow.
b) Lava flows behave as Bingham fluids.
c) Lava flows are laminar.
d) No inflation of the lava flow occurred.

Advancing lava flow fed by a feeding conduit (circular volcanic vent or fissure vent) looses heat by radiation to the surrounding environment by conduction to the substrate below and by convection and conduction to the atmosphere if it is present. The heat loss causes rapid decrease of lava viscosity, which finally arrests the lava flow. This is caused by an enveloping thermal boundary layer within which yield strength and viscosity increases rapidly from all surfaces of the flow inwards (Wilson and Head, 1983). The effect of this process is expressed by theoretical and empirical constant – the Graetz number (Wilson and Head, 1983). The Graetz number relates the rate of heat that is lost from a flow to the rate of heat advection within a flow along its length (Gregg and Fink, 1996). Observations on Earth suggest that lava flow is not moving if the dimensionless Graetz number decreases to about 300 (Wilson and Head, 1983 and references therein). The variation of Graetz number depends on physical properties of the local planetary environment; e.g., lava flows on Venus cool significantly slower due to high ambient temperatures (Wilson and Head, 1983). For thermal diffusivity, which is also included in the calculations, we use the value of 3×10^{-7} m^2 s^{-1} (Hiesinger et al., 2009).

3. Images and softwares

3.1. Images

Last thirty years of remote sensing data brought a large image datasets of Martian surface within large span of resolution variability (from few centimetres to hundreds of meters per pixel). While the first images showed Mars in low resolution did not allow distinguishing relatively small morphological details, the recent high resolution data in visible, infra and ultra light give us a chance to revise and explore our knowledge about all aspects of Martian surface. For the purpose of morphometric analysis of selected lava flows, we have selected images with resolution of around few meters per pixel. This resolution is a reasonable compromise combining coverage of larger areas and sufficient resolution for recognition of small impact craters with diameter around tens of meters.

For our morphometric analysis of selected extrusive features, we used pictures of Martian surface in visible range of light which were taken by *Context Camera* (CTX) on board of NASA mission *Mars Reconnaissance Orbiter* (MRO). This 350 mm focal length camera is designed to obtain grayscale pictures of surface with resolution between 5 to 6 meters per pixel in ideal case. Camera acquires a swath 30 km wide and normally 160 km long (Malin et al., 2007). In some cases we used *High Resolution Stereo Camera (*HRSC) on board of the European Space Agency's *Mars Express* spacecraft. *Mars Orbiter Laser Altimeter* (MOLA) data on board of Mars Global Surveyor were used to establish the topographic profiles across selected lava features (Zuber et al., 1992; Smith et al., 2001) for the morphometric calculations of their

rheological properties. Global gridded MOLA **D**igital **E**levation **M**odel (DEM; cell size: 0.463 km) was used to establish the total volume of each low shield volcano (e.g. Table 6.1) and single-track profiles were used for measurement of lava flows thicknesses (e.g. Figure 5.4).

The CTX camera bridges the global data and high resolution image datasets, namely the gap in coverage between 1.5 to 6 meters per pixel (Malin**,** 2007). The CTX pictures allow describing the subtle morphological features of plain-style volcanism, independent volcanoes and overlapping lava flows. In addition, these provide source data for the absolute ages of the large volcanoes by crater counts technique and basic rheological properties of volcanic landforms by morphometric calculations.

The raw CTX image data are available for download from the *Themis* database (http://themis.asu.edu/). The data were converted for further analysis by USGS Astrogeology image processing software *ISIS3* for correct projection, orientation and illumination (for more information see USGS, 2008).

3.2. Software

3.2.1. ISIS3

The Integrated System for Imagers and Spectrometers (*ISIS*) is a software developed for processing and manipulation of images taken with NASA spacecraft modules (http://isis.astrogeology.usgs.gov/). This software development started more than 30 years ago and originated at the end of Apollo program. The latest *ISIS3* version which was rewritten in the *C++* for *Linux* interface was used for handling of our images.

Few basic operations were used to recount the raw images. First, function "*mroctx2isis*" imports MRO CTX images as an ISIS cube[3], next "*ctxcal*" to radiometrically calibrate the CTX images, than "*spiceinit*" to determine SPICE (*Spacecraft and Planetary ephemeredes, Instrument C-matrix and Event*) kernels for a camera cube and at last "*cam2map*" to convert camera image to a map projection images. In the latter step we had to select appropriate geographical projection with minimal distortion of the shapes of landforms in the area of interest. At last, resolution of the map projected images was chosen. The *Mercator* and *Sinusoidal* projections were found the most suitable for our type of analysis.

Mercator is a cylindrical map projection which was developed by Flemish cartographer Gerardus Mercator in 1569 and it rapidly became a widely used map projection. The distortion is smallest in near-equatorial areas and grows closer to the poles. Sinusoidal projection is a pseudo cylindrical equal-area map

[3] A cube is a 3-dimensional image with axis: samples, lines, and bands.

projection which is based on north-south central meridian. The map distortions are smallest near this central meridian and changes of shapes and sizes of impact craters increase in west-east direction (Kneisl et al., 2010).

Since the distortions of shapes and sizes of impact craters in mercator projection of +/- 30° equatorwards are negligible (Kneisl et al., 2010), we used Mercator projection for all images which cover areas of less than 30° equatorwards on both hemispheres (areas southeast from *Olympus Mons*, Caldera of *Arsia Mons*, *Pavonis Mons*, north from *Biblis Patera*, some volcanoes from *Ceranius Fossae* cluster and *Syria Planum*). When the image covered areas larger than 30° equatorwards, we used sinusoidal projection with central meridian which crossed the images in the middle (in case of the following clusters: *Tempe Terra* and some volcanoes from *Ceranius Fossae*) (see Figure 3.1).

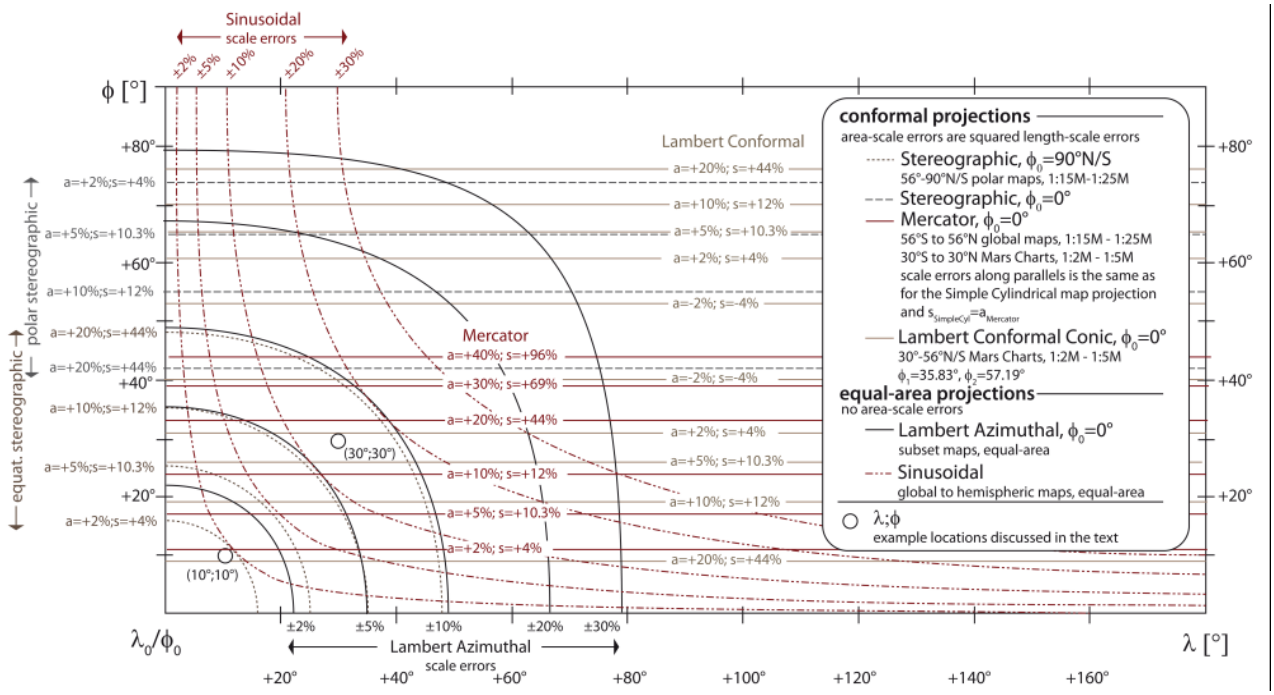

Figure 3.1: Schematic illustration shows distortions in circular shapes caused by different map projections depending on the longitude. Mercator projection is useful for maximal values +/- 30° than error is prohibitively large and other projection has to be used (Kneisl et al., 2010).

The last step of the image data processing was the export of cube images as raster images which were importable to the ArcGIS software environment (script "*isis2std*", producing PNG, JPEG or TIFF formats). The PNG format with PGW file containing information about the coordinate system was used in this study. In few cases, script "*automos*" was used for merging a mosaic of adjacent images.

3.2.2. ArcGIS

The standard "geographic information system" platform *ArcGIS* software family (version 9.2. and 9.3 from ESRI) was used to analyze the raw images, trace the impact craters, and make preliminary interpretations (e.g. delineation of individual object boundaries) in the areas of interest. First, correct projection for the imported data was chosen (projection *Mars 2000 Sphere.prj*). Similar like in ISIS, we had to choose Mercator or Sinusoidal projection depending on latitude of areas of interest. Then we used bilinear interpolation to change sharpness of borders translations to softer and gradual. Bilinear interpolation is a resampling method that uses a weighted average of the four nearest cells to determine a new cell value. New resampled images provided high contrast of crater boundaries for their precise tracing.

The fundamental tool for tracing of individual impact craters in *ArcView* is the *ArcView* extension named *CraterTools* (Figure 3.1) developed by Thomas Kneissl from *Freie Universität* Berlin which produces two types of ESRI shapefiles by manual tracing of crater boundaries; first accounts for dimensions of the selected volcano, second one for the impact craters. ESRI shapefiles are geospatial vector data format and normally includes points, polylines or polygons. The *CraterTools* toolbox allows automatic calculation of crater counts, areas, dimensions and their spatial distributions.

Figure 3.1: Screenshot of CraterTools from ArcView interface. First two active buttons are used for marking impact craters with either two points or three points technique of drawing a circle. The three points technique is more precise. First and last inactive buttons are used to start and terminate the data collection with this tool.

Low shield volcanoes boundaries

Boundaries of low shield volcanoes were established in visible range of *CTX* images. Boundaries of individual volcanoes were clearly recognizable, except for few cases for which idealized boundary shapes were delineated. For the units with incompletely recognizable boundaries, the CSFD technique was applied only to some fraction of the selected unit (e.g. a low shield volcano) (Werner, 2009).

The main goal of this part of the study was to find the boundaries of investigated volcanoes and possible boundaries of their subunits to consider their origin by a single event or multiple lava extrusion. Shapefile including information about total area comprising the volcanoes was then produced by manual tracing of these boundaries in *ArcGIS* environment (see Figure 3.2).

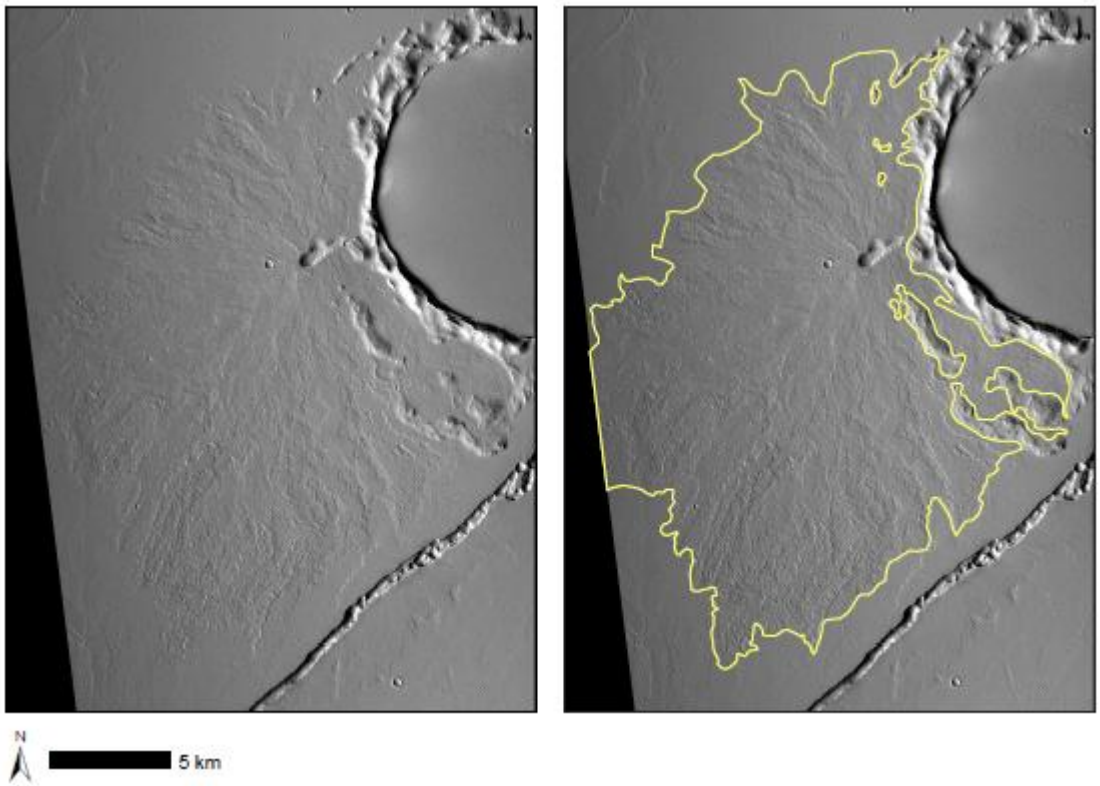

Figure 3.2: An example of low shield volcano in *Ceraunius Fossae* (N. 15) visible on CTX image (left) and mapped boundaries of this volcano (right). This volcano lies on the side of older impact crater which is completely filled by younger lava material.

Crater diameters

For the purpose of the correct age determination from the production function curve, it was necessary to use all impact craters visible irrespective of their degree of erosion or later modification. Craters with elliptical shapes due to impact under sharp angle or secondary craters and craters of non-impact origin like sublimations pits, collapse and volcanic craters were all excluded from the analysis (Werner, 2009) (see Figure 3.3).

The two shapefiles (first with counted crater sizes [km] and second with volcano area [square km]) were then exported into a file for the next statistical analysis using *CraterStats (*http://hrscview.fu-berlin.de/craterstats.html) software (Figure 3.4).

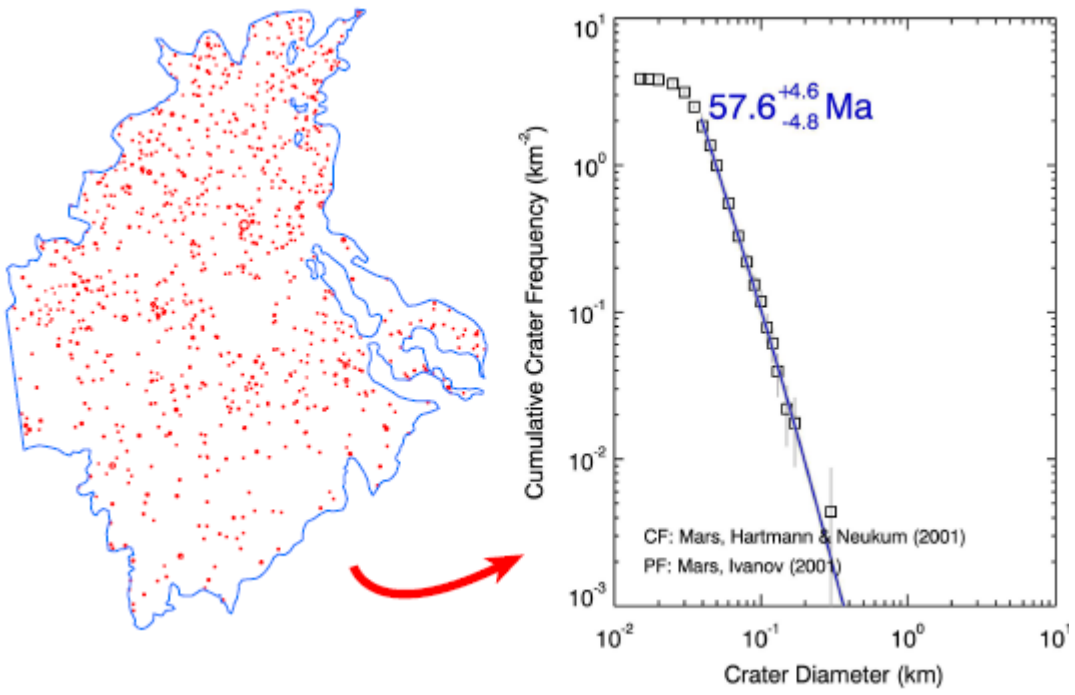

Figure 3.3: An example of impact crater count of volcano No. 15. Blue color marks low shield boundary, red circles are counting impact craters (left). Right picture is production function curve counted by CraterStats fitted with half-line running trough main population of impact craters.

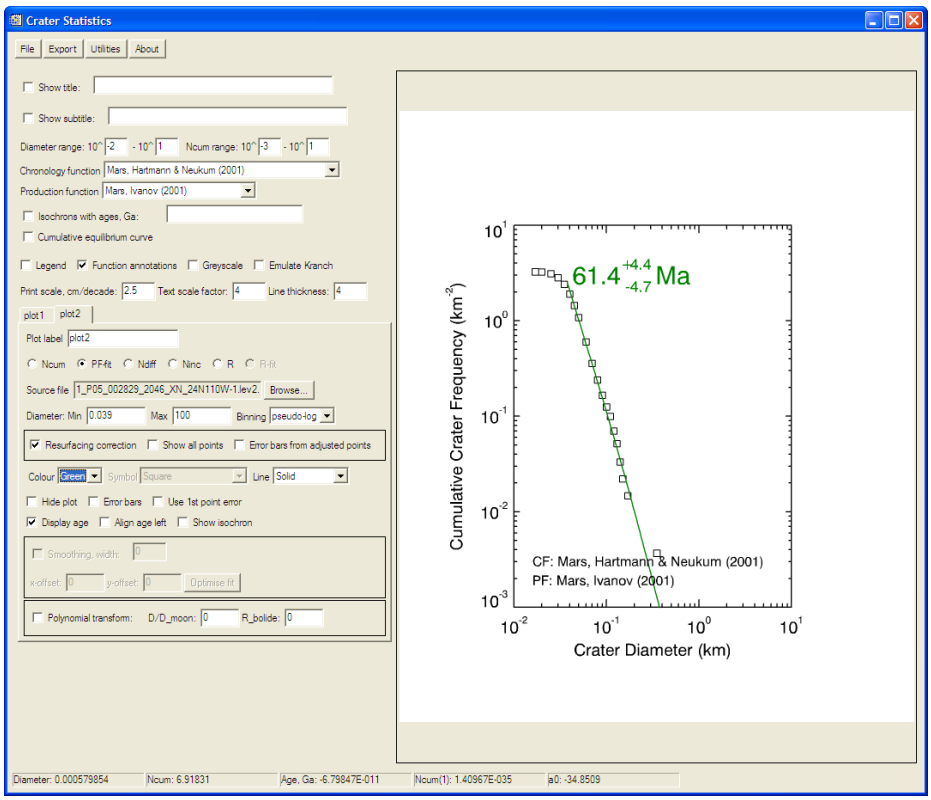

Figure 3.4: Interface of CraterStats developed by Freie Universität Team. Researcher has the ability to set minimum and maximum size of the craters, to be counted for age determination and also choose which plot has to be used. Data file obtained from CraterTools plots the cumulative distribution of impact craters of the area and draw the production function curve characterizing the age of investigated units.

4. Chronology

First part of our research was based on attempt to establish absolute ages of low shield volcanoes in *Tharsis* region. Chronology of low shield volcanoes from this area was not systematically investigated before. For the purpose of volcano geochronology, the CSFD based on *CTX* images (with resolution around 6 meters per pixel) was used. Data from total 61 volcanoes is presented. These data were collected together with other students of the DLR team, namely Felix Jagert and Angelika Hoffmeister.

Low shield volcanoes are volcanic features formed by overlapping lava flows (Hauber et al., 2009). The fact that low shield volcanoes have gentle slopes is an important prerequisite for crater counting analysis, because we can exclude deformations of impact craters caused by steep slopes.

4.1. Clusters in Tharsis

Hauber et al. (2009) found that the low shield volcanoes in the *Tharsis* region do not show any spatial affinity to the huge volcanoes or any other landforms in this region. The low shield volcanoes are typically distributed in groups or "clusters" (Hauber et al., 2009 and see Figure 2.8) and their distribution seems to correlate with the regional tectonic settings like faults or grabens in the area. Our investigation focused on these clusters where the majority of low shield volcanoes in the *Tharsis* are situated.

From each cluster, few low shield volcanoes were processed to receive a first approximation about the ages representing the low shield volcanic episode in the area of interest (see Figure 4.1). Clusters situated in *Tempe Terra*, south part *of Ceraunius Fossae*, south-east from *Olympus Mons*, north from *Biblis Patera*, in caldera of *Arsia Mons*, south from *Pavonis Mons* and in *Syria Planum* were analyzed for this purpose. The selected clusters occur in a -20°S to +40°N belt of the *Tharsis* region and cover subregions with different speed and style of erosion, crater numbers and presence of secondary craters.

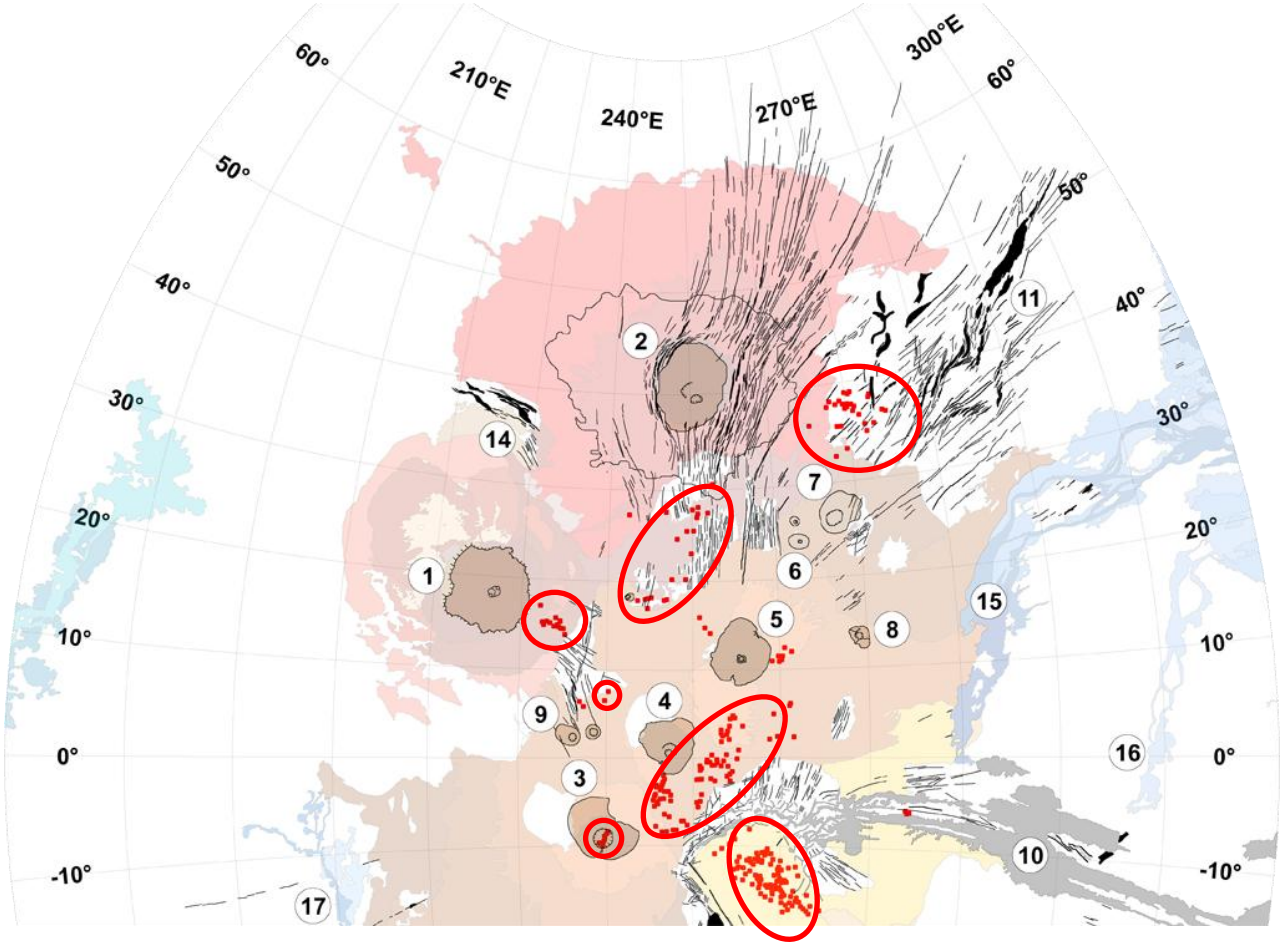

Figure 4.1: Position of investigated clusters in *Tharsis* region (Modified image from Hauber et al. [2009]). Numbers describe the prominent morphological landforms: *Olympus Mons* (1), *Alba Patera* (2), *Arsia Mons* (3), *Pavonis Mons* (4), *Ascraeus Mons* (5), *Ceraunius Tholus* (6), *Ulysses Patera* (7), *Tharsis Tholus* (8), *Biblis Patera* (9), *Valles Marineris* (10), *Tempe Fossae* (11), *Acheron Fossae* (14), *Kasei Vallis* (15), *Maja Valles* (16) and *Mangala Vallis* (17).

4.1.1. Tempe Terra

Presence of low shield volcanoes in the *Tempe Terra* region covering 400,000 km^2 is known from Viking images (Plescia, 1981; Hauber et al., 2002). Low shield volcanoes in this area are situated mainly within a circle of 200 km radius covering ~125,000 km^2, centered at 37.5°N and 274°E (Hauber et al., 2009). This area consists of volcanic units and older and heavy fractured crust (Moore, 2001). Most of the volcanoes are around the *Mareotis Fossae* going in SW-NE direction. All volcanoes in this cluster are situated above the 30°N latitude, therefore the sinusoidal projection was used to minimize the distortion of crater shapes. *Tempe Terra* was earlier recognized as an area formed by volcanic, glacial and eolian activity (Van Gasselt et al., 2003).

Since the westernmost volcanoes including the *Issedon Tholus* were heavily eroded by numerous overlapping impact craters, the boundaries of individual impact craters were recognisable only with difficulties. Considering these difficulties, we decided to map only craters larger than 100 meters.

To the east from *Enipeus Vallis*, an old channel of unknown origin reveals numerous craters with a specific morphology. While in this area the volcanoes are covered by a soil layer that behaves as a semiliquid environment after impact (Gault and Greeley, 1978). Impact craters often look like *rampart craters* (see Figure 4.1a). Possible explanation for these craters is that the impacts produce heat, which melts ice in the ice-rich uppermost soil layer. Produced water is mobilized and freezes in a different part of the structure. The observations of rampart and eroded craters suggest that the thick layer of soil probably contains ice. We also observed a structure suggesting presence of possible iceberg in the past (see Figure 4.1b). This positive sinusoidal landform was interpreted as an *esker*. However, smaller volcanoes situated on the top of the old crust fragments do not reveal rampart craters (and therefore ice-rich soil layer) and most of these craters are covered by younger eolian deposits forming dunes.

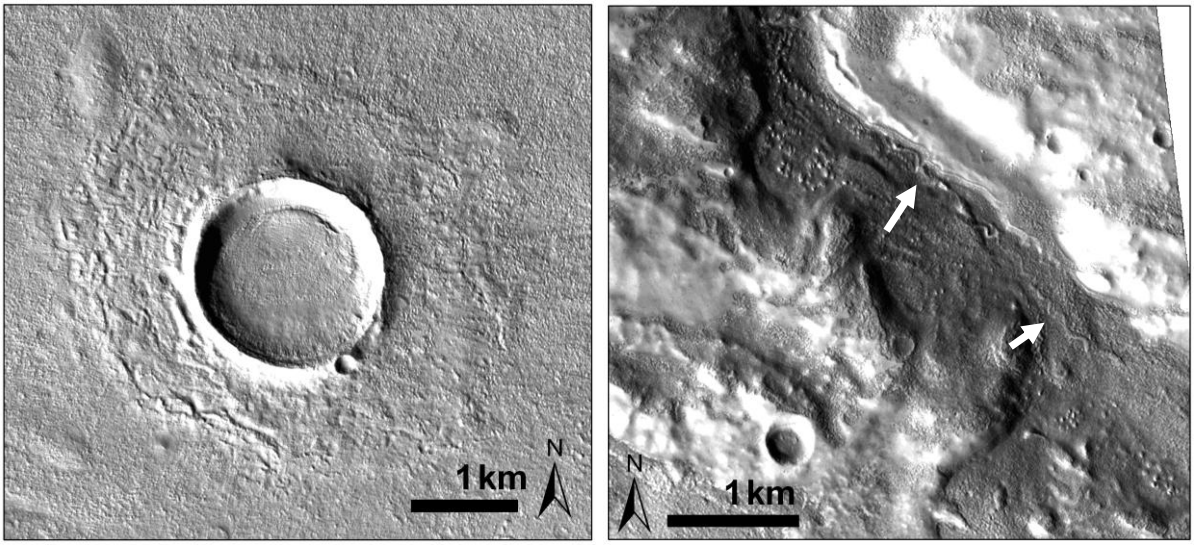

Figure 4.1: a) Detail of possible rampart crater on the flank of low shield volcano No. 27 in *Tempe Terra* with younger smaller crater in the crater rim (CTX image P05_002881_2182_XN_38N092W, centered 38.2° N /267.8°E). b) Sinusoidal positive landform situated in a small valley going from block of old crust in northern part of *Tempe Terra* which might represent an esker-like structure. Altitude decreases from left down corner to upper right corner of the image (CTX image P03_002103_2189_XN_38N091W, centered 39.2° N / 268.6°E).

4.1.2. South part of Ceraunius Fossae

Low shield volcanoes in the southern part of *Ceraunius Fossae* region are often fractured by one or more graben or fault systems of *Ceraunius Fossae* running through all the investigated subregions. Presence of well developed fractures in the mapped lava units suggests that the grabens were probably later reactivated

or are still active (see Figure 4.2).

Impact craters and summit craters of all the investigated volcanoes were clearly recognizable, which suggests low erosion factor of this region.

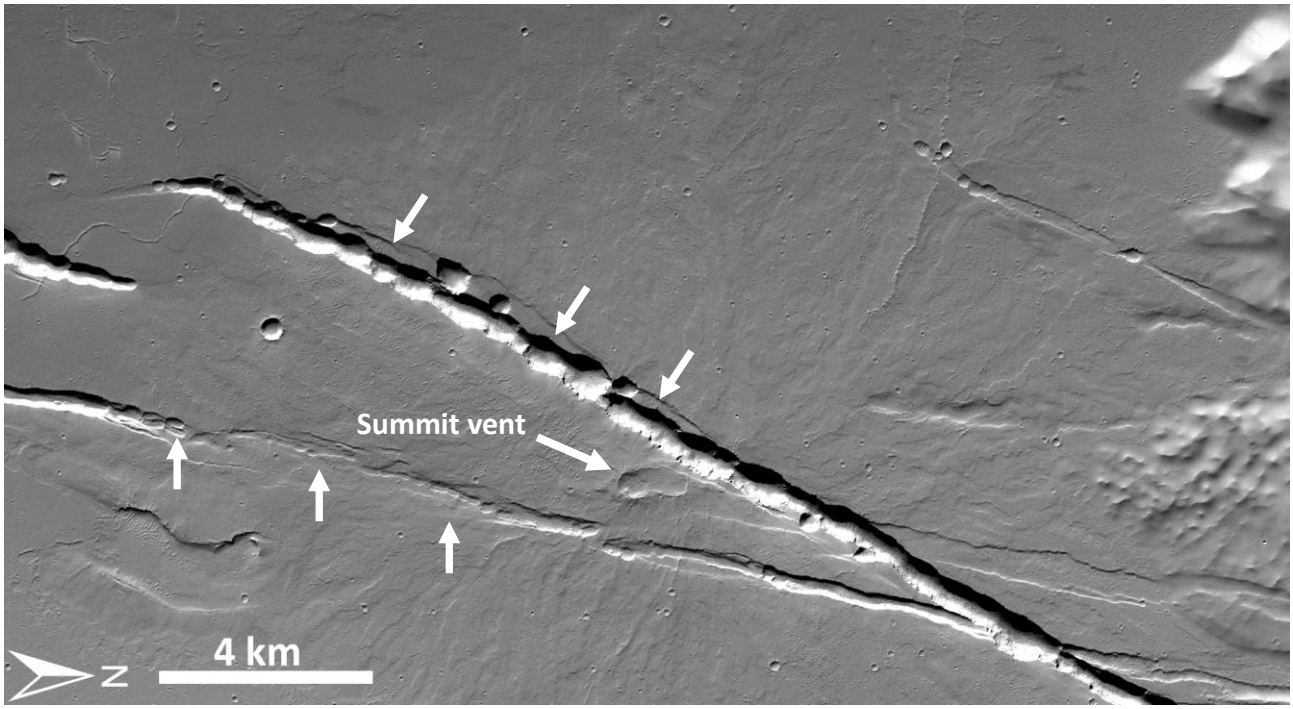

Figure 4.2: Modifications of low shield volcano morphologies via reactivation of underlying fractures is visible in the case of volcano No. 19. Two linear depressions (marked with white arrows) crosscut lava flows that were derived from a small central vent - in the center of the image (P04_002763_2080_XN_28N109W, centered 28.75° N / 250.74° E).

4.1.3. Region located in south-eastern direction from Olympus Mons

This area is typical with dense distribution of abundant low shield volcanoes with overlapping relationships, which allows to determine relative stratigraphy of investigated volcanoes. The impact craters are surrounded by clearly developed rims, therefore the erosion factor is low. The whole area is covered by younger lava flows with well defined boundaries; eolic dust layers or any other newer superficial material is absent. Numerous fissures in the area produced long lava flows associated with plain-style volcanism. These were used for morphometric calculations of rheological properties of lavas (see Table 5.1). Also the contamination by secondary craters was low; we observed only few well bordered clusters of secondary craters.

4.1.4. Northern from Biblis Patera

Low shield volcanoes in this area are different from those observed in any other investigated clusters of *Tharsis*; their cones are much steeper and smaller in lateral extent. Few volcanoes with steep flanks possibly formed by more viscous lavas were also found. Unfortunately, because the eolian erosion in this area was strong, the smaller craters were almost completely destroyed and the larger were heavily eroded as well, therefore the age determination of this area by crater counts technique was almost impossible. On the other hand, interesting new volcanic features in this region were found. These landforms are small conical hills with much steeper slopes than low shield volcanoes and with basal diameter ranging around few kilometres. We interpreted them as possible cinder cones (see Figure 4.3), well known from Earth, that form by accumulation of scoria around the central vent. Five cinder cones are aligned in a linear array oriented in south-north direction.

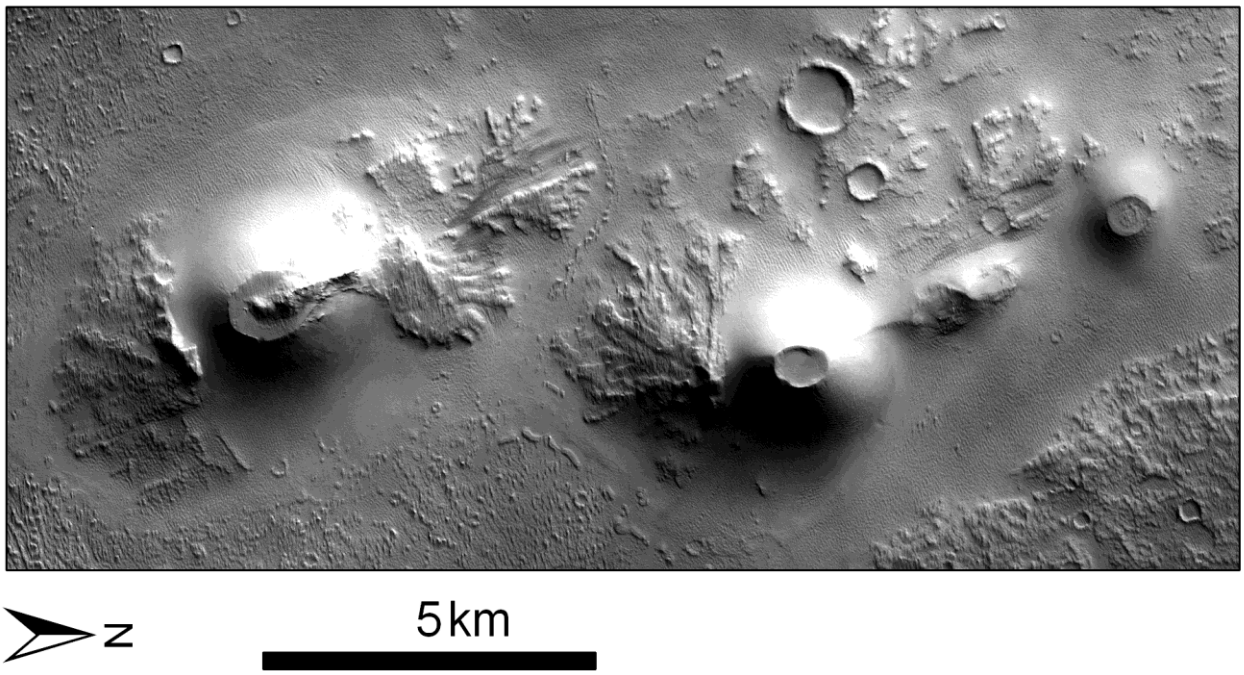

Figure 4.3: Two possible cinder cones with lava flows gravitating from their flanks north from *Biblis Patera*. Lava flows are decorated by flow lobes (CTX image P19_008262_1862_XN_06N123W, centered 5.6° N / 237.0° E).

4.1.5. Caldera of Arsia Mons

Low shield volcanoes in *Arsia Mons* caldera are widely dispersed and partially clustered around the fracture system running across this structure in the SE-NW direction. The elongation of vents and linear structures also correlates with this direction. Low shield volcanoes are overlapped by other volcanoes or by surrounding lava flows and altogether form a compact and relatively smooth bottom of the caldera. The

recognition of exact boundaries between each individual units was difficult and are locally based on subjective interpretations.

Surface of caldera is covered by dark criss-crossing and sometimes smoothly curving streaks (Figure 4.4) which probably resulted from dust devils, atmospheric vortexes that cruise above the surface and redistribute the deposited dust. The presence of dust devils at the caldera of *Arsia Mons* was previously confirmed by Reiss et al. (2009 and references therein).

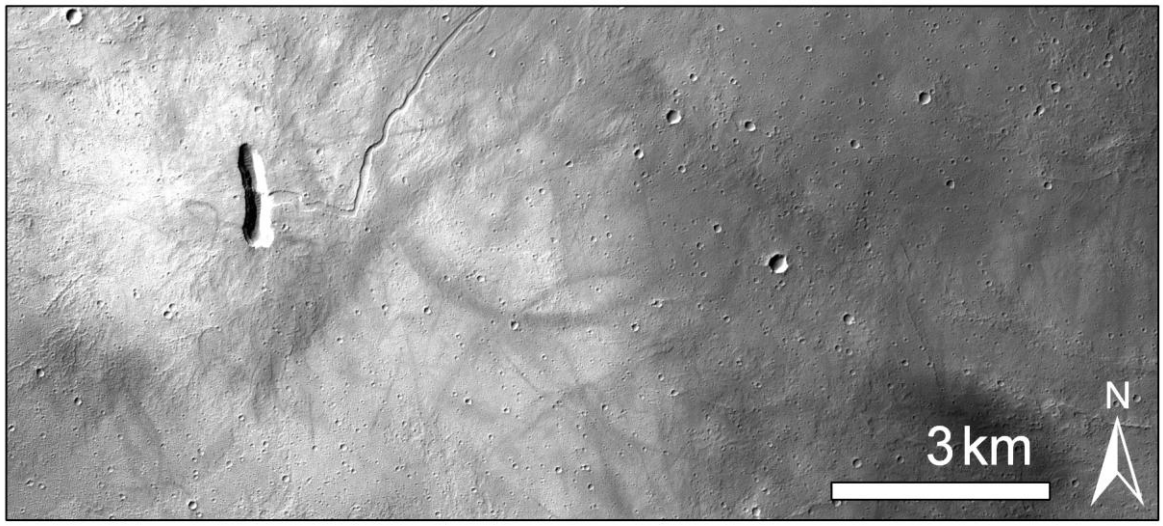

Figure 4.4: Criss Criss-crossing grooves produced probably by dust devils around the summit of an elongated vent of volcano No. 37 with well developed lava channel (CTX image P21_009343_1702_XN_09S120W, centered 9.9° S / 239.27° E).

4.1.6. Southern from Pavonis Mons

Volcanoes southern from *Pavonis Mons* are well developed volcanic landforms formed by clearly visible overlapping lava flows. Exceptions from this general characteristic are volcanoes No. 48 and No. 49. They look that they were formed by material which did not formed well bounded and limited lava flows. However without in-situ observation, this interpretation can not be confirmed (see Figure 4.5). Contamination due to secondary craters in this area is low and crater rims are well preserved.

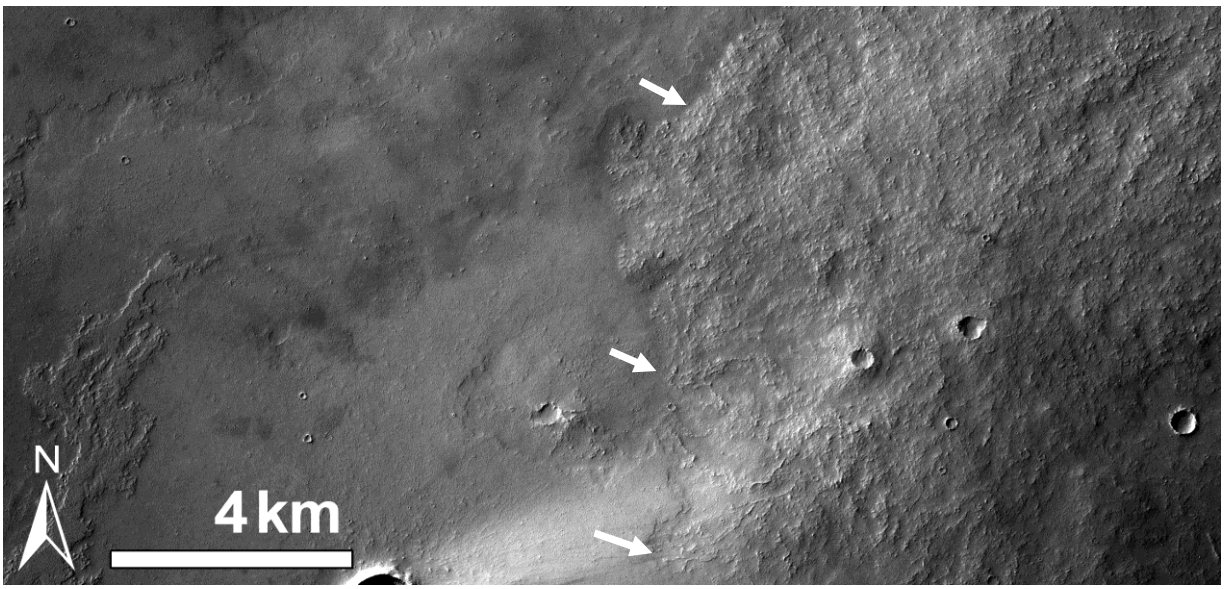

Figure 4.5: Volcano No. 49 (right part of the image) is formed by less fluid lava flows than basaltic flows suggesting different chemistry composition. The volcano is surrounded by low viscous lava flows elongated in SW to NE direction, which are associated with plain-style volcanism. Transition between this two types is marked by arrows (CTX image P22_009725_1750_XI_05S109W, centred 5.76° S / 250.46° E).

Another volcano (No. 47) is segmented by a system of fractures trending in east-western direction which formed a deep graben (see Figure 4.6). This observation clearly suggests that some tectonic processes were younger than the volcanic episode in the area, because these fault bounded tectonic grabens are not filled with lava.

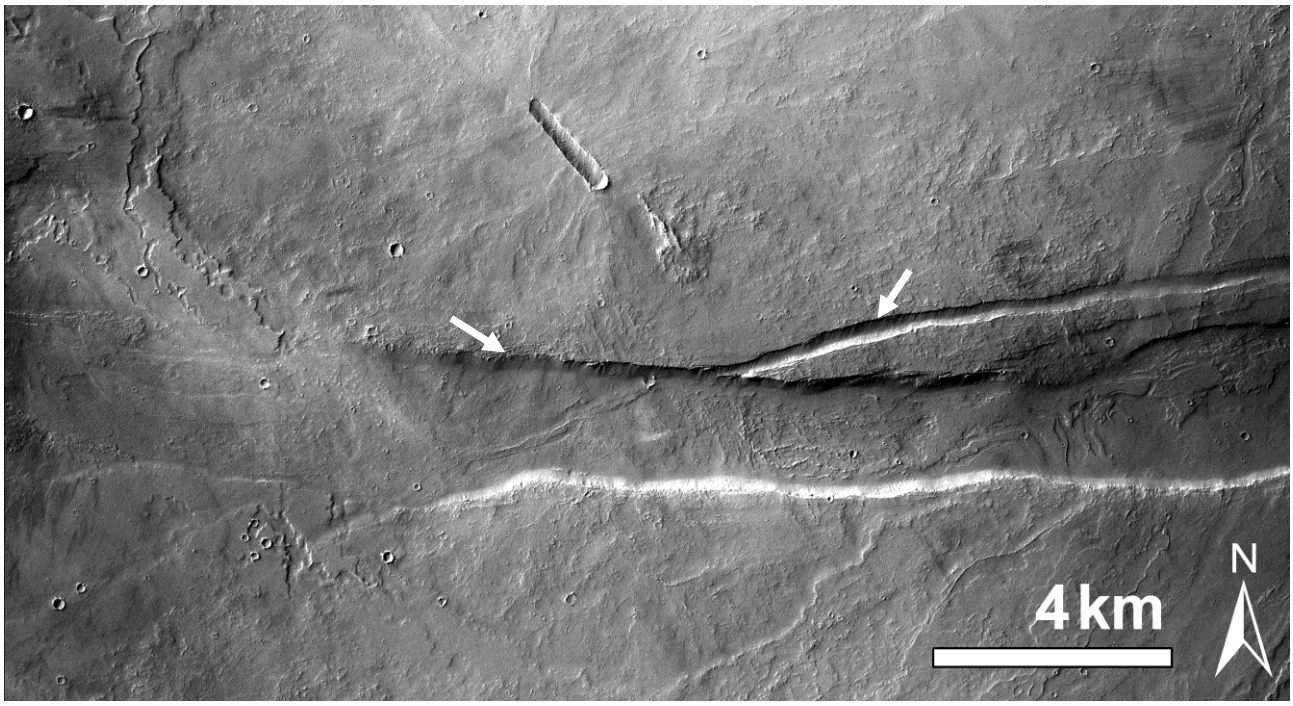

Figure 4.6: Volcano No. 47 was later cut by series of tectonic fractures (arrows) which detached part of volcano in the bottom part of the image. This suggested that tectonic processes were still active after emplacement of low shield volcano. Note that in left side of image are visible lava flows partly covered the biggest fracture (CTX image P22_009725_1750_XI_05S109W, centre 5.2° S / 250.39 E).

4.1.7. Syria Planum

Syria Planum was already identified as a center of volcanic activity (Scott and Tanaka, 1986). Baptista et al. (2008) confirmed that the observed volcanic landforms in *Syria Planum* region may be classified as low shield volcanoes. The age of *Syria Planum* was previously established to be Hesperian. Our observations, based on relative abundance of impact craters, confirm that this unit is the oldest one in the researched field. Amount of impact craters was significantly higher than in other clusters. Although it was sometimes difficult to identify boundaries between the independent shield volcanoes, in one area, their boundaries were clearly defined by darker rims decorating the individual volcanoes (see Figure 4.7). The morphology in the area was obliterated by forces of erosion by impacting and dust coverage. However, despite the high erosion, it was possible to count the craters on surfaces of investigated volcanoes, although the analysis focused only on bigger impact craters (craters larger than 250 meters).

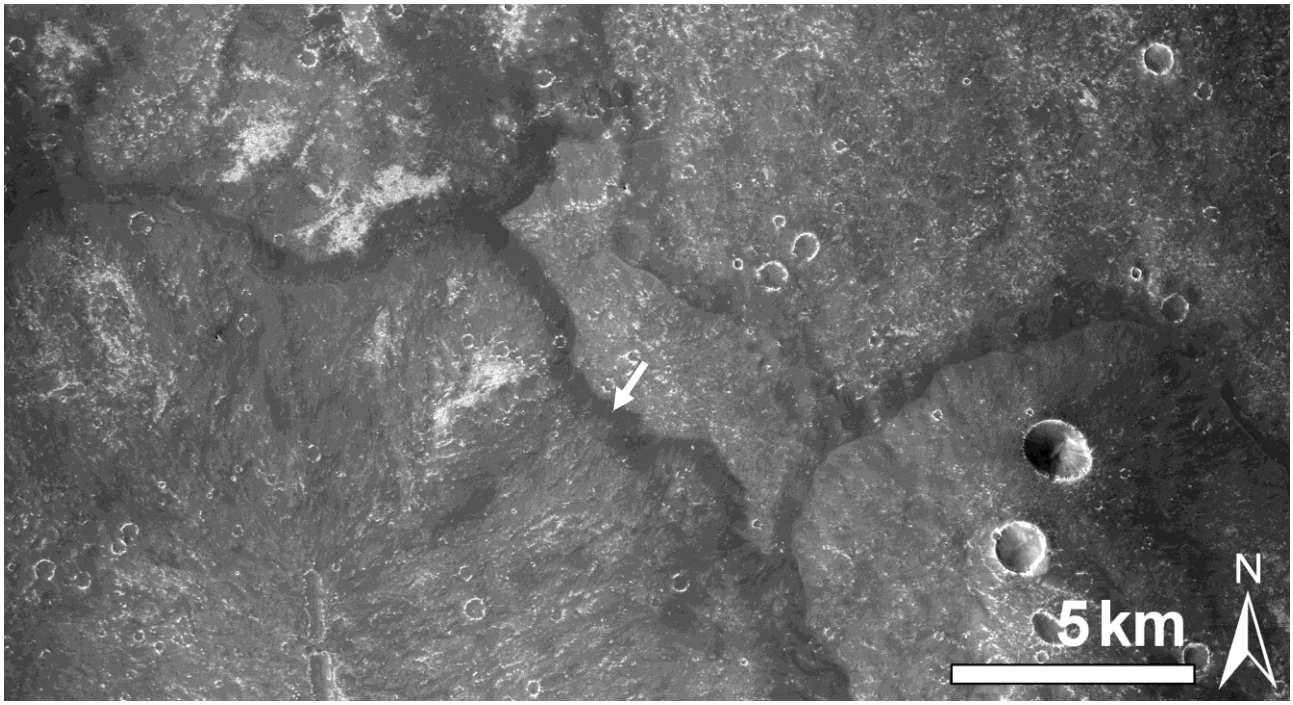

Figure 4.7: Low shield volcanoes in *Syria Planum* with a dark layer. Origin of this darker material is unknown (CTX image P06_003554_1651_XI_14S100W, centered 15.24° S / 259.33° E).

4.2. Approach and Technique

The main tool for absolute age investigation of the different investigated regions was the crater size-frequency distribution method (CSFD) based on cumulative frequency of impact craters in defined to their sizes. For CSFD, logarithmic scale (log (km^{-2})/log (km)) is typically used, because the relative frequency of small craters is high. This reflects the effect of probability; smaller craters are created more often than larger ones (Neukum and Wise, 1976).

Smaller craters form a characteristic bunch in the upper part of the production function curve. This part of the production function curve is strongly affected by given image resolutions and ability of the researcher to distinguish the small craters. Absence of these small impact craters bends the curve and causes a typical hook-shaped upper end of the curve (Hiesinger, 2002) (see Figure 4.8a). To minimize the effect of the latter shortcomings in the CSFD analysis, for tracing and final interpretation, we used 50 meters (around 8 to 10 pixels) as the minimum size of the counted impacts.

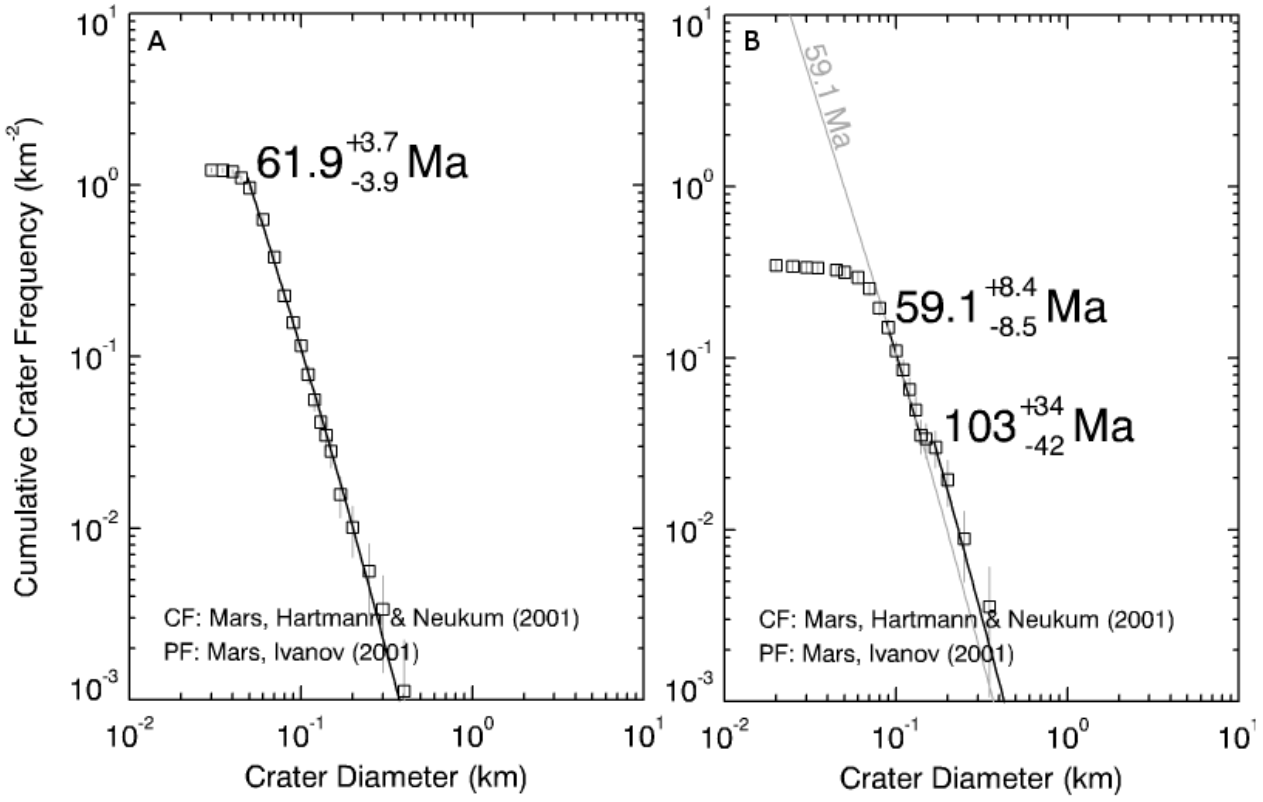

Figure 4.8: Almost linear production function curve for volcano No. 10 (A), which is ideal for single age determination. In contrast, curve for volcano No. 45 (B) revealing a kink suggests the resurfacing effect, which reflects underestimation of older crater population due to their coverage by younger units.

Linear regression was used to fit the data with a straight line (see Figure 4.8a). A kink in a curve for CSFD data for some volcanoes (see Figure 4.8b) means that the analysis was carried out in an area, where the older surface was partly covered by a younger surface suggesting some resurfacing event as described by Hiesinger (2002). Emplacement of a new unit, for example a lava sheet, covers smaller impact craters, while larger craters remain visible as they stick out above the newer layer (e.g. crater D1 in Figure 4.9). Younger impacts then form a new population of impact craters on the newer unit, which is reflected by the upper segment of the curve visible in CSFD diagram. The kink-effect of the production function curve allows indirect estimatation of lava flow thickness covering old and cratered surfaces. However low shield volcanoes could be long lived volcanic features or formed by episodic eruptions so that the suggested resurfacing spans over the entire life of a volcano so that the CSFD curve reflects several impact crater populations.

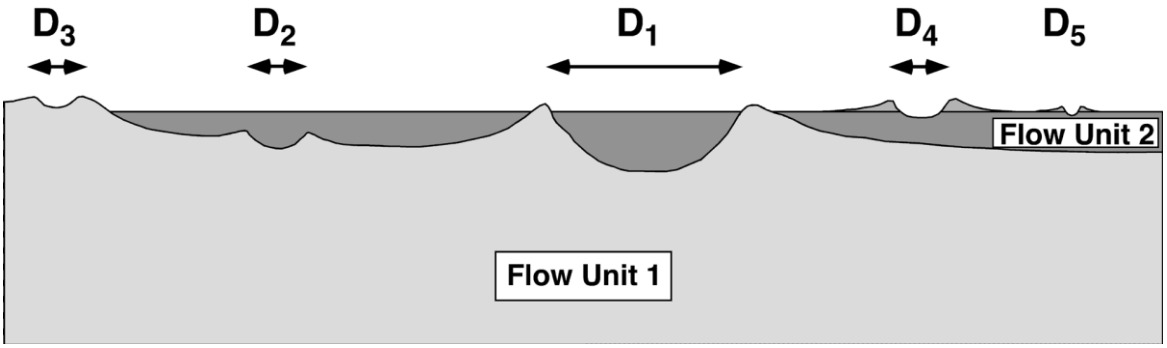

Figure 4.9: Schematic illustration of the resurfacing event. Flow Unit 1 represents older surface which was eroded by population of impact craters and later partly covered with younger surface (Flow Unit 2). Younger surface is than exposed to newer impacts producing new population of impact craters. Partially buried big crater (D_1) with visible rim and younger (D_4, D_5) and older (D_3) smaller craters together form a mixed population (Hiesinger, 2002).

4.3. Uncertainties in absolute ages

There are a few important prerequisites for the age determination using the crater counting technique. The first one requires careful geological mapping of homogeneous units, second craters of non-impact origin are excluded from the crater count. Several morphological features can be mismatched with impact craters, for example sublimation pits, volcanic craters or secondary craters (Werner, 2009). The third prerequisite is careful establishing of shapes and sizes of impact craters by the researcher during the mapping process.

To test the possible error caused by researcher's interpretation, all researchers of our team independently mapped and counted age for selected low shield volcano. It was found that all the researchers got very similar results. We also compared our results with the values established by Werner (2009) for volcano No. 46. The difference was smaller than 3%, which means that the researcher's error is lower, than that

suggested by Hartman et al. (1981).

It should be kept in mind that the CSFD method contains general uncertainty based on possible errors caused in the adaptation of lunar chronology model to Martian conditions. This may cause some shift of the measured data from the correct values (Werner, 2009), but present observation of current Martian cratering rate supports this analogy (Hartman, 2007; Hartman et al., 2008).

4.3.1. Unit boundary identification

The second important prerequisite of the CSFD method requires delineation of a homogenous unit that is characterized by a single age (Werner, 2009). Accuracy during identification of boundaries for selected units is required, since analysis for combination of units leads to distorted results (Figure 4.10).

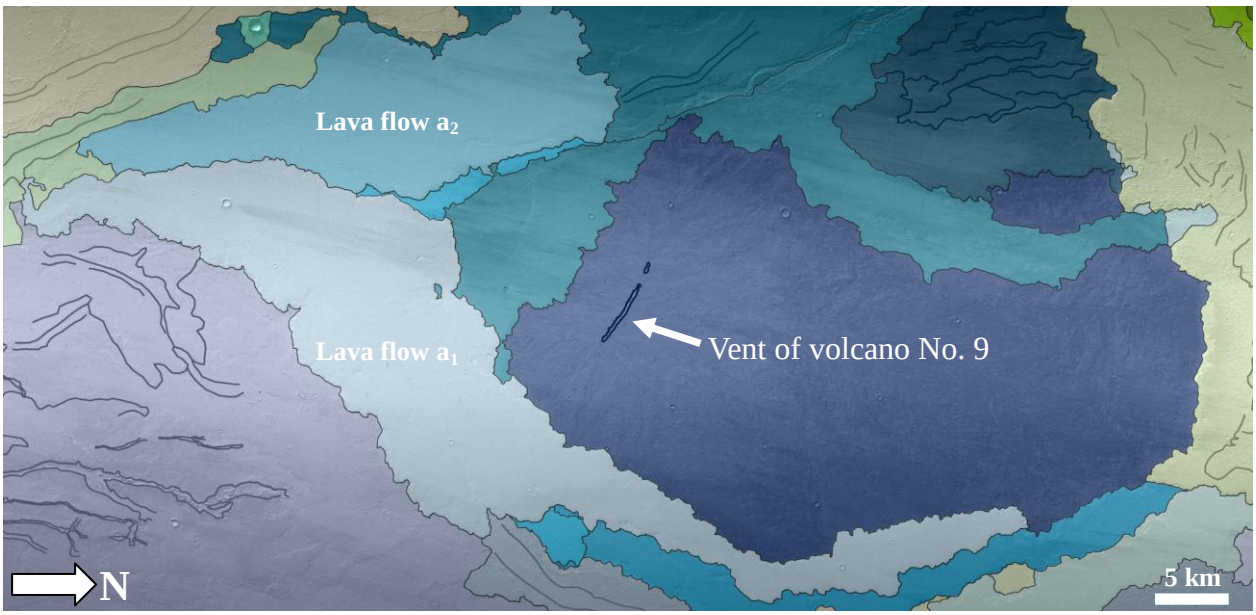

Figure 4.10: An example of a map of individual units used for CSFD and rheological calculations in a region located south-east from Olympus Mons.

Since low shield volcanoes form compact and easily recognisable units, formed by single lava flows, their boundaries are easily established. This is also due to the fact that the low shield volcanoes of the investigated areas are often surrounded by younger lava flows with different surface structure, which renders a high contrast with adjacent smooth surfaces of the low shields (see Figure 4.11a). Boundaries of overlapping volcanoes were also clearly visible, except for few cases. For unclearly defined boundaries, the analysis was applied only to a part of a volcano, which was clearly recognisable as a single unit (Figure 4.11b).

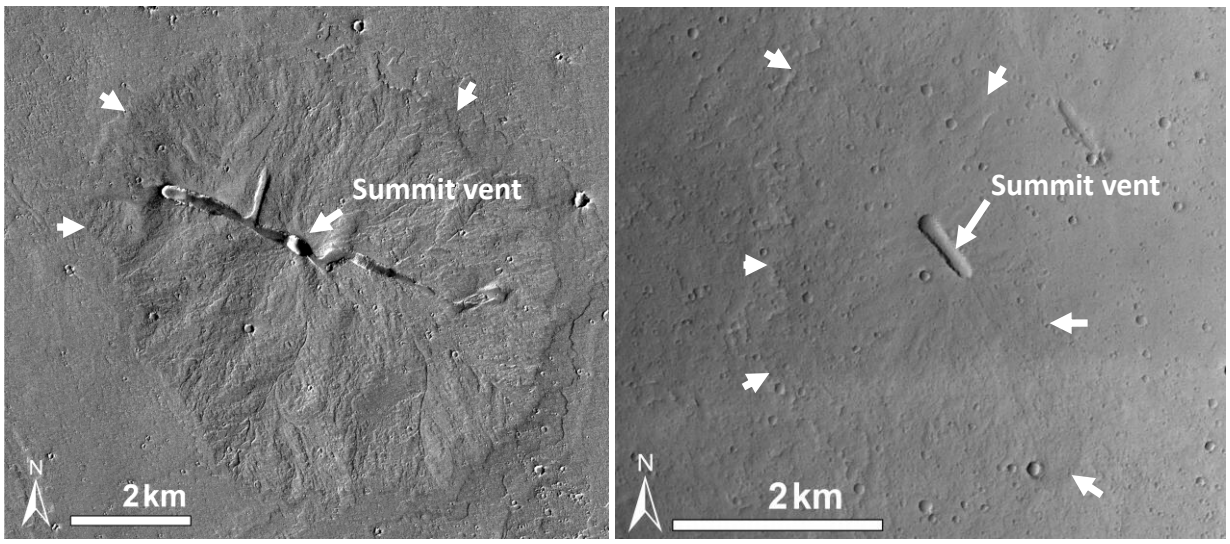

Figure 4.11: Examples of two volcanoes with clearly (A) and faintly (B) visible boundaries. A) Low shield volcanoes surrounded by younger lava flows (No. 14 south-eastern from Olympus Mons), which accentuate the boundaries of the investigated low shield volcano (CTX image P22_009686_1954_XN_15N127W, centered 15.39° N / 232.99° E). B) Overlapping relationship of adjacent volcanoes sometimes smears their mutual boundaries (volcano No. 34 at caldera of *Arsia Mons* (CTX image P03_002157_1709_XN_09S119W, centered 8.65° S / 240.08 E).

4.3.2. Secondary craters

Secondary craters (also called crater chains), that could contaminate the traced crater populations, often form elongated clusters or arrays of pits that formed by the landed ejecta that was thrown out of a larger crater (see Figure 4.12). Their incorporation in the datasets results in a steeper CSFD(s) than predicted by applied crater production functions (Werner, 2009). Secondary craters cause large uncertainities in crater counting, because they are present everywhere on Martian surface. However, since the secondary craters often form clusters of small craters, they are easily recognisable. Werner (2005) and Werner et al. (2009) established that the contamination due to unrecognised secondary craters included in the measurement is less than 10% in case of old surface and less than 5% in most other cases. Lava flows and low shield volcanoes in the present study were relatively young, therefore effect of contaminations by secondary craters on the determined age were well below 10%.

Since secondary craters have diameters generally smaller than 300 meters, Hartman (2005) and McEwen et al. (2005) suggested exclusion of all craters smaller than this size from the CSFD analysis. However, Werner (2009) showed on the basis of crater production functions, that the steepness of the size-frequency curve is not affected if small secondary craters are included. However, it was also found that included secondary craters produce “kinks” on curves for craters with diameter smaller than 100 meters, which could be misinterpreted as a resurfacing event.

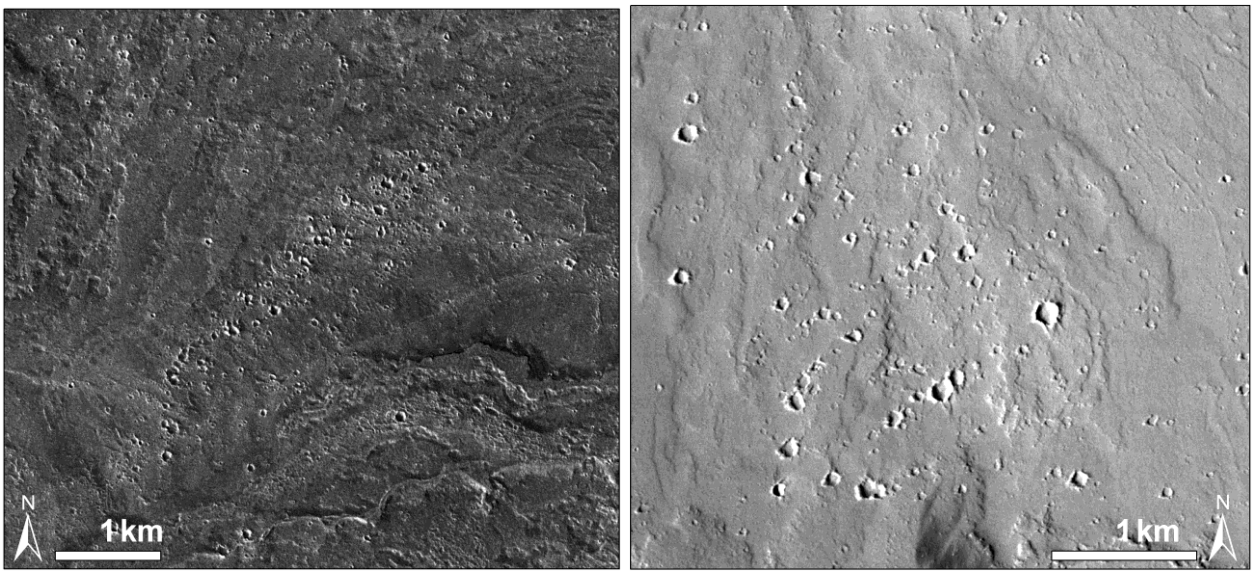

Figure 4.12: A) Secondary craters forming an elongated cluster (CTX image P07_003700_1937_XI_13N127W, centered 15.4° N / 231.92° E) and B) showing more randomly distributed group secondary craters than in (A) (CTX image P04_002763_2080_XN_28N109W, centered 28.26° N / 250.85° E).

In the present study, the secondary cluster contents in selected areas was easily detected, except one volcano in *Ceraunius Fossae* due to a large contamination by secondary craters, which was excluded from our analysis.

4.3.3. Shape of craters

Impact craters show a wide variety of shapes, which reflects either different angle of impact, material at the impact zone, impact velocity or the degree of erosion. For example, impact of a body under a relatively lower angle to the Martian surface causes elongated impact crater which cannot be traced using the *CraterTools*. Erosion changes the shape of impact crater by partial or complete destruction of crater rim and decreases original rim height. Impact craters then seem to be larger than they were originally. The latter difficulty, together with low resolution per pixel it can cause significant errors in age determination from small craters. For this reason we decided to use only craters bigger than 50 meters in diameter in most of the investigated areas; these are represented by more than 10 pixels in diameter on the CFX images.

4.4. Results of chronology

Age estimations were carried out from 61 low shield volcanoes from over 40,000 impact craters in seven different *Tharsis* subregions. Our investigation improved the knowledge about volcanic activity on Mars and also revealed that the volcanic activity enacted more evenly during the Martian history. We confirmed the previously published results regarding few volcanic areas associated with low shield volcanoes that are relatively younger with respect to other regions on Mars. It offers a new angle of view on the Martian history regarding the extent of processes that formed the Martian atmosphere.

Our results are listed in Table A.2 and graphically processed in Figure 4.13 and Figure 4.14. It seems that volcanism occured in *Tharsis* region almost recently as was suggested already before for example by Neukum et al., (2004). We observed wide timescale range of volcanic history, although the ages in each cluster of low shield volcanoes were similar, but they ranged widely in the comparison with other clusters. Especially the results from *Syria Planum* suggest that this region is very old with volcanic activity dating back to 1340 Ma to 2,880 Ma. Also *Tempe Terra* showed old age of volcanism 370 Ma to 1,000 Ma ago. Other clusters such as those south from *Ceranius Fossae* (57 to 133 Ma), southeast from *Olympus Mons* (52 to 111 Ma) and south of *Pavonis Mons* (44 to 105 Ma) revealed younger volcanic activity dating to the Late Amazonian. Low shield volcanoes found north from *Biblis Patera* (196 and 215 Ma) and volcanoes in cluster located in caldera of Arsia Mons (90 to 397 Ma) are marked by intermediate ages between younger and older volcanic activity.

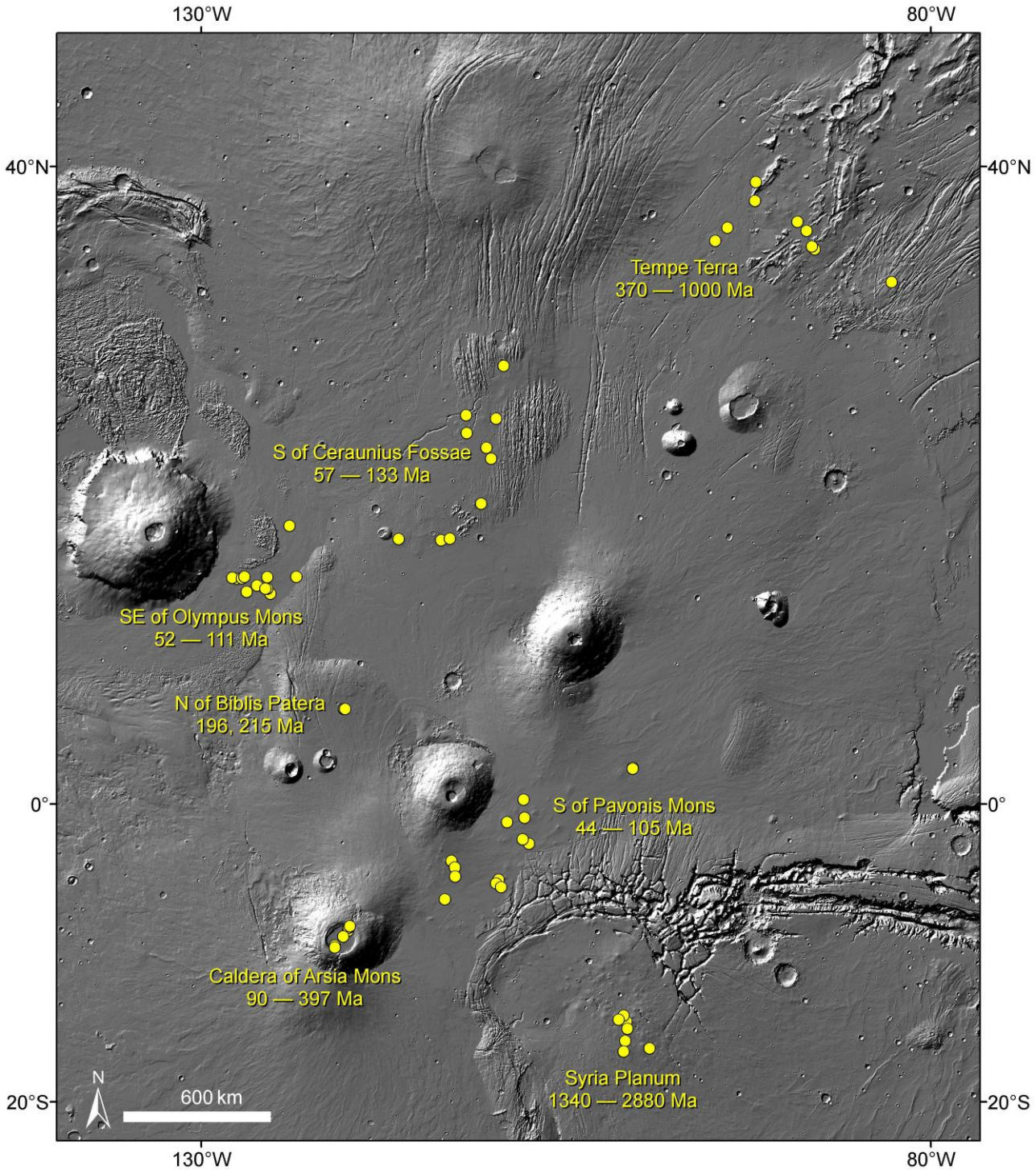

Figure 4.13: Locations of representative surface areas that were selected for age determination and mapping in the CTX images. Several low shield volcanoes in each shield cluster were dated by crater counts; total 61 individual low shield volcanoes were mapped. The absolute ages as determined by crater counting are indicated in yellow text, yellow spots indicate locations of investigated low shield volcanoes (Image: shaded relief from MOLA).

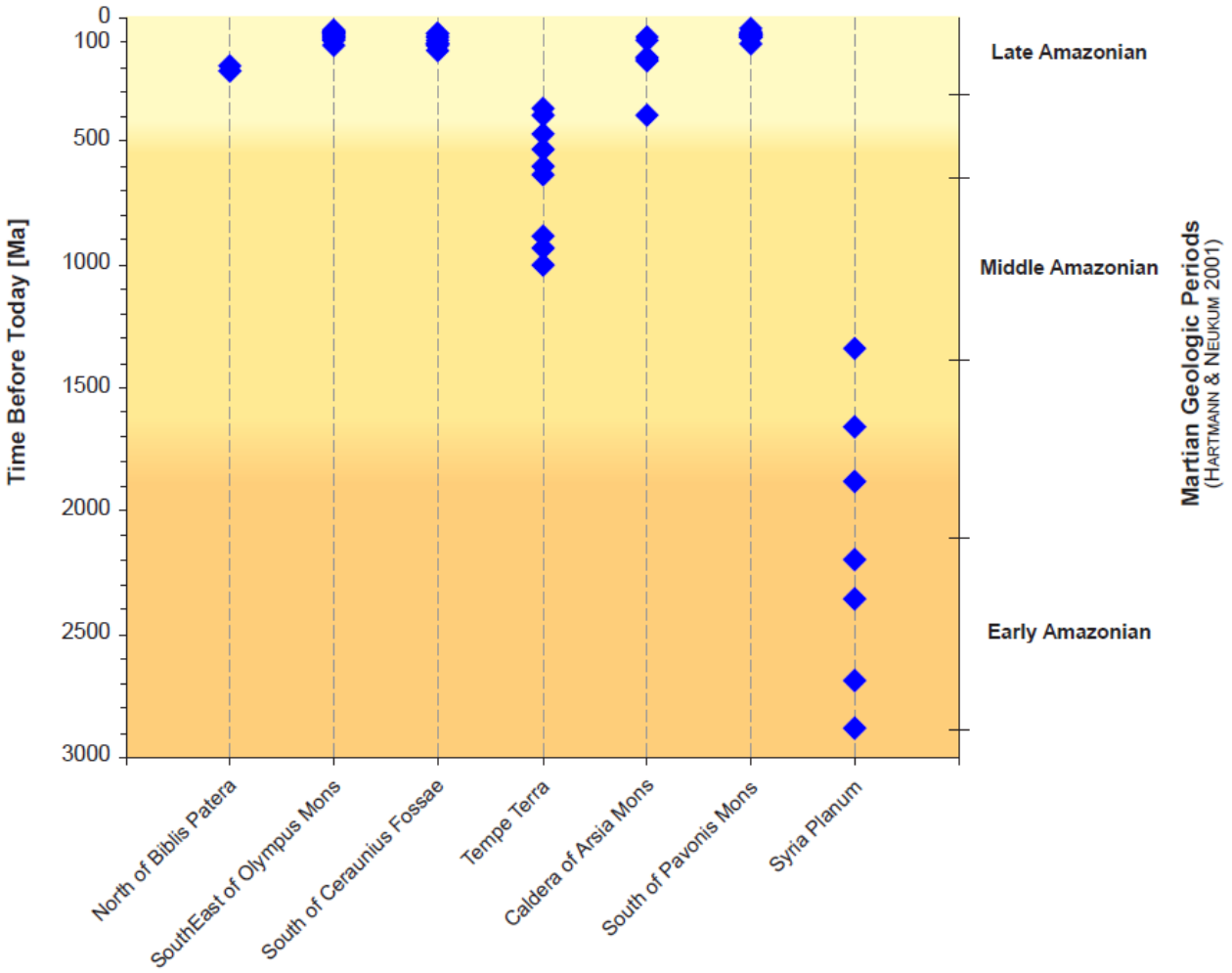

Figure 4.14: Graphical presentation of the CSFD analysis results from total 61 volcanoes selected in the *Tharsis region* of low shield ages. Relatively old ages of *Syria Planum* contrasts with younger ages for the rest of the investigated low shield volcanoes.

4.5. Discussion

Independent volcanoes in clusters have similar ages suggesting that they were probably formed during the same episode of volcanic activity with few exceptions like *Tempe Terra* and *Syria Planum*. These clusters show a large spread in volcano ages ranging on the timescale of billions of years. However, the rest of clusters revealed young volcanic activity of unknown source. Since the effusive products of younger volcanic phases could have buried the evidence for geological units and possibly older volcanic episodes. In other words, it is possible that the mapped clusters piled up on older volcanic products at long living volcanic centres. The fact that not even larger impact craters were preserved suggests that the areas mapped are covered by a thick sequence of lava flows.

There is no evidence for migration of volcanic activity locus throughout the history in the *Tharsis* region. Similarly, mechanism which would explain occurrence and distribution of low shield volcanoes through *Tharsis* remains also unknown. Previously used explanation of *Tharsis* origin concluded that its volcanism originated due to mantle plume below this region (Harder and Christensen, 1996). Hypothetically, a point source under a relatively homogenous crust could produce centrically symmetrical or radially distributed lava effusions on the surface. Radial occurrence of low shield volcanoes and increase of ages in specific directions like on Hawaii or Yellowstone (e.g. Tarduno and Cottrell, 1997 or Pierce and Morgan, 1992) was not confirmed by the present results. Distribution of low shield volcanoes in *Tharsis* is rather random. This is interpreted by partial melting in different domains of relatively thick crust under *Tharsis* and contribution of radioactive heat for magma production (Schumacher and Breuer, 2007).

Volcanic activity in clusters did not show any association with major shield volcanoes except for *Arsia Mons*. These low shield volcanoes might have been products of volcanic activity of *Arsia Mons* itself; another explanation is that the rising magma used only pre-existing supply channels and the low shield volcanoes formed later after the main eruptions of *Arsia Mons* finished. Other clusters are clearly spatially associated with local fractures and fault systems. These volcanoes display elongated fissures and central vents elongated parallel with the directions of the faulting systems (see Table 6.1 for more details).

Our observations also revealed that the low shield volcanoes were cut by younger faults in few cases. This suggests that the tectonic processes forming some of these fault systems in Martian crust were active less than a few tens of millions years ago.

Comparison of absolute ages obtained using the CSFD method and relative ages of adjacent volcanoes was carried out for a group of low shield volcanoes located south-east from *Olympus Mons*. In this region, effusive lava sheets of adjacent volcanoes overlap each other. However, for the case of three clustered volcanoes, this correlation was positive only partially (see Figure 4.15). Relation between two volcanoes established by relative stratigraphy was confirmed for the oldest and medium age volcano. For the pair of the youngest and the medium aged volcano the relative dating correlation was not confirmed by the CSFD method. This is explained by complex history of the medium aged volcano with at least one resurfacing event. Only partial resurfacing event on the volcano might have altered the correct CSFD age (see volcano No. 13 for more details about chronology curve). In summary, although this correlation was not completely confirmed, our goal was to establish primarily the average ages for each cluster rather than ages of individual volcanoes.

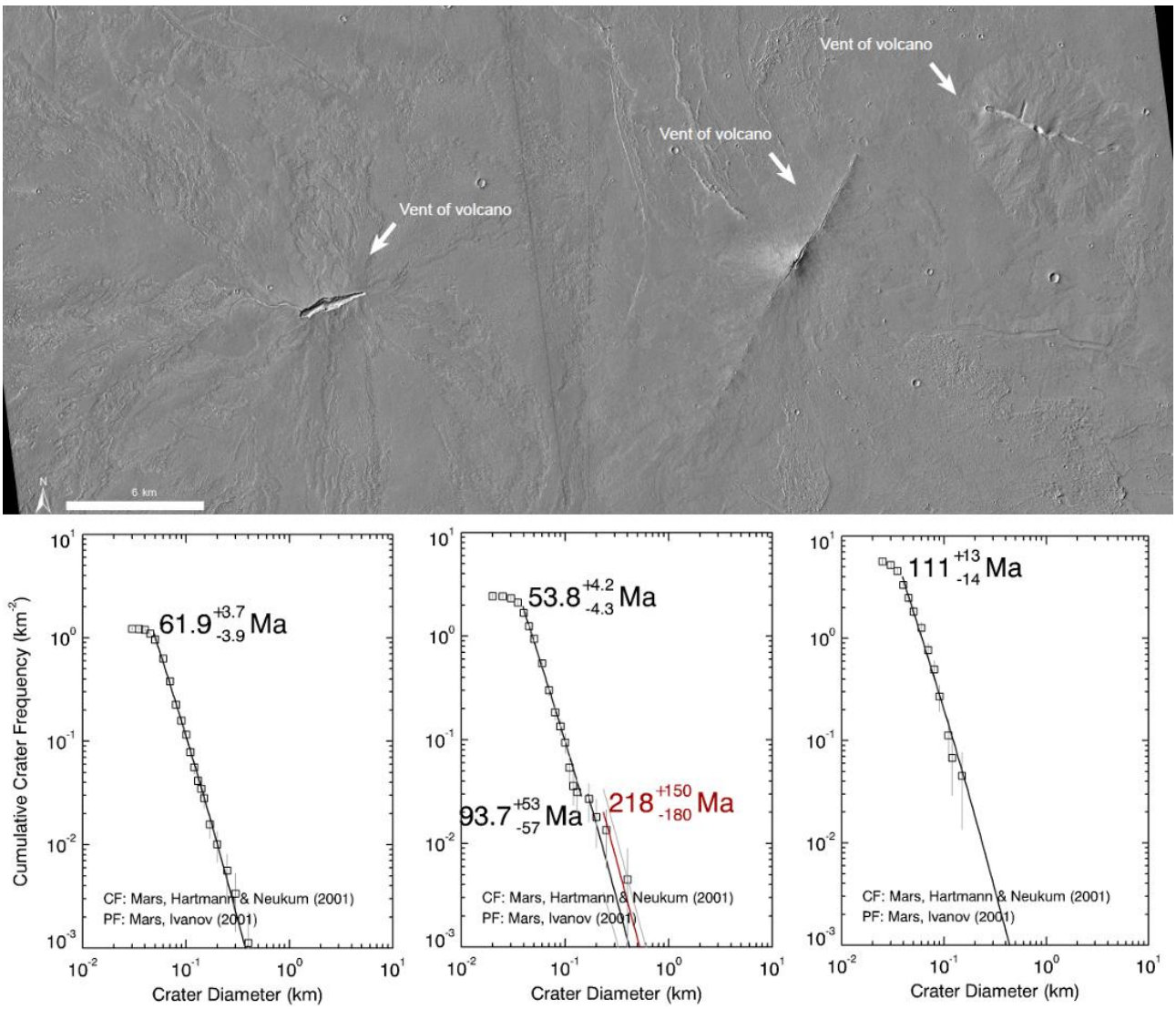

Figure 4.15: Volcanoes No 10, No. 13 and No. 14 (from left to right) located in region located south-easterly from *Olympus Mons*. An experiment based on CSFD absolute ages in comparison with relative stratigraphy. According to the relative stratigraphy, volcano No. 14 is the oldest; No. 13 is younger and is N. 10 is the youngest. Absolute ages do not confirm these age relationships, which is explained by complex effusive history and only partial resurfacing event around 93.7 Ma (mosaic of two CTX image, right one P22_009686_1954_XN_15N127W and left one P19_008473_1952_XI_15N127W, centered 15.3° N / 232.65° E).

4.6. Conclusions of geochronology for low shield volcanoes

We concluded that the volcanic activity forming low shield volcanoes was relatively recent on the long timescale of Martian geological history. Last episodic eruption forming low shield volcanoes occurred from 50 to 130 Ma except for few cases in *Tempe Terra* and *Syria Planum*, which are significantly older. Most of the volcanoes were formed in Late Amazonian, which is in agreement with previously published datings (e. g. Neukum et al., 2004; Werner, 2009 and references therein). We did not observe any development of ages in any direction which could suggest movement of volcanic centre connected with mantle plume migration;

this supports the partial melting scenario as suggested by Schumacher and Breuer (2007).

However, many questions remain unanswered. First, it is not clear whether the volcanic activity forming low shield volcanoes occurred by a single event or multiple events. Considering the limitations of the CSFD method, results of the present research are pertinent only to the youngest superficial layer. Age differences between individual clusters of low shield volcanoes are relatively small suggesting that they were emplaced during a single volcanic episode. Nevertheless, clusters like *Tempe Terra, Syria Planum* and caldera in *Arsia Mons* suggest relatively longer-lasting volcanic activity in the entire *Tharsis* region on the timescale of hundreds of millions or billions of years, respectively. These results suggest that volcanism in *Tharsis* is characterised by multiple-phase activity (see Figure 4.14).

The next question regards to possible volcanic activity on Mars. Is it volcanically inactive for good or is there only a temporary gap between two subsequent volcanic events? Answers to this question will remain speculative, unless we get more information of the processes in Martian crust and mantle. If volcanism occurs on Mars in the future, it will dramatically change our point of view on evolution of Martian atmosphere.

As a side result of our research, we have identified several landforms in *Tempe Terra* regions which we interpreted as products of glacial processes (see Figure 4.1).

5. Rheology

Previous works determined rheological properties of lava flows in few regions on Mars comprising the flanks of *Acreus Mons* (Hiesinger et al., 2007), *Central Elysium Planitia* (Voucher et al., 2009), *Jovis Tholus* (Wilson et al., 2009) etc. of the major aim of this part of the study was to estimate basic rheological properties of erupted lavas forming low shield volcanoes and surrounding plains. These properties can be obtained by morphometric analysis (e. g. Wilson and Head, 1983) using remotely sensed high-resolution data (see or e.g. Hauber et al., 2009 and references therein). Knowledge of the physical properties of the erupted magmas on Mars can extend our knowledge about eruption conditions and mechanisms. Low dip angle of low shield volcano flanks is explained by low viscosity of magmas erupted from vents, high eruption rates or high temperature (Hauber et al., 2009).

An important condition for the morphometric analysis is that the selected lava flow gravitated over an inclined surface (e. g. Baloga, 1987; Baloga et al., 1998; Bruno et al., 1996). Felix Jagert and Petr Brož applied morphometric analysis for rheological properties of 10 lava flows (designated by letters *a* to *f*) on

the basis of CTX images. One part of these flows started in central vents of low shield volcanoes and gravitated on their flanks (see for example Figure 5.1), second part originated on the surrounding plains and were spatially associated with fissures forming plain-style volcanism areas. The morphometric analysis enabled estimation of yield strength, plastic viscosity and effusion rates of the lavas together with volume of each lava flow or respective low shield volcano. Finally, we made comparison of our results with other Martian lavas and effusive products on surfaces of Moon, Earth and Venus.

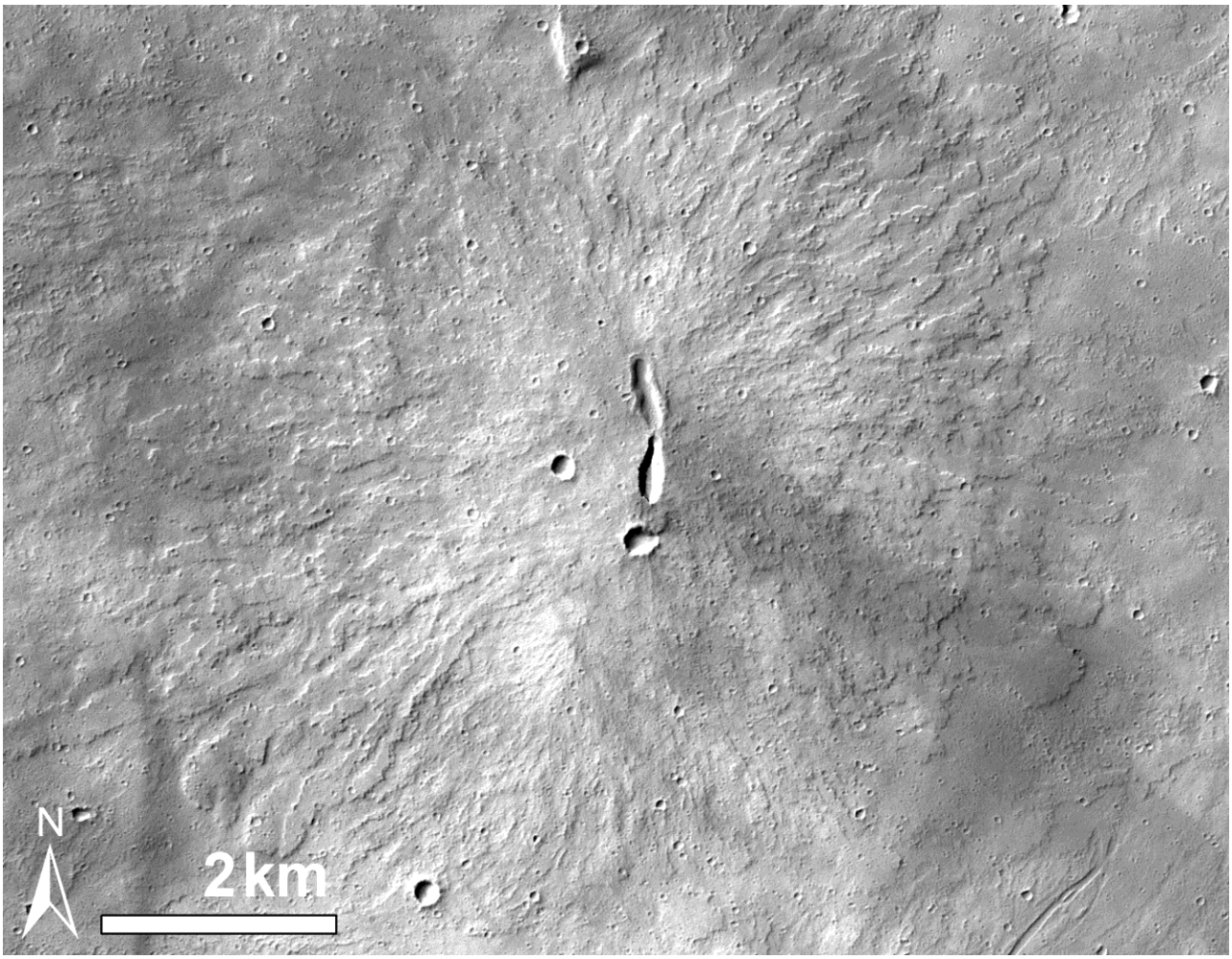

Figure 5.1: Example of low shield volcano with well recognisable overlapping lava flows forming the main body of the cone at caldera of *Arsia Mons* (N. 38). Summit craters are formed by elongated vents (CTX image P21_009343_1702_XN_09S120W, centered 9.77° S / 239.18° E).

5.1. Approach and Technique

For estimation of physical properties of selected lava flows, we used the same basic assumptions as

described in more detail by Hiesinger et al. (2007). The **yield strength** τ of lava flows (Pa), described as the stress at which material begins to deform plastically, **plastic viscosity** η of lava (Pa.s) described as the resistance of material to the shear stress and finally **effusion rate** (m^3/s) are calculated using the following equations (presented by Hiesinger et al. (2007) and references therein).

$$\text{Yield strength (Pa)}$$

$$\tau = h \cdot \rho \cdot g \cdot \sin\alpha \qquad \text{Equation 5.1.1}$$

$$\tau = \rho \cdot g \cdot \frac{h^2}{w} \qquad \text{Equation 5.1.2}$$

$$\text{Effusion rates } (m^3/s)$$

$$Q = Gz \cdot \kappa \cdot x \cdot \frac{w}{h} \qquad \text{Equation 5.1.3}$$

$$\text{Plastic viscosity (Pa.s)}$$

$$\eta = \frac{\rho \cdot h^4 \cdot g}{Q} \qquad \text{Equation 5.1.4}$$

$$\eta = \frac{\rho \cdot g \cdot h^3 \cdot w \cdot \sin\alpha}{n \cdot Q} \qquad \text{Equation 5.1.5}$$

where **h** is the flow height (m), **x** is flow length (m), **w** is the flow width (m), **ρ** is the density ($kg.m^{-3}$), **g** is the gravitational acceleration ($m.s^{-2}$), **α** is angle of slope (degrees), **Gz** is experimental Graetz number (dimensionless), **κ** is the thermal diffusivity (m^2s^{-1}) and **n** is a constant describing shape of a lava flow (Hiesinger et al., 2007).

For both equations 5.1.4 and 5.1.5, it is assumed that the lava flow behaves as a Newtonian fluid, and therefore represent a simplified description, since it is Binghamian rheology is expected for the lava flows (Hiesinger et al., 2007). To establish yield strength we have selected equations 5.1.1 and 5.1.2. presented by

Moore et al., (1978).

It should be mentioned that the absolute values of yield strength and plastic viscosities calculated from these equations are affected by large uncertainties (Sakimoto and Gregg, 2001). Nevertheless, it is quite attractive to compare these with other works from other Martian provinces (Vaucher et al., 2009) and other places in solar system including terrestrial basalts for further speculations about lava properties and their emplacement conditions in different environments on terrestrial planets. These information may be also useful in the future research aimed to determine the quantity of volatiles released from erupted lava for given the bulk volumes of the lava flows and low shield volcanoes in the plain-style volcanic regions.

Using images of flows processed in ArcGIS, we were able to approximately determine the volume of lava forming the flows. For this purpose, we used the whole surface area which was covered by the lava forming single flow and average thicknesses from MOLA PEDR measurements. An important prerequisite for the analysis is that the lava gravitated over a smooth flat topology. This condition was fulfilled, since the selected lava erupted on relatively flat areas without any signs of depressions or bigger humps which might dramatically change the results.

5.2. Lava flows' lengths, widths and thicknesses

Estimation of rheological properties of extrusive lavas from morphometrical measurements is based on the following dimensional characteristics: lava flow length (**x**), width (**w**) and thickness (**h**).

Dimensions of selected lava flows were measured from CTX images in ArcGIS 9.2 interface with pre-instaled tools. Length of each flow was measured by a polygon line connecting centers of several traverse transects across the lava body (Figure 5.2). Lava width represents the average length from all traverse transects (Hiesinger et al., 2007; Vaucher et al., 2009). The resulting average length of lava flows from the morphometric analysis is ~24.44 km, with minimum of ~16 and maximum of ~52.2 km. Lava flow width ranged from ~200 to ~8700 m with average of ~1760 m.

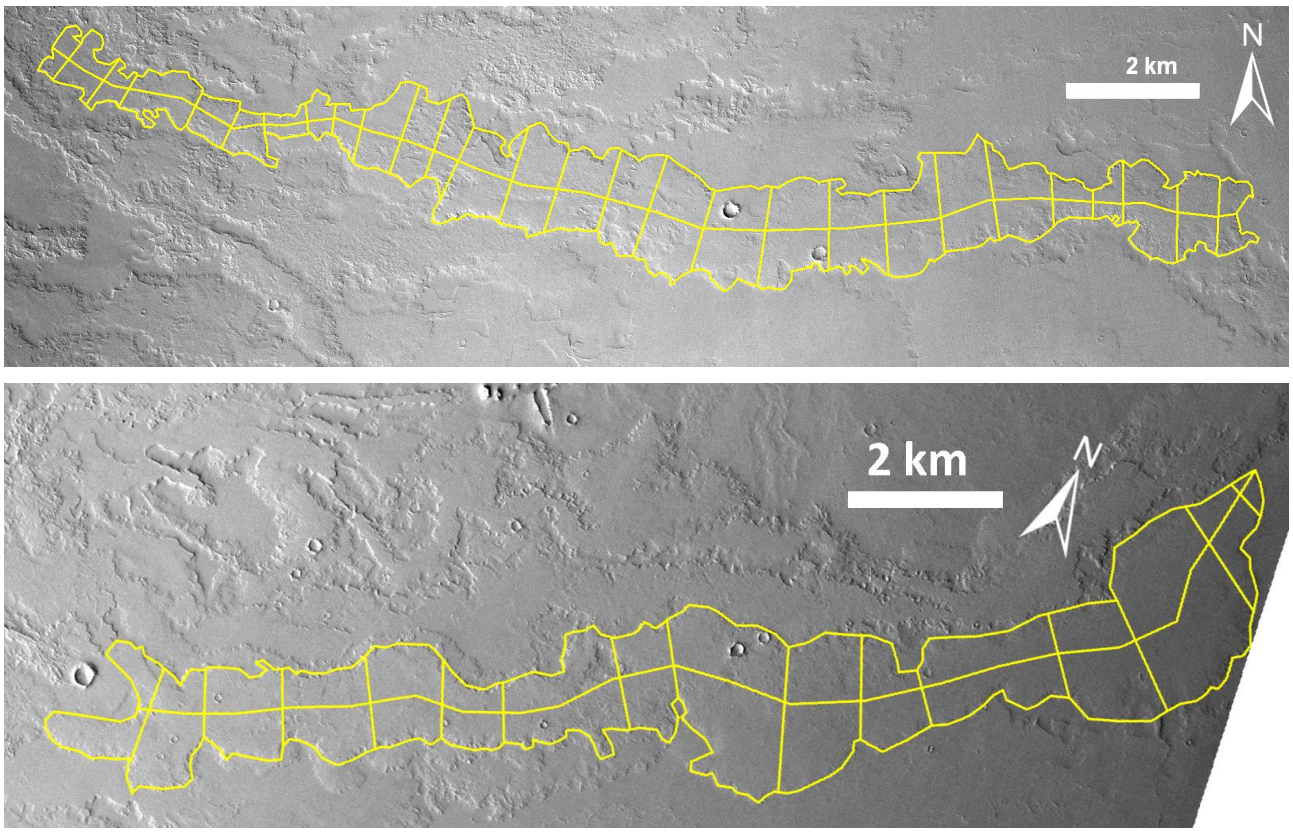

Figure 5.2: Two examples of investigated lava flows *e* (upper) and *f* (downer).

Earlier measurements of lava flow thicknesses were rather inaccurate, because these utilized stereo or photoclinometric techniques (Glaze, 2003). We attempted to employ several techniques to obtain the best results. The methods used comprise the De Hon method (1974), resurfacing-events (Neukum and Horn, 1975; Hiesinger and Head, 2002), single MOLA profiles (Glaze, 2003) and theoretically shadow measurement (Arthur, 1974). At first, we decided to use the shadow measurement method, which is a widely used technique in planetology. Calculation of lava flow thickness is based on lenght of a shadow, which it casts, on the position of the flying probe that collected the image, position of Sun and the latitude. After first preliminary analysis of the CTX images we found out that this method is inappropriate for lava flows in the selected areas because they are only several meters thick and observed shadows were only few pixels long, implying high degree of inaccuracy for possible shadow measurement technique given 6 m/pixel CTX image resolution.

5.2.1. De Hon method (1974)

The second method employed for lava flow thickness measurements was the De Hon method (De Hon, 1974), which was developed by De Hon in 1974 for volcanic lunar maria[4] and does not require any topographic data. This method is based on morphometric analysis of impact craters that were engulfed by lava flow sheets that flooded even the interior of the crater. The estimation of thickness of the lava flow accounts from the diameters and rim heights (h) of the partially burried crater, because there is direct relationship between the rim height and central crater depth (see Figure 5.3). The difference between the exposed rim height and the original rim height then corresponds to the thickness of the lava flow around crater. The De Hon technique is based on empirical formulas which were calculated for different sizes of impact craters (De Hon, 1979). The disadvantage of this method is that the calculated values represent the maximum values for the lava thicknesses. In the case of overlapping flows, the calculation will correspond to the thickness of the whole pile of lava flows, or its part.

$$h = 0.036\ D^{1.014} \text{ for craters} < 15 \text{ km}$$

$$h = 0.399\ D^{0.236} \text{ for craters} > 15 \text{ km}$$

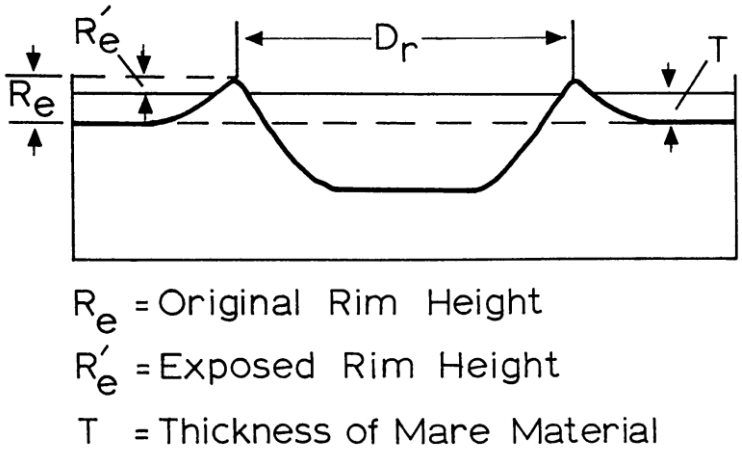

Figure 5.3: Diagram depicting major morphometric parameters of impact craters engulfed by a lava flow used for estimation of lava flow thickness (De Hon, 1974).

Unfortunately, not even this method is suitable for inspection of areas selected for our study due to several reasons. First, the empiric formulas for crater rim height were derived only for relatively big craters. However, since lava flows covered only limited areas in the selected regions and we did not find any crater of suitable size engulfed by a lava flow. Second, it is very difficult to identify the partly flooded impact craters even with the high resolution CTX images. The third reason forbidding application of De Hon's method is that the estimation of exposed rim height again requires shadow length measurement. As already discussed above, this proved as an unsuitable technique due to the low image resolution and relatively short

shadows. Although craters almost completely filled with lava could offer direct evidence for lava flow thicknesses, such craters were not observed in the investigated areas.

5.2.2. Resurfacing-events

Morphometric analysis of Neukum and Horn (1975), improved by Hiesinger and Head (2002) is kind of extension De Hon method. It is based on analysis of CSFD data, which reflect the maximum diameters of craters completely buried by younger lava flows. This crater diameter is indicated by a "kink" on the impact crater production function curve, corresponding to the resurfacing event. Given the maximum crater dimensions buried by lava flows, it is then easy to indirectly estimate the lava flow thickness of the resurfaced area.

The method was tested on investigated lava flows. The results were unsuccessful, because the CSFD in the selected area didn't show any clear signs of the resurfacing events possibly due to the small extent of selected area.

5.2.3. MOLA - *Mars Orbiter Laser Altimeter*

The most precise method for measurements of the lava flow thickness is achieved by Mars Orbiter Laser Altimeter (MOLA) as described by Glaze (2003). In contrast to previous methods described above, which are based on indirect estimates, this method offers direct and precise surface height measurements from satellite-borne technical equipment.

Topographic data used for measurement of lava flow thicknesses in this study were taken by MOLA onboard of *Mars Global Surveyor* orbiting Mars from 1997 to 2006. MOLA was taking spot measurements of elevations by a laser beam of the pulse repetition rate of 10 Hz reflected from the planet surface along the ground track of the spacecraft orbiting the planet along the polar orbit. It made over 670 million measurements and generated nearly 9,500 orbital profiles from September 1999 to June 2001 (Som, 2008). The diameter of laser beam had around 75 meters (Smith et al**.,** 1999) when it reached the Martian surface. The spaces between each two measured spots were about 300 meters in the north-south direction (Smith et al., 2001). The spacing in the west-east direction depended on the actual latitude; it was smallest in the polar regions and in the order of several kilometres near the equatorial areas. Where the beam reached a flat surface (slope <2°), the vertical accuracy was ~1 m (Smith et al., 2001).

[4] Lunar maria are dark volcanic plains on Moon formed by basaltic lava.

Glaze (2003) successfully used single MOLA tracks from ***P**recision **E**xperiment **D**ata **R**ecords* (PEDRs) to determine the longitudinal thickness profile of each individual lava flow. This technique benefits from the gridded topography derived from MOLA and provides precise elevation transects across the MOLA tracks and offers higher resolution than DEM. Lava flows and low shield volcanoes are morphologically indistinct, their identification on the background of the plains is difficult. The reason is, that the coverage by MOLA measurements never included the whole Martian surface because of the spacing between two measurements especially in equatorial areas. For this reason DEM model was generally interpolated from these tracks with distortions because of gaps between tracks. However, it is not possible to find out the position of these tracks in DEM model and sizes of these gaps. Second issue is that the gridded DEM model is a uniform grid without precise information about the exact topographical values. It is useful for large objects, but useless for small.

MOLA PEDR profiles have a vertical precision of 37.5 cm (Garvin et al., 2000b) which is satisfactory for determination of height profiles across the low lava flows. The profiles reveal sharp morphology of lava flows in individual transects (Glaze, 2003). Due to the location of our investigated lava flows near the equator, single measurements were sometimes used to refine the thicknesses. As already mentioned, the MOLA tracks in equatorial area were sometimes spaced at distances of few kilometers, therefore we selected lava flows oriented in north-south direction and transected by the MOLA PEDR profiles. The north-south orientation of the profiles was required for slope angle calculation for the respective lava flows. The measurement(s) from PEDR profiles indicated that the background slope (not the lava flow slope) in the investigated region was less than 1°.

Fitting of MOLA PEDR profiles with the CTX images (Figure 5.4) enabled precise localization and precise thickness measurement for each lava flow. Thickness of the lava flow was measured from several points along the profile, because the lava flow thickness can show irregularities, which are not related to the primary emplacement event (erosion, impact craters etc.) (Glaze, 2003). Arithmetic mean of the measured values was then recorded. This method also provided the basement inclination upon which the lava flow streamed downslope. This parameter is also required for calculations of yield strength and plastic viscosity for the investigated lava flow. MOLA gridded topography data were not sufficient for slope measurements due to low resolution of 28 pixel per degree.

Average slopes of the lava flows generated by low shield volcanoes range between 0.16 to 0.23°, which is typical for low shield volcanoes in plain-style volcanic regions (see Table 6.1 or Hauber et al., 2009). Measured thicknesses for the set of selected lava flows ranges between 3.5 and 7.5 meters, which is much less than expected and previously established for Martian flows (e. g. Hiesinger et al., 2007 or Vaucher et

al., 2009), but is in agreement with values for equivalent terrestrial lava flows. On the other hand, given the limited dataset for only 10 lava flows, these results should be regarded as preliminary.

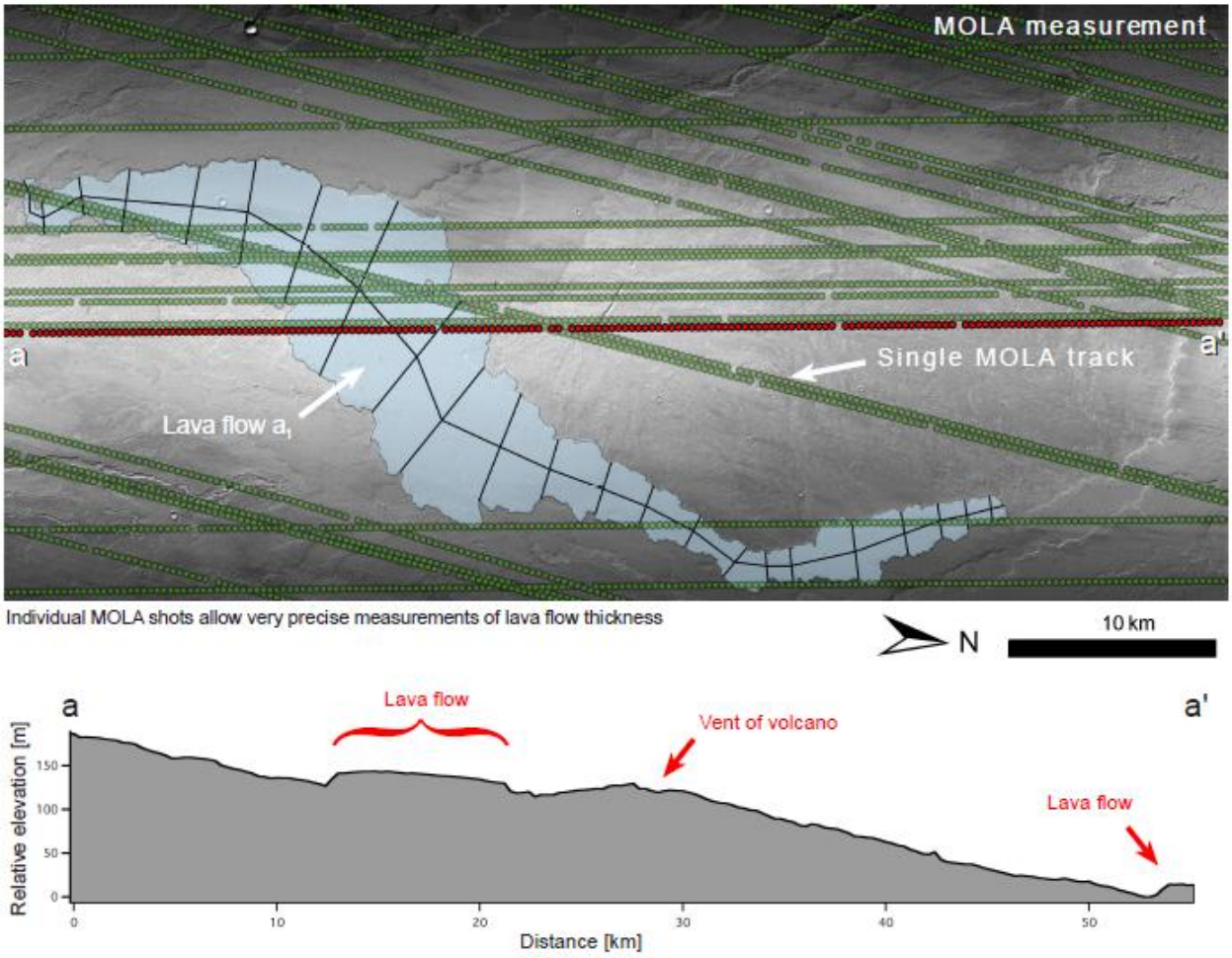

Figure 5.4: a) Several PEDR MOLA profiles superposed on the CTX image and transecting an area with few lava flows and a low shield volcano (No. 9) east from Olympus Mons (image centred -123.82°E 18.64°N). One of the investigated lava flows a_1 is traced by light blue polygon; the black line transects corresponded to measured length and width of the flow. Red dots mark the PEDR track used for the a-a' profile depicted in b). b) Elevation of MOLA PEDR profile across the CTX image without vertical exagartation, same scale as for the CTX image. The lava flows and top of shield volcano No. 9 are marked with arrows.

5.2.4. Rock Densities

Physical properties of Martian rocks are unfortunately poorly established due to the lack of Martian rock samples. Estimates of the porosities of Martian volcanic rocks range from 25 to 75% (Wilson and Head, 1994), suggested density variation ranges between 725 and 2,960 $kg.m^{-3}$ (Wilson and Head, 1994; Longhi, 1990). SNC meteorites[5], which were most probably derived from Mars and landed on Earth are characterized by densities of 2,750 to 2,960 $kg.m^{-3}$ (Longhi, 1990). These values are close to densities of

2,500 kg.m^{-3} (e.g. Hiesinger et al., 2007) and 2,800 kg.m^{-3} (e.g. Vaucher et al., 2009) for Martian lavas considered in different studies. We decided to use both of the latter values for our calculations to consider effect of density on the final results. Values of densities are fundamental for calculation of both yield strength and plastic viscosity. In contrast, the effusion rates do not depend on density. Hiesinger (2007) demonstrated that for example ±50% error in density will produce same error for calculated density value (e.g., the ±50% error changes densities from 1,250 to 3,750 kg.m^{-3}).

5.2.5. Thermophysical parameters

Thermophysical parameters (Graetz number and thermal diffusivity), present in the equation 5.1.3 and later via Q in equations 5.1.4 and 5.1.5, control primarily the plastic viscosity. The first is the experimental dimensionless Graetz number relating the rate of heat loss from a flow to the rate of heat advection within a flow along its length (e.g. Gregg and Fink, 1996) and reflects the effect of heat loss on lava flow diffluence. It was observed that basaltic lavas on Earth flow for the empiricaly derived Graetz number reaching a value of 300 (Pinkerton and Sparks, 1976). However, considering different physical conditions on Mars related to Earth (thinner atmosphere, cooler surface or different compositions lava) the correct values of the Graetz number for Martian conditions are rather speculative (Vaucher et al.; 2009). In spite of this uncertainty, we use the value of 300 for the Graetz number (Pinkerton and Sparks, 1976) in the present study. For thermal diffusivity value of 3×10^{-7} m^{2}s^{-1} is used corresponding to the andesitic rocks like average value of possible thermal diffusivity (e.g. Vaucher et al., 2009; Hiesinger et al., 2007).

5.2.6. Other parameters

Gravitational acceleration on Mars measured by space probes is 3.71 m.s^{-2}. The next parameter in Jeffrey´s equation (equation 5.1.5) is a constant n which reflects lava flow shapes, with 3 being used for relatively broad flows and 4 for narrow flows (Hiesinger et al., 2007). Slopes were measured using the MOLA PEDR profile.

[5] General term used for family of Martian meteorites founded on Earth; shergottites, nakhlites, and chassignites.

5.3. Discussion of errors in the analysis

Remote sensing data allow investigating lava flows without the *in situ* observation, however, it should be kept in mind that there are several problems which alter the results. First of all, the used equations (5.1.1, 5.1.2, 5.1.3, 5.1.4 and 5.1.5) represent only very simplified description of the complex fluid mechanics of lava extrusion. A major assumption in this description is that these lava flows represent emplacement of lava flows along an inclined flat surface without barriers deviating the flow direction. The equations are also valid only for *aa* lavas (Vaucher et al., 2009). Loss of heat after eruption via conduction, radiation and convection to the surrounding environments induces viscosity decrease by crystallization and increased bonding strength between molecules forming the melt. On the other hand, insulating crust covering the top of a lava flow decreases heat loss of a flow (Witter and Harris, 2007) and promotes lateral diffluence of the basaltic flow on long distances. It could cause more effective transport of lava to longer distance and change observed flows' rheological dimension (Vaucher et al., 2009). Temperature, chemical composition, SiO_2 and volatile content significantly control lava viscosity (Dingwell et al., 1996, Potuzak et al., 2004, Hauber et al., 2009 and references therein). In general, regarding the temperature effect, we can expect that the viscosity of lava at the source (circular or fissure vent) should be lower than the viscosity near the forehead of a lava flow. Considering the yield strength of the lava, it can represent both the internal yield strength and/or the strength of the growing crust enveloping the lava (Lyman et al., 2005).

The calculated physical properties correspond to the two chosen values of densities (2,500 and 2,800 $kg.m^{-3}$ respectively). Arithmetic mean for yield strength and for viscosity is calculated for the respective equations (5.1.1, 5.1.2 and 5.1.4, 5.1.5 respectively) in attempt to minimize errors by using more equations with different input parameters in equations, namely the slope angle in the case of equations 5.1.1 and 5.1.5. To test the degree of error in the final calculations, Hiesinger et al., (2007) chose artificial deviations of ±10, ±30, and ±50% from all the input parameters. He found out, that the error for yield strength can vary between +225% to -175% for yield strength and between +390 to -240% for viscosities.

Given the high resolution around 6 meters per pixel (the lengths of investigated flows range between 16 to 52 km and widths between 930 to ~4500 m) for CTX images and vertical precision of 37.5 cm with MOLA PEDRs, the errors in the calculations are probably much smaller than those suggested by Hiesinger et al., (2007).

5.4. Results

In this part of study we observed and measured 10 lava flows to determine composition of low shield volcanoes and surrounding plains developed during a plain-style volcanic event in *Tempe Terra*, *Ceraunius Fossae*, near *Pavonis Mons* and south-east from *Olympus Mons*. The morphometric analysis was not successful for the two selected lava flows. In one case, the boundary of the flow could not be reliably established (in *Tempe Terra*); second flow was affected by significant morphological irregularities possibly suggesting deformation after emplacement or significant selective erosion (south-east from *Olympus Mons*). For this reason calculated parameters are presented only for 8 lava flows (see Table 5.1). Two flows (a_1 and a_2) were derived from a fissure vent associated with plain-style volcanism south-east from *Olympus Mons*, four flows (*b*, *c*, d_1 and d_2) are products of a low shield volcano near *Ceraunius Fossae* and two flows (*e* and *f*) were erupted from a low shield volcano near *Pavonis Mons*.

ID	Flow Lenght (m)	Area (km^2)	Flow Width (m)	Flow Height (m)	Slope (°)	Volume (km^3)	Yield strength a (Pa)	Yield strength b (Pa)	Ave. Yield Strength (Pa)	Effusion Rate (m^3/s)	Viscosity 1 (Pa.s)	Viscosity 2 (Pa.s)	Ave. Viscosity (Pa.s)
a_1	52194	196.03	3098	5.96	0.20	1.17	1.98E+02	1.07E+02	1.52E+02	2.44E+03	4.82E+03	2.23E+03	3.52E+03
a_2	24645	107.54	4442	7.36	0.17	0.79	2.01E+02	1.14E+02	1.57E+02	1.34E+03	2.04E+04	9.03E+03	1.47E+04
b	24593	27.97	931	5.18	0.18	0.14	1.49E+02	2.69E+02	2.09E+02	3.98E+02	1.69E+04	3.11E+03	9.99E+03
c	18332	24.10	1211	6.09	0.20	0.15	1.93E+02	2.86E+02	2.39E+02	3.28E+02	3.91E+04	8.83E+03	2.40E+04
d_1	22311	-	1125	4.77	0.16	-	1.27E+02	1.88E+02	1.58E+02	4.74E+02	1.02E+04	2.28E+03	6.24E+03
d_2	18814	-	1142	5.60	0.20	-	1.81E+02	2.56E+02	2.19E+02	3.45E+02	2.65E+04	6.26E+03	1.64E+04
e	18598	20.36	1019	3.96	0.22	0.08	1.42E+02	1.43E+02	1.43E+02	4.31E+02	5.32E+03	1.75E+03	3.54E+03
f	16029	21.38	1139	3.54	0.23	0.08	1.34E+02	1.03E+02	1.18E+02	4.64E+02	3.15E+03	1.37E+03	2.26E+03

for density 2,500 $kg.m^3$

ID	Flow Lenght (m)	Area (km^2)	Flow Width (m)	Flow Height (m)	Slope (°)	Volume (km^3)	Yield strength a (Pa)	Yield strength b (Pa)	Ave. Yield Strength (Pa)	Effusion Rate (m^3/s)	Viscosity 1 (Pa.s)	Viscosity 2 (Pa.s)	Ave. Viscosity (Pa.s)
a_1	52194	196.03	3098	5.96	0.20	1.17	2.21E+02	1.20E+02	1.71E+02	2.44E+03	5.39E+03	2.50E+03	3.94E+03
a_2	24645	107.54	4442	7.36	0.17	0.79	2.25E+02	1.27E+02	1.76E+02	1.34E+03	2.29E+04	1.01E+04	1.65E+04
b	24593	27.97	931	5.18	0.18	0.14	1.66E+02	3.01E+02	2.34E+02	3.98E+02	1.89E+04	3.48E+03	1.12E+04
c	18332	24.10	1211	6.09	0.20	0.15	2.17E+02	3.20E+02	2.68E+02	3.28E+02	4.38E+04	9.89E+03	2.68E+04
d_1	22311	-	1125	4.77	0.16	-	1.42E+02	2.11E+02	1.77E+02	4.74E+02	1.14E+04	2.56E+03	6.98E+03
d_2	18814	-	1142	5.60	0.20	-	2.03E+02	2.87E+02	2.45E+02	3.45E+02	2.97E+04	7.02E+03	1.84E+04
e	18598	20.36	1019	3.96	0.22	0.08	1.59E+02	1.61E+02	1.60E+02	4.31E+02	5.96E+03	1.96E+03	3.96E+03
f	16029	21.38	1139	3.54	0.23	0.08	1.50E+02	1.15E+02	1.32E+02	4.64E+02	3.53E+03	1.54E+03	2.53E+03

for density 2,800 $kg.m^3$

Table 5.1: Results of lava flows measurements.

The lengths of investigated flows range between 16 and 52 km and widths between 930 to ~4500 m. Similarly to low shield volcanoes, lava flows have very low slopes, typically less than 0.5°, ranging between 0.16 to 0.23 with height of 3.5 to 7.5 meters. Volumes of the flows range from 0.08 to 1.17 km^3. It is clear that lava flows forming low shield volcanoes have significantly smaller volumes (from 0.08 to 0.14 km^3) than the flows associated with plain style volcanism (from 0.79 to 1.17 km^3).

Calculated yield strength, depending on the used equation, from 1.07×10^2 to 2.56×10^2 Pa, if we

average the yield strengths derived from equations 5.1.1 and 5.1.2, we obtained minimal value 1.18×10^2 and maximal 2.39×10^2 Pa for density 2,500 kg.m^{-3} and 1.15×10^2 to 3.2×10^2 Pa with average values 1.32×10^2 and 2.68×10^2 Pa for density of 2,800 kg.m^{-3}. These results are for example by two orders smaller than those calculated by Hiesinger et al. (2007) on the eastern flank of *Ascraeus Mons*, but are in the same range as presented by Vaucher et al. (2009) or Wilson's (2009) and they are in the same range as devised for terrestrial basaltic rocks from Hawaiian shields (Moore, 1987 and Shaw et al., 1968).

Name	Object	Yield strength (Pa)	Effusion Rate (m^3/s)	Viscosity (Pa.s)	Source	Note
Makaopuhi, Hawaii	Earth	1.0E+02	-	-	Shaw et al. (1968)	
Mauna Loa, Hawaii	Earth	3.5E+02 - 7.2E+03	4.17E+02 – 5.56E+02	1.4E+02 - 5.6E+06	Moore (1987)	
Mare Imbrium	Moon	2.0E+02	-	-	Booth and Self (1973)	
Mairan Domes	Moon	5.3E+04 – 13.1E+04	48.0 – 51.5	1.3 – 11.5E+08	Wilson and Head (2003)	
Artemis Festoon Lobe 1	Venus	4.12E+04	1.02E+04	7.12E+06	McColley and Head (2004)	
Atalanta Festoon	Venus	1.22E+05	9.52E+02	2.34E+09	McColley and Head (2004)	
Arsia Mons	Mars	0.39E+03 – 3.1E+03	5.6E+03 – 4.3E+04	9.7E+05	Warner and Gregg (2003)	
Olympus Mons	Mars	8.8E+03 – 4.5E+04	-	2.3E+05 – 6.9E+06	Hulme (1976)	
Flows near Ascraeus Mons	Mars	2.0E+02 – 1.3E+05	23 – 4.04E+02	1.8E+04 – 4.2E+07	Hiesinger et al., 2007	density 2500 kg/m^3
Large flows at Central Elysium Planitia	Mars	1.0E+02 – 5.0E+05	-	2.5E+05	Vaucher et al. (2009)	density 2800 kg/m^3
Small flows at Central Elysium Planitia	Mars	<2.0E+02	-	>1.0E+03	Vaucher et al. (2009)	density 2800 kg/m^3
Flows east from Jovis Tholus	Mars	1.00E+02	5.00E+03	1.00E+02	Wilson (2009)	density 2500 kg/m^3
a_1	Mars	1.52E+02	2.44E+03	3.52E+03	-	density 2500 kg/m^3
a_1	Mars	1.71E+02	2.44E+03	3.94E+03	-	density 2800 kg/m^3
e	Mars	1.43E+02	4.31E+02	3.54E+03	-	density 2500 kg/m^3
e	Mars	1.60E+02	4.31E+02	3.96E+03	-	density 2800 kg/m^3

Table 5.2: Comparison of investigated flow a1 and e with other results from Earth, Moon, Venus and Mars.

Effusion rates of investigated flows calculated from Equation 5.1.3, range from 3.28×10^2 to 2.48×10^3 ms^{-3}. These results are one or two orders higher than effusion rates established for flows near *Acreaus Mons* (Hiesinger et al., 2007), but still in the range of terrestrial volcanoes and some other volcanic provinces on Mars like lava flows east from *Jovis Tholus* (Wilson, 2009).

Using Jeffrey´s equation (Equation 5.1.5) and method using relationship between effusion rate, thickness and density (Equation 5.1.4), we estimated the average values of viscosities as an arithmetic mean from these two results. For the lower value of density (2,500 kg.m^{-3}), we obtained viscosities ranging from 1.37×10^3 to 3.91×10^4 Pa.s with average viscosities from equations 5.1.4 and 5.1.4 of 2.26×10^3 and 2.40×10^4 Pa.s and for higher density from 1.54×10^3 to 4.38×10^4 Pa.s with average values of 2.53×10^3 and $2.68 \times$

10^4 Pa.s. These values are significantly smaller than viscosities of volcanic rocks calculated for *Mare Imbrium* on Moon and volcanic regions on Venus and also smaller than large shields on Mars like *Olympus Mons* or *Arsia Mons* (Table 5.2). However, calculated values in the present study are in agreement with similar small lava flows near *Elysium Planitia* and also with viscosities known from terrestrial shield volcano *Mauna Loa* on Hawaii. This comparison suggests a good agreement with previous studies elaborating properties of basalts.

5.5. Discussion

Our results show relatively low values of yield strength and viscosity in all cases of investigated flows that are within the range of previously observed small lava flows in other areas on Mars and also at *Central Elysium Planitia*. Respective values are however two orders of magnitude smaller than yield strength and three to four orders of magnitude smaller than viscosities measured on the flanks of giant shield volcanoes like *Olympus Mons* or *Arsia Mons*. This discrepancy indicates that low shield volcanoes and plain-style volcanism are associated with less viscous magmas then that forming the huge shields.

Hauber et al. (2009), Hiesinger et al. (2007), Vaucher et al. (2009), Wilson et al., (2009) and others summarized possible explanations of low viscosities of erupted lava as following:

a) Low viscosity is caused by low silica content in melt which in the case of basaltic magmas is less than 45% for ultrabasic, and from 45 to 52% for basic composition.
b) Relatively high temperature of erupting lava.
c) High effusion rates.
d) Low crystal content in the erupted lavas.
e) Presence of significant amount of dissolved volatiles in melt (e.g. water).
f) Combination of those factors.

Unfortunately the relative contribution of the above stated factors can not be determined only from the morphometric measurements. Due to young observed ages of low shield volcanoes and investigated lava flows, it is surprising that melting occurred relatively recently and released enough heat to produce low viscosity magmas widely spread throughout *Tharsis* and *Elysium* regions. Schumacher and Breuer (2007) explained that the lower thermal conductivity of thicker crust and heat release provided by radioactive element in the crust made an insulating layer leading to increase of temperature in some areas of the upper mantle. This process may theoretically lead partial melting in large depths in recent Martian mantle producing hot melt than the melt produced in relatively shallower parts. Fast transport of superheated crystal-poor magma may finally cause volcanic activity of plain-style volcanic regions like in *Tharsis*.

However, this explanation was later partly rejected by other authors (see Vaucher et al., 2009 and references therein) for example due to relatively thin crust in the *Central Elysium Planitia* (Wieczorek and Zuber, 2004). Wilson et al. (2009) argued that low viscosity observed around *Jovis Tholus* may suggest that these lavas likely represent primitive mantle melts erupted from greater depths than the magmatic products of shallow crustal sources.

Another theory (Richet et al., 1996; Dingwell et al., 1996) explaining the low viscosity of low-shield volcano forming magmas is the high content of dissolved water and/or dramatic depression of the liquidus temperature (Vaucher et al., 2009). Ascent of water-rich magmas would be accompanied by outgassing (release of volatiles) following the critical bubble nucleation at depth of several hundred meters to few kilometres in the Martian crust (Wilson and Head, 1994). It is however possible that the released water vapour never reached the surface due to recondensation and deposition in rock pores on the contact with colder crust in depth (Vaucher et al., 2009). In contrast, Wilson et al. (2009) concluded that at least small amount of dissolved water vapour (0.1 to 0.2 mass%) was present in the erupted lava.

High effusion rates are confirmed by specific morphologies of volcanic bodies, known as sinuous rilles[6], in *Tempe Terra* and at one place in *Syria Planum* described by Hauber et al. (2009). Sinuous rilles in *Tempe Terra* (Figure 5.5) are formed by elliptical depressions at their head and by channel outgoing from its head (Hauber et al., 2009). These cylindrical depressions are probably formed by lava erupted via lava fountains fast erupted lava, ejected pyroclastic material falling back to the surface where they could form lava lake. This leads to the turbulent movements in a lava lake and thermal erosion of bedrock (Wilson and Head, 2001). This lake was probably feedingthe lava flow forming the adjacent sinuous rille.

The average length of the lava flow in this study was established to be around 24.44 km, which is in good agreement with the results of Wilson (2009) together with low values of viscosity and yield strength. Much larger flows reaching several hundreds of kilometres are known from Mars. Why the less viscous lavas do not form longer lava flows? One explanation was discussed by Keszthelyi and Self (1998) who noted that longer lava flows (longer than 100 km) gravitated over steep flanks of more than 5°. Observation of Martian surface suggests that longer Martian lava flows occur only on the flanks of huge shield volcanoes and not on low shield volcanoes with gentle slopes (Hauber et al., 2009).

Thicknesses of investigated lava flows ranges around 5 meters which is atypically less than for lava flows observed around huge Martian volcanoes. This confirms the previously established measurements by Wilson et al. (2009) who suggested that flows associated with fissure eruptions are unusually thin.

[6] Usually long, winding valley with steep sides.

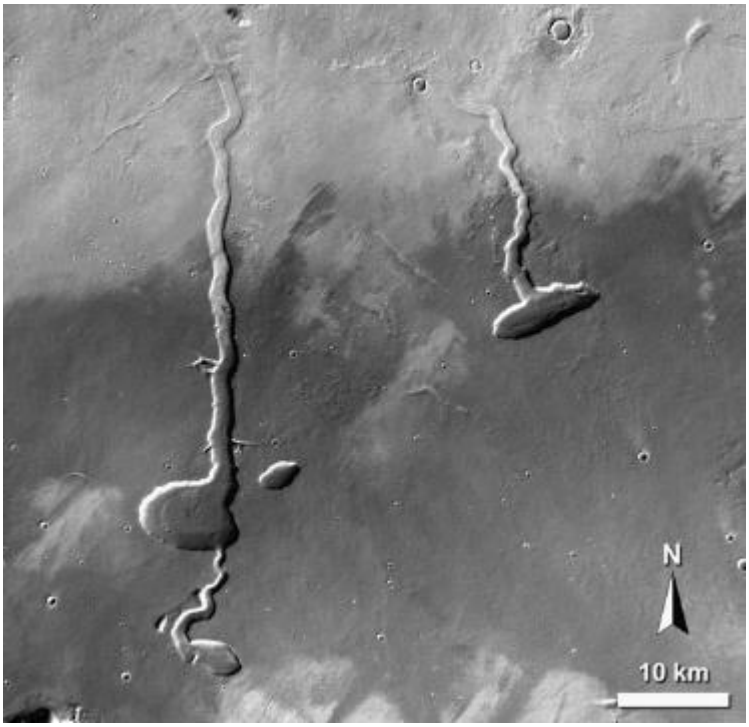

Figure 5.5: Several elliptic depressions and outgoing channels interpreted like sinious rilles in the *Tempe Terra*. Detail of HRSC image h1594_0000.nd (centered 38.6°N / 269.78°E). From Hauber et al., 2009.

5.6. Conclusions of rheological properties

On the basis of similarities between viscosity and yield strength values with terrestrial shield volcanoes on Hawaii, calculated properties from chemical composition of rocks in landing site in *Gusev* crater (Greeley et al., 2005), calculated properties of Martian meteorites (Lodders, 1998) and our results, we conclude that the investigated lava flows have very low viscosity and composition corresponding from basaltic to andesitic rocks. However, low values of thicknesses, yield strengths, high effusion rates and low viscosities suggest that volcanism forming low shield volcanoes is a result of unusual composition, unusual pre-eruptive conditions (level of temporary storage), or unusual eruption conditions as was already suggested by Wilson and Head (1994) and observed by Wilson et al. (2009).

We clearly observed low viscosity flows covering older surfaces and forming volcanic landforms characteristic for plain-style volcanism. Although the major reason for the calculated low viscosities is not resolved, properties of Martian lavas calculated in this study are similar to their terrestrial analogues. We did not find any differences between lava flows forming low shield volcanoes and large surrounding lava plains; it leads us to conclusion that both these landforms were created by the same magma type and one source.

6. Volumes of low shield volcanoes

Morphological parameters of low shield volcanoes have been already comprehensively described by other authors (e.g. see Hauber et al., 2009) so we focused only on the determination of volumes and morphological characteristics of their summit areas (Table 6.1). This offers an opportunity for future project aiming to calculate average number of lava flows forming each low shield volcano and compare the dimensions of Martian low shield volcanoes with their terrestrial equivalents (their total area and volume, see Figure 6.1). The determination of volumes and basal areas was determined using the DTM-Tool program from MOLA DEM data with resolution of ~463 m per cell in combination with CTX images. Although the low resolution of MOLA-DEM is inappropriate for small landforms like single lava flows, since low shield volcanoes covering very large areas (in our study range from ~6 to ~2930 km^2 with average ~355 km^2) this analysis is possible.

The volume values of the low shield volcanoes probably represent their lower limits, since it can be partly buried by younger lava flows or by other low shield volcanoes. Our shield age determination suggested that volcanic activity was distributed on a long timescale, therefore the likelihood that volcanoes overlapped each other, is high.

Calculated volumes for 37 volcanoes are represented in Table 6.1 and range from ~0.177 to 172 km^3, which is in agreement with previously published data by Baptista et al. (2008) and Hauber et al. (2009). Low lower limit of calculate volumes could be an artefact of low resolution DEM model used for volcanoes smaller than 30 km^2 (Hauber et al., 2009).

Figure 6.1c shows that the low shield volcanoes on Mars have differ from their analogs on Earth, in general they are formed by smaller volumes of magma and their flanks dip at shallower angles. Typical terrestrial shield volcano is characterized by slope angles ranging from 4° to 8° (see Hauber et al., 2009 and references therein) and around 2.7° on Icelandic shields (Rossi, 1996), which is still significantly more than for low shields on Mars with average slope angles of 0.43° (Hauber et al., 2009). This fact together with our estimations of rheological properties supports the idea that the low shield volcanoes originated from low viscosity lava of basaltic to andesitic composition.

ID	Region	Area of volume count (km^2)	Mean relief (m)	Mean slope (°)	Volume (km^3)	Vent	Direction N (°)
1	N of Biblis Patera	103.514	44	0.44	1.5211	s	-
2	N of Biblis Patera	15.178	45	1.16	0.2253	s	-
3	SE of Olympus Mons	393.379	55	0.28	7.175	f	132.2/109.2
4	SE of Olympus Mons	-	-	-	-	f	145.2
5	SE of Olympus Mons	640.735	56	0.22	11.9689	f	139.7/115.2
6	SE of Olympus Mons	60.35	9	0.11	0.1767	s/f	117.7
7	SE of Olympus Mons	231	33	0.22	2.5619	m	163,5
8	SE of Olympus Mons	45.896	12	0.18	0.1804	s	-
9	SE of Olympus Mons	393.44	17	0.09	2.24	f	115.1
10	SE of Olympus Mons	-	-	-	-	f	70.6
11	SE of Olympus Mons	33.131	21	0.38	0.235	s	124.2
12	SE of Olympus Mons	246.931	12	0.08	1.0015	f	46.2
13	SE of Olympus Mons	226.415	13	0.09	1.0015	f	29.9
14	SE of Olympus Mons	39.586	35	0.56	0.4606	s/f	111.4
15	S of Ceraunius Fossae	271.96	17	0.10	1.5273	s	-
16	S of Ceraunius Fossae	-	-	-	-	s	-
17	S of Ceraunius Fossae	-	-	-	-	s	-
18	S of Ceraunius Fossae	-	-	-	-	s	-
19	S of Ceraunius Fossae	325.305	46	0.26	5.0133	s	-
20	S of Ceraunius Fossae	755.86	31	0.11	7.8120	m	-
21	S of Ceraunius Fossae	-	-	-	-	f	38
22	S of Ceraunius Fossae	164.666	28	0.22	1.5311	f	155.7
23	S of Ceraunius Fossae	665.76	50	0.20	11.0187	f	184.9
24	S of Ceraunius Fossae	-	-	-	-	s	-
25	Tempe Terra	2932.5	176	0.33	172.378	m	53.5
26	Tempe Terra	-	-	-	-	m	15.9
27	Tempe Terra	-	-	-	-	s	-
28	Tempe Terra	287.021	23	0.14	2.2383	s	-
29	Tempe Terra	-	-	-	-	s	-
30	Tempe Terra	29.945	117	2.16	1.1630	m	41.2
31	Tempe Terra	134.56	124	1.09	5.58	m	73.6
32	Tempe Terra	-	-	-	-	m	69.4
33	Tempe Terra	-	-	-	-	m/f	65.3
34	Caldera of Arsia Mons	5.803	7	0.28	0.0128	s	-
35	Caldera of Arsia Mons	40.475	18	0.30	0.2494	s	-
36	Caldera of Arsia Mons	-	-	-	-	s	-
37	Caldera of Arsia Mons	53.41	70	0.97	1.2417	f	6.1
38	Caldera of Arsia Mons	33.941	18	0.31	0.204	f	175.2
39	Caldera of Arsia Mons	-	-	-	-	s	-
40	S of Pavonis Mons	-	-	-	-	s	-
41	S of Pavonis Mons	324.501	67	0.38	7.2758	s	-
42	S of Pavonis Mons	-	-	-	-	s	-
43	S of Pavonis Mons	-	-	-	-	f	16.6
44	S of Pavonis Mons	324.849	71	0.40	7.634	s	-
45	S of Pavonis Mons	615.566	121	0.50	24.841	m	49.4
46	S of Pavonis Mons	-	-	-	-	s	-
47	S of Pavonis Mons	183.067	73	0.55	4.4778	s	138.2
48	S of Pavonis Mons	84.888	18	0.20	0.5167	m	90
49	S of Pavonis Mons	-	-	-	-	m	-
50	S of Pavonis Mons	570.512	125	0.53	23.738	m	-
51	S of Pavonis Mons	71.629	42	0.50	1.0005	f	35.4
52	S of Pavonis Mons	-	-	-	-	f	6.8
53	S of Pavonis Mons	-	-	-	-	f	19.2
54	Syria Planum	-	-	-	-	s	-
55	Syria Planum	490.961	129	0.59	21.1804	f	164.6
56	Syria Planum	549.438	142	0.61	25.9855	f	176.1
57	Syria Planum	631.072	141	0.57	29.5982	s	-
58	Syria Planum	-	-	-	-	m	22.4
59	Syria Planum	757.23	101	0.37	25.5938	s	-
60	Syria Planum	396.853	40	0.20	5.2312	m	11.4

Table 6.1: Volumes, slopes and morphological characteristics of the summit areas of respective low shield volcanoes (s - single vent, m – multi vents, f – fracture).

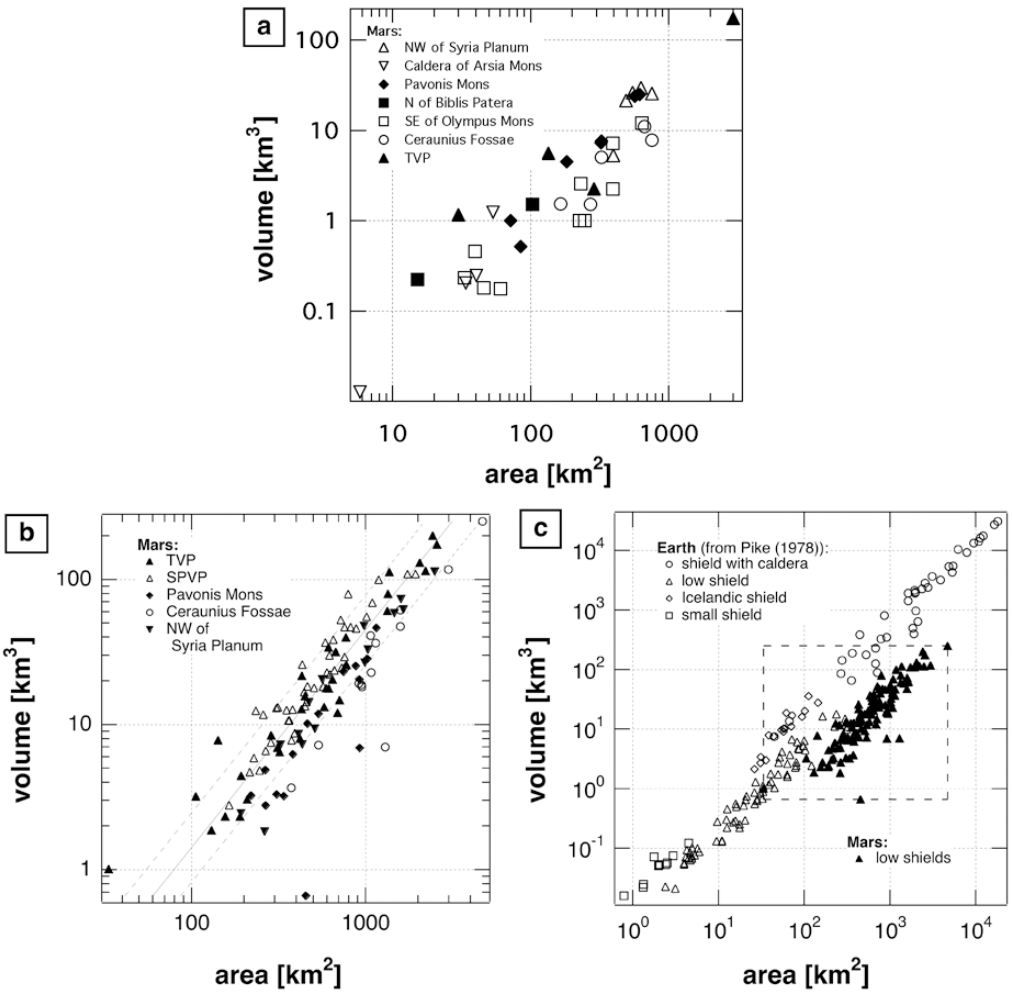

Figure 6.1: Morphometric properties of low shield volcanoes on Mars in comparison to other shields. The plots show the volume of respective shield versus its basal area, (a) dimensional characteristics of low shield volcanoes in this study. In plot (b) (representing results published by Hauber et al., 2009 for bigger volcanoes), inclined lines with a slope coefficient of ~3/2 correspond to constant values of flank slope, assuming a cone as geometric model for a volcanic shield. Solid line is the best fit for cone with flanks around 0.43°, dotted lines are 0.25° and 0.75° (from Hauber, 2009). (c) Comparison between low shield volcanoes in *Tharsis* and terrestrial basaltic shields listed by Pike (1978). All terrestrial shields have steeper slopes than their Martian equivalents (from Hauber 2009).

7. Results

We processed 61 volcanoes, over 40,000 impact craters and 10 lava flows (team work on DLR, cooperation with Felix Jagert and Ernst Hauber) in attempt to extend the recent knowledge about the plain-style volcanism in *Tharsis* region on Mars. Our main goal was to establish the absolute ages of low shield volcanoes using the CSFD method, basic rheological properties of erupted material forming low shield volcanoes and surrounding plains and volumes of independent lava flows and the volcanic cones. The major results of this study are listed bellow:

a) We confirmed previously observed clustering behaviour of low shield volcanoes in *Tharsis* region described by Hauber et al. (2009) together with no close spatial relationship between shield volcano clusters and large volcanoes like *Olympus Mons*, *Tharsis Montes*, *Alba Patera* or *Valles Marineris*. We concluded that formation of the clusters was probably prescribed by regional tectonic settings without any affinity to huge volcanoes, which is in agreement with the previous studies.
b) Our investigation confirmed that CSFD method is appropriate to establish absolute ages of low shield volcanoes due to their low slope angle. Their absolute age determination in combination with relative stratigraphy dating methods can help dating features (faults, grabens) which are not suitable for CSFD dating.
c) Absolute ages confirmed the previously established hypothesis that the plain-style volcanism with low shield volcanoes is relatively young. Most of the investigated volcanoes are from 50 to 130 Ma old (Late Amazonian) with two exceptions of *Tempe Terra* and *Syria Planum* which are significantly older (Middle and Early Amazonian). We also found out that absolute ages are relatively similar in individual clusters; however ages in *Tempe Terra* and *Syria Planum* are more evenly distributed throughout the Martian history (see Figure 4.14).
d) An open question remains, if plain-style volcanism was caused by a single or multiple-episode event. Only the youngest surface superficial layer was analyzed by the CSFD method. It looks that the last episode of eruptions occurred recent past, which supports further speculations about the geological activity of Mars; does the recent situation represent only an interim between two subsequent volcanic phases, or is the volcanic activity already extinct?
e) We did not observe any directional trend of volcanic activity migration of in any direction in the *Tharsis* region as it is known from arrays of volcanoes above mantle plumes on Earth.

Radial distribution between individual clusters was not confirmed either. This leads us to conclude that the more probable explanation for volcanic activity on Mars is the partial melting as suggested by Schumacher and Breuer (2007) than the (super)plume model.

f) Similar calculated physical properties of lava flows forming low shield volcanoes and lavas forming plains in plain-style volcanic regions suggest that the source of magma was the same for both types of landforms.

g) Lava forming the investigated landforms had low viscosity, low yield strength and relatively high effusion rates and all these properties in comparable range with their terrestrial analogues. A comparative study between our results and terrestrial, Venusian and Martian volcanoes revealed that the most probable rock composition forming low shield volcanoes corresponds to basaltic or andesitic rocks. Basaltic composition is in the agreement with models of Martian lithosphere and mantle.

h) Relatively recent volcanic activity could have significantly affected Martian atmosphere by gasses exsolved from the erupted magma. Although this question was not object of this diploma thesis, our contribution for future investigation of this problem is the attempted estimation of the total volumes of each low shield volcano and volume of lava forming each lava flow. The next possible step will be establishing the quantity of lava flows forming each low shield volcano and attempt to count total volume of gases from each volcano.

i) Volume measurements of low shield volcanoes supported the results obtained by Hauber et al. (2009) that Martian low shield volcanoes have not direct analogues on Earth because they are flatter than terrestrial shield volcanoes. This confirms that the low shield volcanoes on Mars consist of low viscosity material which is in the agreement with our rheological conclusions. However reason of this low viscous magma is still enigmatic (e.g. low content of Si-, high amount of Mg- or Fe-, high temperature during eruption, high amount of dissolved volatiles respectively water vapour or combination of these factors).

8. References

Anderson, J.A., Sides, S.C., Soltesz, D.L., Sucharski, T.L, and Becker, K.J., (2004) *Modernization of the Integrated Software for Imagers and Spectrometers* (abs. 2039), LPSC XXXV.

Arthur, D. W. G. (1974), *Lunar Crater Depths from Orbiter IV Long-Focus Photographs*, Icarus 23, 116-133.

Arvidson, R.E., Boyce, J., Chapman, C., Cintala, M., Fulchignoni, M., Moore, H., Neukum, G., Schultz, P., Soderblom, L., Strom, R., Woronow, A., Young, R., (1979) *Standard techniques for presentation and analysis of crater size-frequency data*. Icarus 37, 467–474.

Baloga, S. M. (1987) *Lava flows as kinematic waves*. J. Geophys. Res. 92, 9271-9279

Baloga, S. M., Glaze, L.S., Peitersen, M.N., Crisp, J.A. (2001) *Influence of volatile loss on thickness and density profiles o active basaltic flow lobes*. J. Geophys. Re. 106, 13395-13405.

Baptista, A., N. Mangold, V. Ansan, P. Lognonne, D. Williams, J. Bleacher, P. Masson, and G. Neukum (2008) *A swarm of small shield volcanoes on Syria Planum, Mars, analyzed using Mars Express HRSC data*, J. Geophys. Res., 113, E09010, doi:10.1029/2007JE002945.

Barlow, N.G. (2008) *Mars. An Introduction to its Interior, Surface and Atmosphere*, Cambridge Planetary Science. Cambridge University Press, ISBN 9780521852265.

Bleacher, J.E., Glaze, L.S., Greeley, R., Hauber, E., Baloga, S.M., Sakimoto, S.E.H., Williams, D.A., Glotch, T.D., 2009. Spatial and alignment analyses for a field of small volcanic vents south of Pavonis Mons and implications for the Tharsis province, Mars. J. Volcanol. Geotherm. Res. 185, 96–102.

Booth, B., and Self S. (1973) *Rheological features of the 1971 Mt. Etna lavas, Philos*, Trans. R. Soc. London, Ser. A, 274, 99–106.

Brož P. (2008), *Mapování vulkanické aktivity na Marsu v oblasti Tharsis*, bachelor work at Charles University in Prague.

Bruno, B.C., Baloga, S.M., Taylor, G.J. (1996) *Modeling gravity-driven glows on an inclined plane*. J. Geophys. Res. 101, 11565-11577.

Burr, D. (2005) *Clustered streamlined forms in Athabasca Valles, Mars: evidence for sediment deposition during floodwater ponding*. Geomorphology 69, 242–252.

Carr M.H. (2006) The Surface Of Mars, Cambridge University Press (United Kingdom), ISBN 9780521872010

Carr M.H. & Head, James W., I. (2009) *Geologic history of Mars*, Earth. Planet. Sci. Lett.. doi: 10.1016/j.epsl.2009.06.042

Comer, R. P., Solomon S. C., and Head J. W. (1985) *Mars: Thickness of the Lithosphere from the Tectonic Response to Volcanic Loads*, Rev. Geophys., 23(1), 61–92.

Davidson, J., De Silva, S., (2000) *Composite volcanoes*, in: Sigurdsson, H. (Ed.), Encyclopedia of Volcanoes. Academic Press, San Diego, pp. 663–681.

De Hon R. A. (1974) *Thickness of mare material in the Tranquillitatis and Nectaris basins*, Lunar Science Conference, 5th, Houston, Tex., March 18-22, 1974, Proceedings. Volume 1. (A75-39540 19-91) New York, Pergamon Press, Inc., 1974, p. 53-59.

De Hon R. A. (1979) *Thickness of the western mare basalts*, Lunar and Planetary Science Conference, 10th, Houston, Tex., March 19-23, 1979, Proceedings. Volume 3. (A80-23677 08-91) New York, Pergamon Press, Inc., 1979, p. 2935-2955.

Dingwell, D.B., Romano, C., Hess, K.U. (1996) *The effect of water on the viscosity of a haplogranitic melt under P-T-X conditions relevant to silicic volcanism*. Contrib. Mineral. Petrol. 124, 19–28.

Garvin, J.B., Sakimoto, S.E.H., Frawley, J.J., Schnetzler, C.C. (2000b) *North polar region craterforms on Mars: Geometric characteristics from the Mars Orbiter Laser Altimeter*, Icarus 144, 329-352.

Garvin, J.B., Sakimoto, S.E.H., Frawley, J.J., Schnetzler, C.C., Wright, H.M. (2000a) *Topographic evidence for geologically recent near-polar volcanism on Mars*, Icarus 145, 648–652.

Gault, D. E.; Greeley, R. (1978), *Exploratory experiments of impact craters formed in viscous-liquid targets - Analogs for Martian rampart craters*, Icarus, vol. 34, June 1978, p. 486-495. DOI: 10.1016/0019-1035(78)90040-4.

Glaze L. S., Baloga S. M., Stofan E. R. (2003) A methodology for constraining lava flow rheologies with MOLA, Icarus, Volume 165, Issue 1, p. 26-33.

Greeley R. (1982) The *Snake River Plain, Idaho - Representative of a new category of volcanism*, Journal of Geophysical Research, vol. 87, Apr. 10, 1982, p. 2705-2712.

Greeley R. and Schneid B.D. (1991) *Magma Generation on Mars: Amounts, Rates, and Comparisons with Earth, Moon, and Venus*, Science, 15 November 1991, Vol. 254. no. 5034, pp. 996 – 998, DOI: 10.1126/science.254.5034.996.

Greeley R. and Spudis P. D. (1981) *Volcanism on Mars*, Reviews of Geophysics and Space Physics, 19, 13–43.

Greeley, R., Foing, B.J., McSween, H.Y., Neukum, G., Pinet, P., van Kan, M., Werner, S.C., Williams, D.A., Zegers, T.E.

(2005) *Fluid lava flows in Gusev crater, Mars*. J. Geophys. Res. 110. E05008.
Gregg, T. K. P., and Fink J. H. (1996) *Quantification of extraterrestrial lava flow effusion rates through laboratory simulations*, J. Geophys. Res., 101, 16,891–16,900.
Harder, H. and Christensen, U. (1996*) A one-plume model of Martian mantle convection*, Nature 380, 507–509.
Hartmann W. K. and Neukum G. (2001) Cratering *Chronology and the Evolution of Mars*, Space Science Reviews, v. 96, Issue 1/4, p. 165-194.
Hartmann, W.K. (2005) *Martian cratering. 8. Isochron refinement and the chronology of Mars*, Icarus 174, 294–320.
Hartmann, W.K. (2007) *Martian cratering. 9. Toward resolution of the controversy about small craters*, Icarus 189, 274–278.
Hartmann, W.K., (1999) *Martian cratering. VI. Crater count isochrons and evidence for recent volcanism from Mars Global Surveyor*, Meteorit. Planet. Sci. 34, 167–177.
Hartmann, W.K., Cruikshank, D.P., Degewij, J., Capps, R.W. (1981), *Surface materials on unusual planetary object Chiron*, Icarus 47, 333–341.
Hartmann, W.K., Neukum, G., Werner, S. (2008) *Confirmation and utilization of the "production function" size-frequency distributions of martian impact craters*. Geophys. Res. Lett. 35, doi:10.1029/2007GL031557. L02205.
Hasenaka, T., (1994), *Size, distribution, and magma output rate for shield volcanoes of the Michoacán–Guanajuato volcanic field, Central Mexico*. J. Volcanol. Geotherm. Res. 63, 13–31.
Hauber E., Bleacher J., Gwinner, K., Williams D., Greeley R. (2009) The topography and morphology of low shields and associated landforms of plains volcanism in the Tharsis region of Mars, Journal of Volcanology and Geothermal Research, v. 185, iss. 1-2, p. 69-95.
Hauber, E., (2007) *Plains volcanism on Mars Revisited: the topography and morphology of low shields and related landforms*. 7th International Conference on Mars, LPI Contribution No. 1353 (CD-ROM), abstract 3287.
Hauber, E., Kronberg, P.,Wolf, U., Neukum, G. (2002) *Tempe Volcanic Province Revisited: New Evidence for Mid-Late Amazonian Plains Volcanism on Mars, and a Hotspot Beneath Tempe Terra?* In: Lunar Planet. Sci., vol. XXXIII. Lunar and Planetary Institute, Houston (CD-ROM), abstract 1516.
Head, J. W. and Wilson L. (1998) *Tharsis Montes as composite volcanoes?: 1. The role of explosive volcanism in edifice construction and implications for the volatile contents of edifice*, 29th Annual Lunar and Planetary Science Conference, March 16-20, 1998, Houston, TX, abstract no. 1127.
Hiesinger H., Head J. W., Neukum, G. (2007) Young lava flows on the eastern flank of Ascraeus Mons, Journal of Geophysical Research, Volume 112, Issue E5, doi: 10.1029/2006JE002717.
Hiesinger, H., Head J. W., Wolf U., Jaumann R., and Neukum G. (2002) *Lunar mare basalt flow units: Thicknesses determined from crater size-frequency distributions*, Geophys. Res. Lett., 29(8), 1248, doi:10.1029/2002GL014847.
Hodges C.A. and Moore H.J. (1994) *Atlas of volcanic features on Mars*, USGS Prof. Paper 1534, 194 p.
Hodges, C.A. (1980) *Tempe-Mareotis volcanic province of Mars. Reports of Planetary Geology Program*, 1979–1980, NASA-TM 81776, 181–183.
Hulme, G. (1974) *The interpretation of lava flow morphology*. Geophys. J. Astron. Soc. 39, 361–383.
Hulme, G. (1976) *The determination of the rheological properties and effusion rate of an Olympus Mons lava*, Icarus, 27, 207– 213.
Ivanov, B.A. (2001), *Mars/Moon Cratering Rate Ratio Estimates*, pace Science Reviews, v. 96, Issue 1/4, p. 87-104 (2001).
Jaeger, W.L., Keszthelyi, L.P., McEwen, A.S., Dundas, C.M., Russell, P.S. (2007) *Athabasca Valles, Mars: a lava-draped channel system*, Science 317, 1709–1711.
Jaumann, R., Neukum, G., Behnke, T., Duxbury, T. C., Eichentopf, K., Flohrer, J., Gasselt, S. V., Giese, B., Gwinner, K., Hauber, E., Hoffmann, H., Hoffmeister, A., Köhler, U., Matz, K.-D., McCord, T. B., Mertens, V., Oberst, J., Pischel, R., Reiss, D., Ress, E., Roatsch, T., Saiger, P., Scholten, F., Schwarz, G., Stephan, K., Wählisch, M., the HRSC Co-Investigator Team (2006) *The high-resolution stereo camera (HRSC) experiment on Mars Express: Instrument aspects and experiment conduct from interplanetary cruise through the nominal mission*, Planetary and Space Science, Volume 55, Issue 7-8, p. 928-952.
Jaumann, R., Neukum, G., Behnke, T., Duxbury, T.C., Eichentopf, K., Flohrer, J., Van Gasselt, S., Giese, B., Gwinner, K., Hauber, E., Hoffmann, H., Hoffmeister, A., Köhler, U., Matz, K.-D., McCord, T.B., Mertens, V., Oberst, J., Pischel, R., Reiss, D., Ress, E., Roatsch, T., Saiger, P., Scholten, F., Schwarz, G., Stephan, K., Wählisch, M., The HRSC Co-Investigator Team (2007) *The high-resolution stereo camera (HRSC) experiment on Mars Express: instrument aspects and experiment conduct from interplanetary cruise through the nominal mission*. Planet. Space Sci. 55, 928–952.
Keszthelyi, L., Self, S. (1998) Why *are there long channelized flows on Venus and Mars, but not the Earth?* Lunar Planet. Sci. XXIX abstract 1426.

Kiefer, Walter S. (2008) *Planetary science: Forming the martian great divide*, Nature 453, 1191-1192 (26 June 2008) | doi:10.1038/4531191a.

Kneissl T., van Gasselt S. and Neukum G. (2010 Accepted manuscript) Map-projection-independent crater size-frequency determinationin GIS environments – new software tool for ArcGIS, Planetary and Space Science, doi:10.1016/j.pss.2010.03.015.

Kneissl, T., Neukum, G.. (2008) *Indications for a non-volcanic origin of conical mounds at the mouth of Chasma Boreale, Mars*, EPSC Abstracts 3, Abstract EPSC2008-A-00259.

Lissauer, J.J., Squyres, S.W., and Hartmann, W.K. (1988) *Bombardment History of the Saturn System*, J. Geophys. Res. 93, 13,776–13,804.

Lodders, K. (1998) *A survey of shergottite, nakhlites and chassigny meteorites wholerock compositions*, Meteorit. Planet. Sci. 33. 83-A190.

Longhi, J. (1990) *Magmatic processes on Mars: Insights from SNC meteorites*, Proc. Lunar Planet. Sci. Conf. 21st, 716– 717.

Lyman, A., Kerr, R., Griffiths, R. (2005). *Effect of the internal rheology and surface cooling on the emplacement of lava flows*. J. Geophys. Res. 110 (B8). B08207.

Malin, M.C., Bell, J.F., Cantor, B.A., Caplinger, M.A., Calvin,W.M., Clancy, R.T., Edgett, K.S., Edwards, L., Haberle, R.M., James, P.B., Lee,S.W., Ravine, M.A., Thomas, P.C.,Wolff, M.J. (2007) *Context camera investigation on board the Mars Reconnaissance Orbiter*, J.Geophys.Res.112. doi:10.1029/2006JE002808. CiteIDE05S04.

Marinova, Margarita M., Aharonson, Oded, Asphaug, Erik (2008) *Mega-impact formation of the Mars hemispheric dichotomy*, Letter in Nature 453, 1216-1219 doi:10.1038/nature07070.

McColley, S. M., and J. W. Head (2004) *Venus festoon deposits: Analysis of characteristics and modes of emplacement*, Lunar Planet. Sci. [CDROM], XXXV, Abstract 1376.

McEwen, A.S., Preblich, B.S., Turtle, E.P., Artemieva, N.A., Golombek, M.P., Hurst, M., Kirk, R.L., Burr, D.M., Christensen, P.R. (2005) *The rayed crater Zunil and interpretations of small impact craters on Mars*, Icarus 176, 351–381.

McGovern, P., Solomon, S., Smith, D., Zuber, M., Simons, M., Wieczorek, M., Phillips, R., Neumann, G., Aharonson, O., Head, W. (2004) *Correction to localized gravity/topography admittance and correlation spectra on Mars: Implications for regional and global evolution*. J. Geophys. Res. 109, doi:10.1029/2004JE002286.

McSween H.Y. Jr. (1999*) Meteorites and Their Parent Planets*, Cambridge University Press, Cambridge, UK, 310 pp., ISBN 0-521-58751-4.

Milazzo, M. P., Jaeger, W. L., Keszthelyi, L., McEwen, A. S., Beyer, R. A. (2009) *Discovery of columnar jointing on Mars*, 39th Lunar and Planetary Science Conference, (Lunar and Planetary Science XXXIX), held March 10-14, 2008 in League City, Texas. LPI Contribution No. 1391., p.2062.

Moore, H. J. (1987) *Preliminary estimates of the rheological properties of 1984 Mauna Loa lava*, in Volcanism in Hawaii, vol. 2, edited by R. W. Decker, T. L. Wright, and P. H. Stauffer, U.S. Geol. Surv. Prof. Pap., 1350, 1569– 1588.

Moore, H. J., and Schaber G. G. (1975) *An estimate of the yield strength of the Imbrium flows*, Proc. Lunar Sci. Conf 6th, 101-118, 1975.

Moore, H.J., Hodges, C.A. (1980) *Some Martian volcanic centers with small edifices*, Reports of Planetary Geology Program-1988, pp. 266–268. NASA-TM 82385, Washington, D.C.

Mouginis-Mark, P.J. (1981) *Ejecta emplacement and modes of formation of martian fluidized ejecta craters*, Icarus 45, 60–76.

Murray, J.B., Muller, J., Neukum, G.,Werner, S.C., van Gasselt, S., Hauber, E., Markiewicz, W.J., Head, J.W., Foing, B.H., Page, D., Mitchell, K.L., Portyankina, G., HRSC Co-Investigator Team (2005) *Evidence from the Mars Express High Resolution Stereo Camera for a frozen sea close to Mars' equator*. Nature 434, 352–356.

Neukum G. (1983) *Meteoritenbombardement und Datierung planetarer Oberflächen*. Habilitation Dissertation for Faculty Membership, Univ. of Munich, 186pp, 1983.

Neukum, G. & Wise, D.U. (1976) *Mars: A Standard Crater Curve and Possible New Time Scale*, Science. 194, S. 381-1387. doi: 10.1126/science.194.4272.1381.

Neukum, G., Hiller, K. (1981) *Martian ages*, J. Geophys. Res. 86 (15), 3097–3121.

Neukum, G., Horn, P. (1976) *Effects of lava flows on lunar crater population*, The Moon, vol. 15, June-July 1976, p. 205-222. Research supported by the Bundesministerium fuer Forschung und Technologie and Deutsche Forschungsgemeinschaft.

Neukum, G., Ivanov, B., and Hartmann, W.K. (2001) *Cratering Records in the Inner Solar System in Relation to the Lunar Reference System*, Space Sci. Rev.

Neukum, G., Jaumann, R., Hoffmann, H., Hauber, E., Head, J.W., Basilevsky, A.T., Ivanov, B.A., Werner, S.C., van Gasselt, S., Murray, J.B., McCord, T., HRSC Co-Investigator (2004) *Recent and episodic volcanic and glacial activity on Mars revealed by the High Resolution Stereo Camera*. Nature 432, 346–351.

Neumann, G.A., Abshire, J.B., Aharonson, O., Garvin, J.B., Sun, X., Zuber, M.T. (2003) Mars Orbiter Laser Altimeter pulse width measurements and footprint-scale roughness. Geophys. Res. Lett. 30, 1561. doi:10.1029/2003GL017048.

Nyquist, L.E., Wooden, J., Bansal, B., Wiesmann, H., McKay, G., and Bogard, D.D. (1979) *Rb-Sr Age of the Shergotty Achondrite and Implications for Metamorphic Resetting of Isochron Ages*, Geochim. Cosmochim. Acta 43, 1057–1074.

Okubo, C.H., Martel, S.J. (1998*) Pit crater formation on Kilauea volcano, Hawaii,* J. Volcanol. Geotherm. Res. 86, 1–18.

Potuzak, M., Giordano, D., Courtial, P., Dingwell, D., (2004). The effect of iron on the rheological properties of silicate melts. Geophys. Res. Abstr. 6 abstract 05036.

Phillips, R. J., Zuber M. T., Solomon S. C., Golombek M. P., Jakosky B. M., Banerdt W. B., Smith D. E., Williams R. M. E., Hynek B. M., Aharonson O., Hauck S. A. (2001) *Ancient geodynamics and global-scale hydrology on Mars*. Science 291, 2587–2591.

Pierce, K. L. and Morgan, L. A., 1992, The track of the Yellowstone hot spot: Volcanism, faulting, and uplift, in Link, P. K., Kuntz, M. A., and Platt, L. B., eds., Regional Geology of Eastern Idaho and Western Wyoming: Geological Society of America Memoir 179, p. 1-53.

Pike, R. J. (1978) *Volcanoes on the inner planets: Some preliminary comparisons of gross topography*, Proc. Lunar Planet. Sci. Conf. 9th, 3239–3273.

Pinkerton, H., Sparks, R., (1976) *The 1975 sub-terminal lavas, mount Etna: A case history in the formation of a compound lava field.* J. Volcanol. Geotherm. Res. 1, 167–182.

Plescia J.B. (1981) *The Tempe volcanic province of Mars and comparisons with the Snake River Plains of Idaho*, Icarus, *45*, 586-601.

Plescia, J.B., Saunders, R.S. (1979) *The chronology of the martian volcanoes*. Lunar Planet. Sci., 2841–2859.

Plescia, J.B., 2004. Morphometric properties of Martian volcanoes. J. Geophys. Res. 109. doi:10.1029/2002JE002031. CiteID E03003.

Reiss, D., Lüsebrink, D., Hiesinger, H., Kelling, T., Wurm, G., Teiser, J. (2009) *High Altitude Dust Devils on Arsia Mons, Mars: Testing the Greenhouse and Thermophoresis Hypothesis of Dust Lifting*, 40th Lunar and Planetary Science Conference, (Lunar and Planetary Science XL), held March 23-27, 2009 in The Woodlands, Texas, id.1961.

Richet, P., Lejeune, A.-M., Holtz, F., Roux, J. (1996) *Water and the viscosity of andesite melts*. Chem. Geol. 128, 185–197.

Rossi, M. (1996) *Morphology and mechanism of eruption of postglacial shield volcanoes in Iceland. Bull*. Volcanol. 57, 530–540.

S. van Gasselt, E. Hauber, R. Jaumann (2003) *Permafrost-related Morphologies in Tempe Terra, Observations and Morphometry*, Sixth International Conference on Mars, July 20-25 2003, Pasadena, California, abstract no.3189.

Sakimoto, S.E.H. (2008) Martian *Small Volcanic Shields and Shield Fields*, in: Lunar Planet. Sci., vol. XXXIX. Lunar and Planetary Institute, Houston (CD-ROM), abstract 1658.

Sakimoto, S.E.H., Garvin, J.B., Bradley, B.A., Wong, M., Frawley, J.J. (2001) *Small Martian North Polar Volcanoes: Topographic Implications for Eruptive Styles*, in: Lunar Planet. Sci., vol. XXXII. Lunar and Planetary Institute, Houston (CD-ROM), abstract 1808.

Sakimoto, S.E.H., Gregg, T.K.P., Hughes, S.S., Chadwick, J. (2003) *Re-assessing plains-style volcanism on Mars. 6th International Conference on Mars*, Lunar and Planetary Institute, Houston (CD-ROM), abstract 3197.

Schumacher, S., Breuer, D. (2007) *An alternative mechanism for recent volcanism on Mars*. Geophys. Res. Lett. 34. L12202.

Schupack, B.B., Sakimoto, S.E.H. (2006) *Eruption Styles of Small Martian Shield Volcanoes and Indications of Post-flow Tectonic Deformation on Syria Planum, from MOLA, TES, and THEMIS Data,* Lunar Planet. Sci., vol. XXXVII. abstract 1157.

Scott, D. H., and K. L. Tanaka (1986) *Geologic map of the western equatorial region of Mars*, U. S. Geol. Surv. Misc. Invest. Ser., Map I-1802-A.

Shaw, H. R., T. L. Wright, D. L. Peck, and R. Okamura (1968) The viscosity of basaltic magma: An analysis of field measurements in Makaopuki lava lake, Hawaii, Am. J. Sci., 266, 225–264.

Sigurdsson, H. et al. (1999) *Encyclopedia of Volcanoes*, Academic Press, San Diego, pp. 663–681.

Sleep, N.H. and Phillips, R.J., (1979) *An isostatic model for the Tharsis province*, Geophys. Res. Lett. 6, 803–806.

Smith, D E.; Zuber M.T., Frey H.V., Garvin J. B., Head J. W., Muhleman D. O., Pettengill G. H., Phillips R. J., Solomon S. C., Zwally H. J., Banerdt W. B., Duxbury T. C., Golombek M. P., Lemoine F. G., Neumann G. A., Rowlands D. D., Aharonson O., Ford P. G., Ivanov A. B., Johnson C. L., McGovern P. J., Abshire J. B., Afzal R. S., Sun X. (2001) *Mars Orbiter Laser Altimeter: experiment summary after the first year of global mapping of Mars*. J.

Geophys. Res. 106, 23689–23722.
Smith, D. G., Neumann G.,. Arvidson R. E, Guinness E. A. and Slavney S. (1999) *Mars Global Surveyor Laser Altimeter Precision Experiment Data Record*, NASA Planetary Data System. MGS-M-MOLA-3-PEDR-L1AV1.0.
Solomon, S.C., Head, J.W., (1982) *Evolution of the Tharsis province of Mars: the importance of heterogeneous lithospheric thickness and volcanic construct*, J. Geophys. Res. 87, 9755–9774.
Som S. M., Greenberg H. M., Montgomery D. R. (2008) *The Mars Orbiter Laser Altimeter dataset: Limitations and improvements*, International Journal of Mars Science and Exploration, vol. 4, p.14-26.
Spohn T., Sohl F., Breuer D. (1998), *Mars*, The Astron Astrophys Rev (1998) 8: 181–236.
Tanaka, K.L. (1986) *The Stratigraphy of Mars*, Proc. 17th Lunar Planet. Sci. Conf., J. Geophys. Res. 91, suppl., 139–158.
Tarduno, John A. and Cottrell, Rory D. (1997), *Paleomagnetic evidence for motion of the Hawaiian hotspot during formation of the Emperor seamounts*, Earth and Planetary Science Letters, Volume 153, Issue 3-4, p. 171-180.
Vaucher, J., Baratoux, D., Toplis, M. J., Pinet, P., Mangold, N., Kurita, K. (2009) *The morphologies of volcanic landforms at Central Elysium Planitia: Evidence for recent and fluid lavas on Mars*, Icarus, Volume 200, Issue 1, p. 39-51, doi:10.1016/j.icarus.2008.11.005.
Walker, G.P. L. (1972) *Compound and simple lava flows and flood basalts*. Bull. Volcanol. 35, 579–590.
Warner, N. H., and Gregg T. K. P. (2003) *Evolved lavas on Mars? Observations from southwest Arsia Mons and Sabancaya volcano, Peru*, J. Geophys. Res., 108(E10), 5112, doi:10.1029/2002JE001969.
Warner, N.H., Farmer, J.D., (2008) *Martian north polar conical mounds: a reassessment of the volcanic origin hypothesis*, Lunar Planet. Sci. XXXIX Abstract 1475.
Werner, S.C., Ivanov, B.A., Neukum, G., (2009) *Theoretical analysis of secondary cratering on Mars and an image-based study on the Cerberus Plains*, Icarus, Volume 200, Issue 2, p. 406-417, doi:10.1016/j.icarus.2008.10.011.
Werner, S.C., Neukum, G., The HRSC Co-Investigator Team, (2005) *Major volcanic constructs seen from Mars Express HRSC—New insights into their evolutionary history*. In: Proc. Lunar Sci. Conf. 36. No. 1766.
Werner, S.C., Van Gasselt, S., Neukum, G., (2003) *Continual geological activity in Athabasca Valles, Mars*. J. Geophys. Res. 108. doi:10.1029/2002JE002020. CiteID 8081.
Werner, S. C. (2005) *Major Aspects of the Chronostratigraphy and Geologic Evolutionary History of Mars*, Dissertation zur Erlangung des Grades eines Doktors der Naturwissenschaften, am Fachbereich Geowissenschaften der Freien Universit¨at Berlin Berlin.
Werner, S. C. (2009) *The global martian volcanic evolutionary history*. Icarus, 201, 44-68.
Wieczorek, M.A., Zuber, M.T., (2004) *Thickness of the martian crust: Improved constraints from geoid-to-topography ratios*, J. Geophys. Res. 109 (E1), doi:10.1029/2003JE002153. 01009.
Williams, D. A., Greeley R., Werner S. C., Michael G.., Crown G.., Neukum G., and Raitala J. (2008), *Tyrrhena Patera: Geologic history derived from Mars Express High Resolution Stereo Camera*, J. Geophys. Res., 113, E11005, doi:10.1029/2008JE003104.
Williams, D. A., Greeley R., Zuschneid W., Werner S. C., Neukum G., Crown D. A., Gregg T. K. P., Gwinner K., and Raitala J. (2007) *Hadriaca Patera: Insights into its volcanic history from Mars Express High Resolution Stereo Camera*, J. Geophys. Res., 112, E10004, doi:10.1029/2007JE002924.
Wilson, L., and Head J. W. (1983), *A comparison of volcanic eruption processes on Earth, Moon, Mars, Io, and Venus*, Nature, 302, 663– 669.
Wilson, L., and Head J. W. (1994*), Mars: Review and analysis of volcanic eruption theory and relationships to observed landforms*, Rev. Geophys., 32, 221– 263.
Wilson, L., Mouginis-Mark P.J., Tyson S., Mackown, J., Garbeil H. (2009) *Fissure eruptions in Tharsis, Mars: Implications for eruption conditions and magma sources*, Journal of Volcanology and Geothermal Research, v. 185, iss. 1-2, p. 28-46.
Wise, D.U., Golombek, M.P., McGill, G.E. (1979) *Tharsis province of Mars: geologic sequence, geometry, and a deformation mechanism*, Icarus 38, 456–472.
Witter, J. B. and Harris A. J. L., (2007) Field measurements of heat loss from skylights and lava tube systems, Journal of Geophysical Research, vol. 112.
Zhong, S. (2002) *Effects of lithosphere on the long-wavelength gravity anomalies and their implications for the formation of the Tharsis rise on Mars*, J. Geophys. Res. 107, 8–1–8-13. doi:10.1029/2001JE001589.
Zhong, S., Roberts, J.H., (2003) On the support of the Tharsis rise on Mars. Earth Planet. Sci. Lett. 214, 1–9.
Zuber, M.T. (2001) The crust and mantle of Mars, Nature, 412, 220-227.
Zuber, M.T., Smith, D.E., Solomon, S.C., Muhleman, D.O., Head, J.W., Garvin, J.B., Abshire, J.B., Bufton, J.L. (1992) *The Mars observer laser altimeter investigation*, J. Geophys. Res. 97, 7781–7797.

Internet references

United States Geological Survey (USGS) (2009), *ArcMap 8.x and 9.x Planetary Projection Tutorial*, http://webgis.wr.usgs.gov/pigwad/tutorials/planetarygis/arcmap_projections.htm. Date of access 2010/4/28.

United States Geological Survey (USGS) (2008): *ISIS Workshop. Working with Mars Reconnaissance Orbiter CTX Data*., http://isis.astrogeology.usgs.gov/IsisWorkshop/index.php/Working_with_Mars_Reconnaissance_Orbiter_CTX_Data. Date of access 2010/4/28.

9. List of figures

10. List of tables

11. Appendix

11.1. Positions of volcanoes

Table A.1. Table contains ID numbers using in master thesis for easer orientation with they exactly position due Martian coordinates, simplification via region and exact CTX name.

ID	Position (° N / ° E)	Region	Name of CTX picture
1	6.51 / 239.79	N from Biblis Patera	P20_008776_1867_XN_06N120W
2	6.51 / 239.87	N from Biblis Patera	P20_008776_1867_XN_06N120W
3	14.82 / 233.83	SE from Olympus Mons	P07_003634_1955_XN_15N126W
4	14.27 / 234.75	SE from Olympus Mons	P13_006258_1932_XN_13N125W
5	14.61 / 234.54	SE from Olympus Mons	P13_006258_1932_XN_13N125W
6	14.61 / 234.42	SE from Olympus Mons	P13_006258_1932_XN_13N125W
7	15.38 / 234.55	SE from Olympus Mons	P13_006258_1932_XN_13N125W
8	15.4 / 236.53	SE from Olympus Mons	P13_006192_1972_XN_17N123W
9	18.73 / 236.06	SE from Olympus Mons	P13_006192_1972_XN_17N123W
10	15.27 / 232.47	SE from Olympus Mons	P19_008473_1952_XI_15N127W
11	14.4 / 233.14	SE from Olympus Mons	P19_008473_1952_XI_15N127W
12	15.33 / 232.14	SE from Olympus Mons	P19_008473_1952_XI_15N127W
13	15.3 / 232.81	SE from Olympus Mons	P19_008473_1952_XI_15N127W
14	15.39 / 232.99	SE from Olympus Mons	P19_008473_1952_XI_15N127W
15	23.73 / 249.57	S from Ceraunius Fossae	P05_002829_2046_XN_24N110W
16	23.03 / 249.88	S from Ceraunius Fossae	P05_002829_2046_XN_24N110W
17	20.17 / 249.20	S from Ceraunius Fossae	P08_004029_2000_XN_20N110W
18	25.53 / 250.22	S from Ceraunius Fossae	P06_003396_2048_XN_24N109W
19	28.75 / 250.74	S from Ceraunius Fossae	P04_002763_2080_XN_28N109W
20	17.79 / 246.45	S from Ceraunius Fossae	P08_004306_1974_XI_17N113W
21	17.87 / 243.55	S from Ceraunius Fossae	P17_007853_1982_XI_18N116W
22	25.74 / 248.18	S from Ceraunius Fossae	P13_006007_2053_XI_25N111W
23	24.65 / 248.22	S from Ceraunius Fossae	P13_006007_2053_XI_25N111W
24	17.89 / 247.06	S from Ceraunius Fossae	P15_007075_1980_XN_18N112W
25	35.98 / 265.25	Tempe Terra	P03_002024_2164_XN_36N094W
26	36.71 / 266.09	Tempe Terra	P22_009566_2169_XN_36N093W
27	38.18 / 267.97	Tempe Terra	P05_002881_2182_XN_38N092W
28	39.18 / 268.04	Tempe Terra	P05_002881_2182_XN_38N092W
29	35.51 / 272.05	Tempe Terra	P03_002182_2159_XN_35N088W
30	35.67 / 271.86	Tempe Terra	P03_002182_2159_XN_35N088W
31	33.66 / 277.33	Tempe Terra	P18_008234_2139_XN_33N082W
32	36.54 / 271.51	Tempe Terra	P20_008867_2168_XI_36N088W
33	37.04 / 270.88	Tempe Terra	P20_009012_2174_XI_37N089W
34	-8.65 / 240.08	Caldera of Arsia Mons	P03_002157_1709_XN_09S119W
35	-8.44 / 240.11	Caldera of Arsia Mons	P03_002157_1709_XN_09S119W
36	-8.34 / 240.2	Caldera of Arsia Mons	P03_002157_1709_XN_09S119W
37	-9.66 / 239.17	Caldera of Arsia Mons	P21_009343_1702_XN_09S120W
38	-9.77 / 239.18	Caldera of Arsia Mons	P21_009343_1702_XN_09S120W
39	-9.04 / 239.75	Caldera of Arsia Mons	P04_002513_1709_-9_03x239_756
40	-2.71 / 252.48	S from Pavonis Mons	P12_005730_1791_XI_00S107W
41	-1.23 / 250.98	S from Pavonis Mons	P07_003673_1774_XN_02S108W
42	-3.89 / 247.17	S from Pavonis Mons	P20_008934_1756_XI_04S112W
43	-4.33 / 247.4	S from Pavonis Mons	P20_008934_1756_XI_04S112W
44	-4.96 / 247.42	S from Pavonis Mons	P20_008934_1756_XI_04S112W
45	-2.41 / 252.04	S from Pavonis Mons	P02_001906_1776_XI_02S108W
46	-6.51 / 246.72	S from Pavonis Mons	P20_008789_1735_XN_06S113W
47	-5.18 / 250.39	S from Pavonis Mons	P22_009725_1750_XI_05S109W
48	-5.42 / 250.23	S from Pavonis Mons	P22_009725_1750_XI_05S109W
49	-5.69 / 250.57	S from Pavonis Mons	P22_009725_1750_XI_05S109W
50	-0.93 / 252.17	S from Pavonis Mons	P08_004095_1790_XI_01S107W
51	0.3 / 252.12	S from Pavonis Mons	P08_004095_1790_XI_01S107W
52	2.49 / 259.6	S from Pavonis Mons	P19_008538_1827_XN_02N100W
53	2.42 / 259.59	S from Pavonis Mons	P19_008538_1827_XN_02N100W
54	-16.51 / 260.75	Syria Planum	P13_006244_1654_XN_14S099W
55	-14.74 / 259.17	Syria Planum	P06_003554_1651_XI_14S100W
56	-15.22 / 259.22	Syria Planum	P06_003554_1651_XI_14S100W
57	-14.34 / 258.97	Syria Planum	P21_009105_1641_XI_15S100W
58	-16.01 / 259.08	Syria Planum	P21_009105_1641_XI_15S100W
59	-14.62 / 258.62	Syria Planum	P06_003264_1642_XN_15S101W
60	-16.71 / 258.97	Syria Planum	P06_003264_1642_XN_15S101W

11.2. Investigated parameters of low shield volcanoes

Table A.2. Volumes, slopes and morphological characteristics of the summit areas of respective low shield volcanoes (s - single vent, m – multi vents, f – fracture).

ID	Region	Area of crater count (km^2)	Area of volume count (km^2)	Mean relief (m)	Mean slope (°)	Volume (km^3)	Vent	Direction N (°)	Age (My)	Resurfacing
1	N from Biblis Patera	105.48	103.514	44	0.44	1.5211	s	-	196	None
2	N from Biblis Patera	18.71	15.178	45	1.16	0.2253	s	-	215	None
3	SE from Olympus Mons	394.18	393.379	55	0.28	7.1750	f	132,2/109,2	59	None
4	SE from Olympus Mons	115.11	-	-	-	-	f	145.2	51.8	None
5	SE from Olympus Mons	638.49	640.735	56	0.22	11.9689	f	139,7/115,2	68.2	None
6	SE from Olympus Mons	60.32	60.35	9	0.11	0.1767	s/f	117.7	74.7	None
7	SE from Olympus Mons	242.11	231	33	0.22	2.5619	m	163.5	53.2	None
8	SE from Olympus Mons	46.22	45.896	12	0.18	0.1804	s	-	93	None
9	SE from Olympus Mons	406.74	393.44	17	0.09	2.2400	f	115.1	54.3	94.6
10	SE from Olympus Mons	1722.56	-	-	-	-	f	70.6	61.9	None
11	SE from Olympus Mons	39.02	33.131	21	0.38	0.2350	s	124.2	85.9	None
12	SE from Olympus Mons	258.42	246.931	12	0.08	1.0015	f	46.2	73.5	None
13	SE from Olympus Mons	222.55	226.415	13	0.09	1.0015	f	29.9	53.8	93.7
14	SE from Olympus Mons	44.27	39.586	35	0.56	0.4606	s/f	111.4	111	None
15	S from Ceraunius Fossae	271.82	271.96	17	0.10	1.5273	s	-	57.6	None
16	S from Ceraunius Fossae	787.94	-	-	-	-	s	-	68.8	None
17	S from Ceraunius Fossae	635.48	-	-	-	-	s	-	70	None
18	S from Ceraunius Fossae	1172.39	-	-	-	-	s	-	57.4	None
19	S from Ceraunius Fossae	234.52	325.305	46	0.26	5.0133	s	-	99.4	62.3
20	S from Ceraunius Fossae	601.9	755.86	31	0.11	7.8120	m	-	106	none
21	S from Ceraunius Fossae	1595.99	-	-	-	-	f	38	104	276
22	S from Ceraunius Fossae	123.92	164.666	28	0.22	1.5311	f	155.7	96.8	none
23	S from Ceraunius Fossae	582.28	665.76	50	0.20	11.0187	f	184.9	82.5	932
24	S from Ceraunius Fossae	1257.12	-	-	-	-	s	-	126	none
25	Tempe Terra	2932.502	2932.502	176	0.33	172.3780	m	53.5	1004	none
26	Tempe Terra	293.46	-	-	-	-	m	15.9	885	none
27	Tempe Terra	1202.67	-	-	-	-	s	-	601	none
28	Tempe Terra	382.27	287.021	23	0.14	2.2383	s	-	534	none
29	Tempe Terra	703.36	-				s	-	469	none
30	Tempe Terra	29.66	29.945	117	2.16	1.1630	m	41.2	930	none
31	Tempe Terra	139.66	134.56	124	1.09	5.5800	m	73.6	639	none
32	Tempe Terra	1501.51	-	-	-	-	m	69.4	394	980
33	Tempe Terra	1197.7	-	-	-	-	m/f	65.3	369	1180
34	Caldera of Arsia Mons	6.033	5.803	7	0.28	0.0128	s	-	397	none
35	Caldera of Arsia Mons	39.44	40.475	18	0.30	0.2494	s	-	89.5	none
36	Caldera of Arsia Mons	118.83	-	-	-	-	s	-	162	none
37	Caldera of Arsia Mons	56.8	53.41	70	0.97	1.2417	f	6.1	168	none
38	Caldera of Arsia Mons	35.08	33.941	18	0.31	0.2040	f	175.2	176	none
39	Caldera of Arsia Mons	160.18	-	-	-	-	s	-	76.8	none
40	S from Pavonis Mons	329.39	-	-	-	-	s	-	54.1	78.8
41	S from Pavonis Mons	304.05	324.501	67	0.38	7.2758	s	-	43.8	none
42	S from Pavonis Mons	816.65	-	-	-	-	s	-	67.8	none
43	S from Pavonis Mons	583.67	-	-	-	-	f	16.6	76.6	none
44	S from Pavonis Mons	319.15	324.849	71	0.40	7.6340	s	-	75.7	none
45	S from Pavonis Mons	562.08	615.566	121	0.50	24.8410	m	49.4	59.1	103
46	S from Pavonis Mons	694.57	-	-	-	-	s	-	105	none
47	S from Pavonis Mons	189.56	183.067	73	0.55	4.4778	s	138.2	73.8	none
48	S from Pavonis Mons	80.14	84.888	18	0.20	0.5167	m	90	75.6	none
49	S from Pavonis Mons	155.92	-	-	-	-	m	-	66.3	none
50	S from Pavonis Mons	590.83	570.512	125	0.53	23.7380	m	-	77.6	none
51	S from Pavonis Mons	76.27	71.629	42	0.50	1.0005	f	35.4	72.5	none
52	S from Pavonis Mons	12.25	-	-	-	-	f	6.8	68.6	none
53	S from Pavonis Mons	940.74	-	-	-	-	f	19.2	62.7	none
54	Syria Planum	214.24	-	-	-	-	s	-	2880	none
55	Syria Planum	493.6	490.961	129	0.59	21.1804	f	164.6	1340	none
56	Syria Planum	543.13	549.438	142	0.61	25.9855	f	176.1	2200	none
57	Syria Planum	630.48	631.072	141	0.57	29.5982	s	-	1660	none
58	Syria Planum	470.82	-	-	-	-	m	22.4	2690	none
59	Syria Planum	784.91	757.23	101	0.37	25.5938	s	-	1880	none
60	Syria Planum	367.47	396.853	40	0.20	5.2312	m	11.4	2360	none

b

11.3. Image catalogue of investigated low shield volcanoes

This catalogue contains all investigated low shield volcanoes in all clusters in *Tharsis* region. It is composed by two images for each volcano. First is *CTX* image with *ArcGIS* shapefile showing boundaries of volcanoes marked by yellow line. All these images are up north oriented with different scale (see each scale bar for detail). Second image is chronology curve produced by *CraterStats*. Few cases are red marked indicating unclear age of curve.

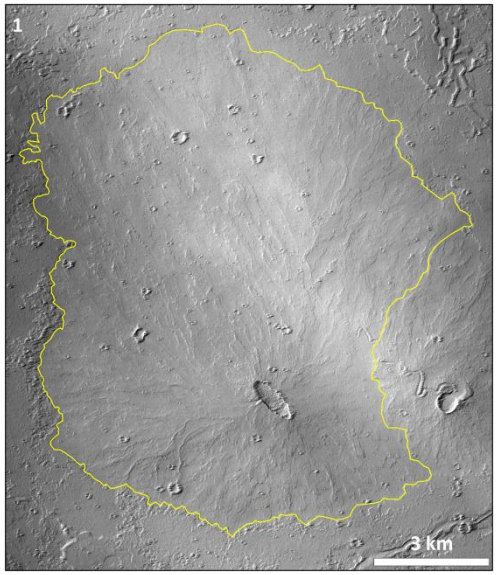

No. 1 (Northern from Biblis Patera)

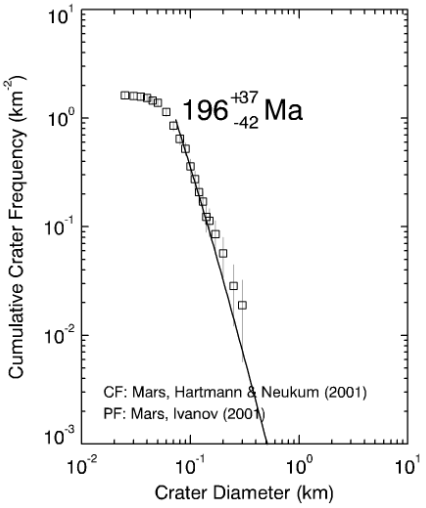

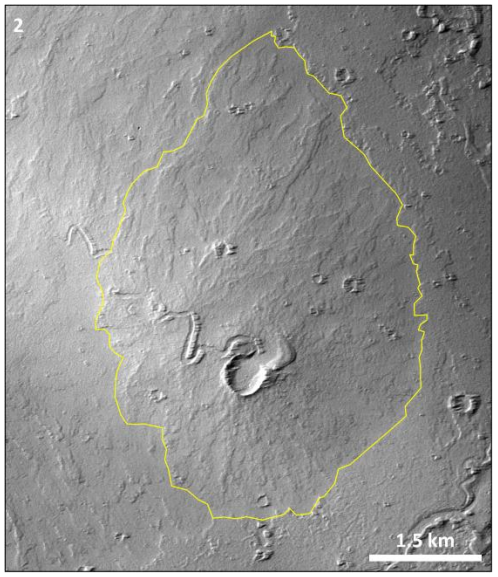

No. 2 (Northern from Biblis Patera)

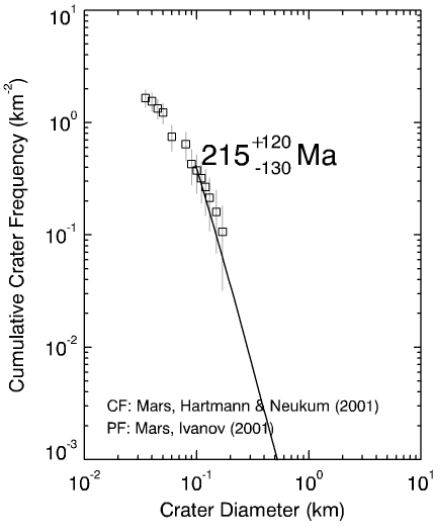

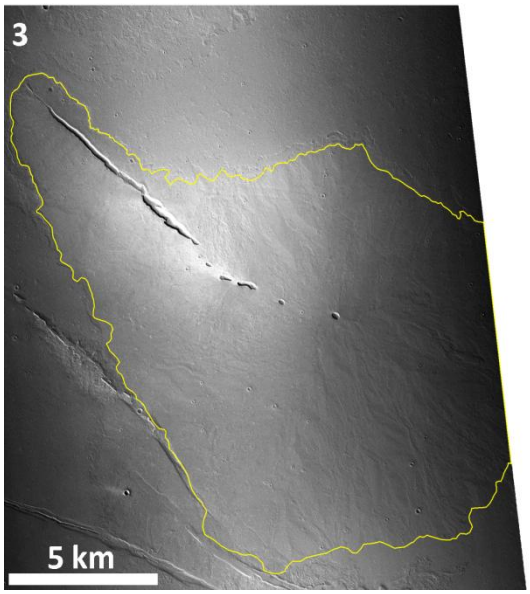

No. 3 (SE from Olympus Mons)

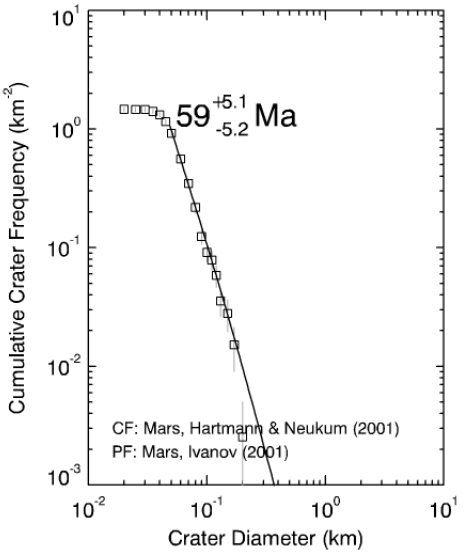

d

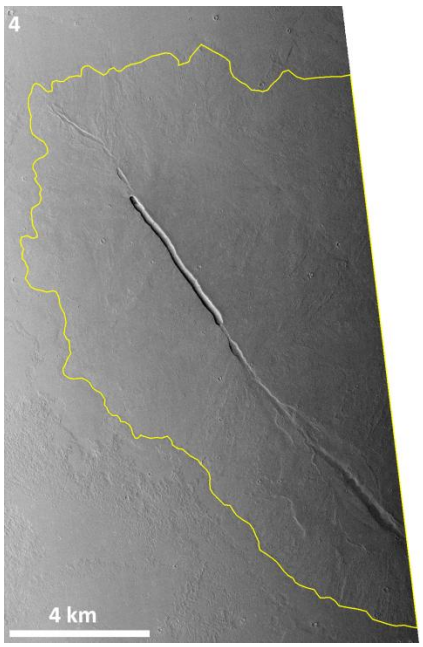

No. 4 (SE from Olympus Mons)

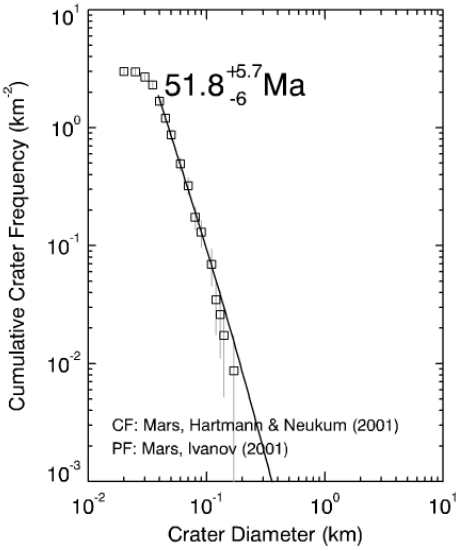

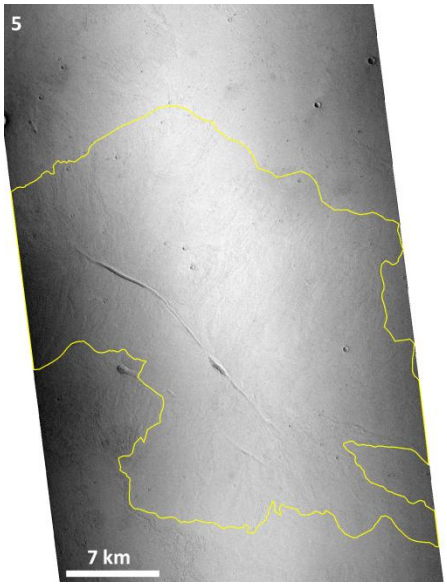

No. 5 (SE from Olympus Mons)

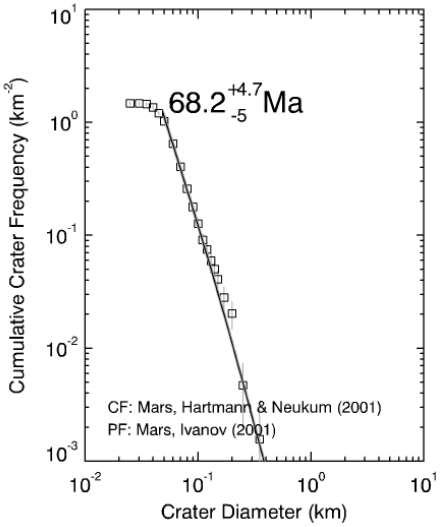

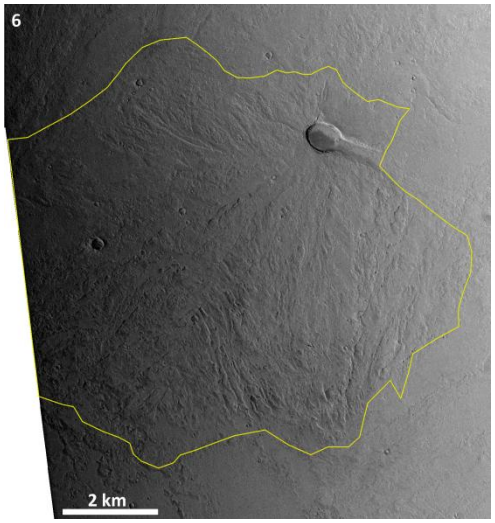

No. 6 (SE from Olympus Mons)

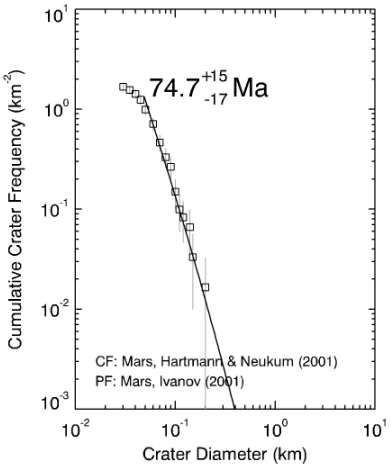

e

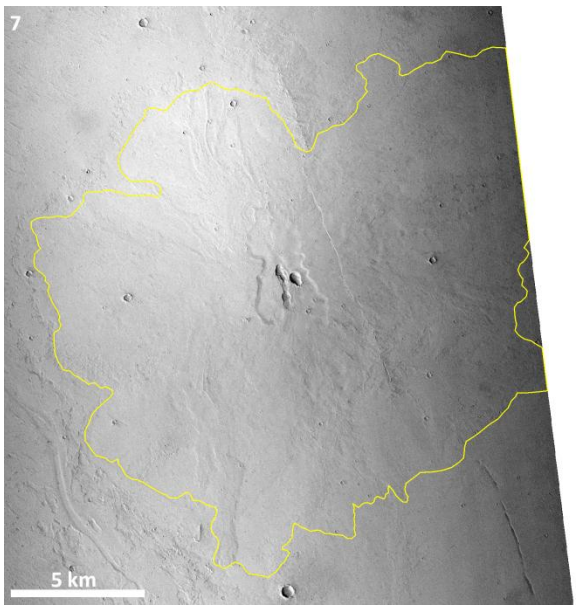

No. 7 (SE from Olympus Mons)

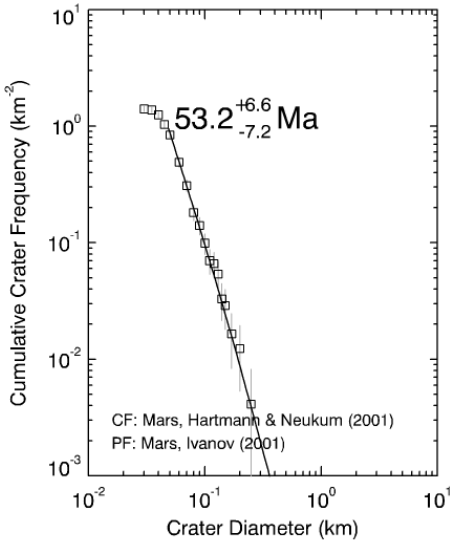

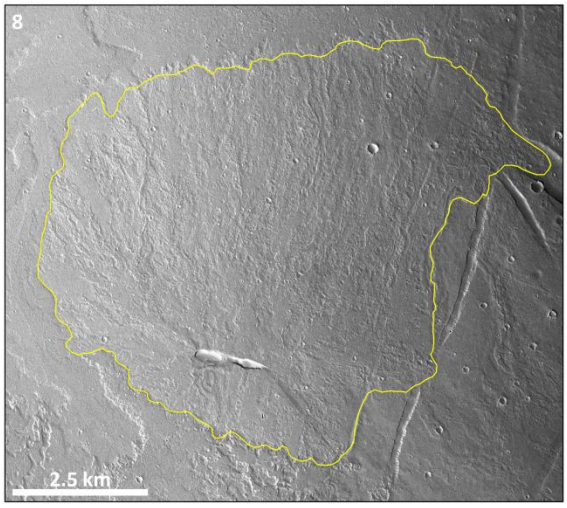

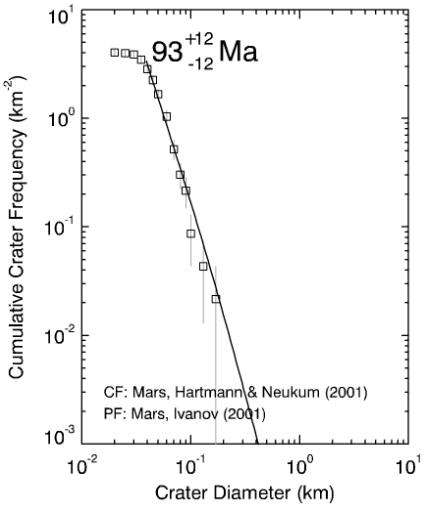

No. 8 (SE from Olympus Mons)

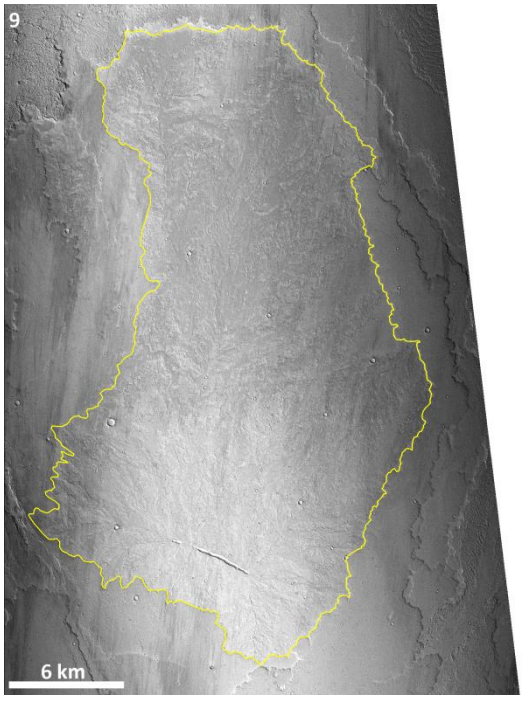

No. 9 (SE from Olympus Mons)

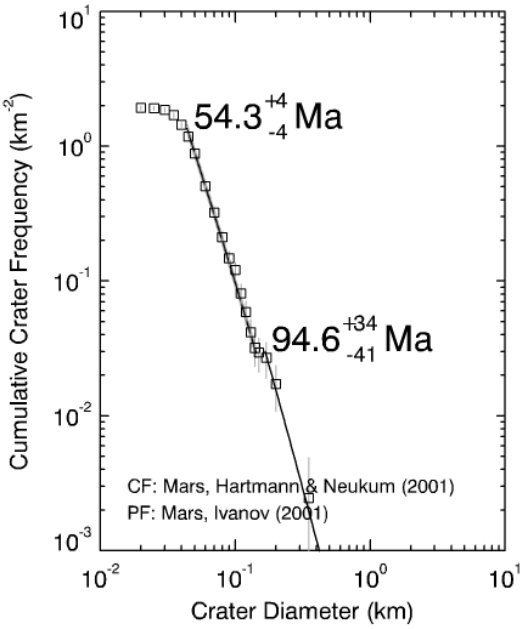

f

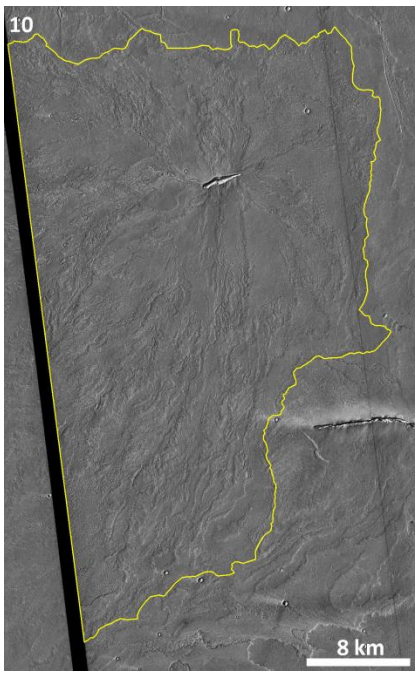

No. 10 (SE from Olympus Mons)

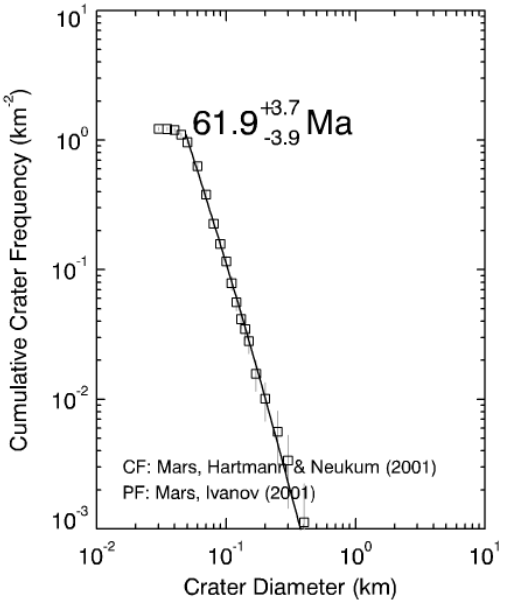

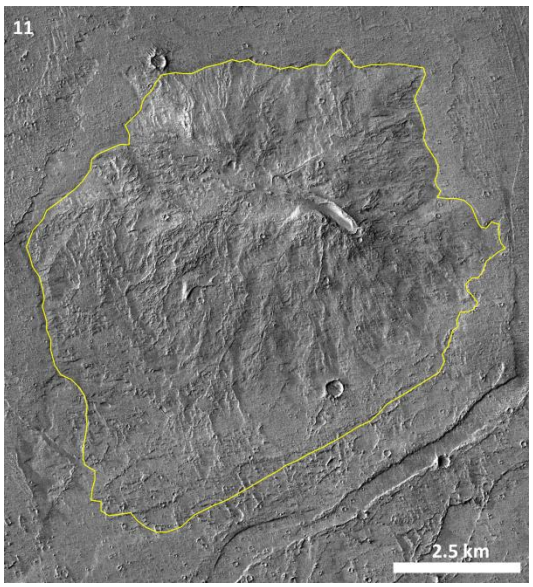

No. 11 (SE from Olympus Mons)

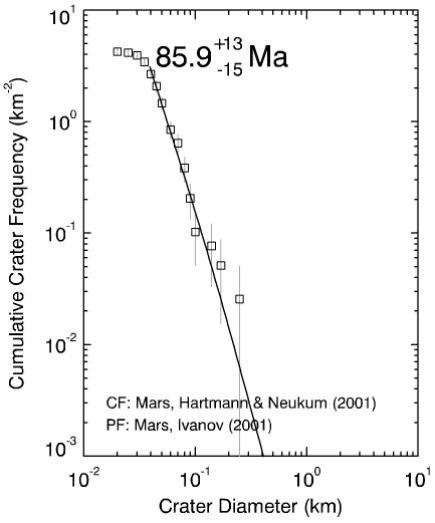

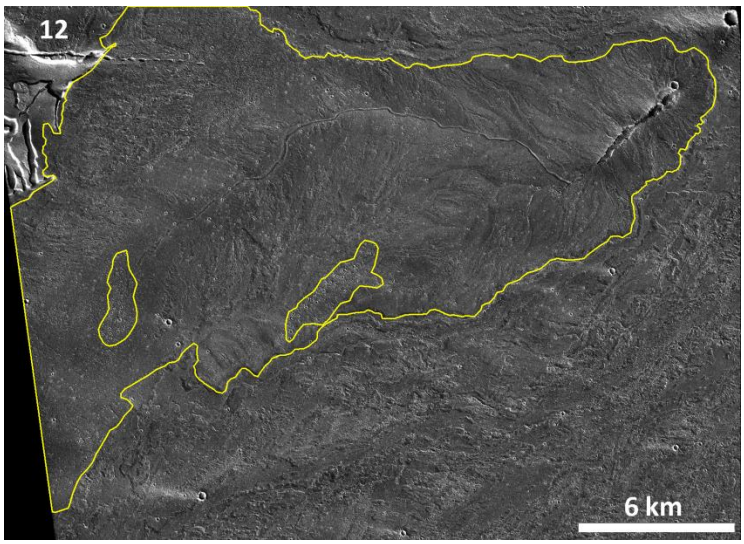

No. 12 (SE from Olympus Mons)

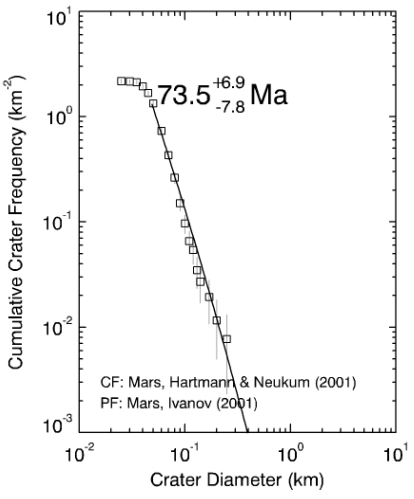

g

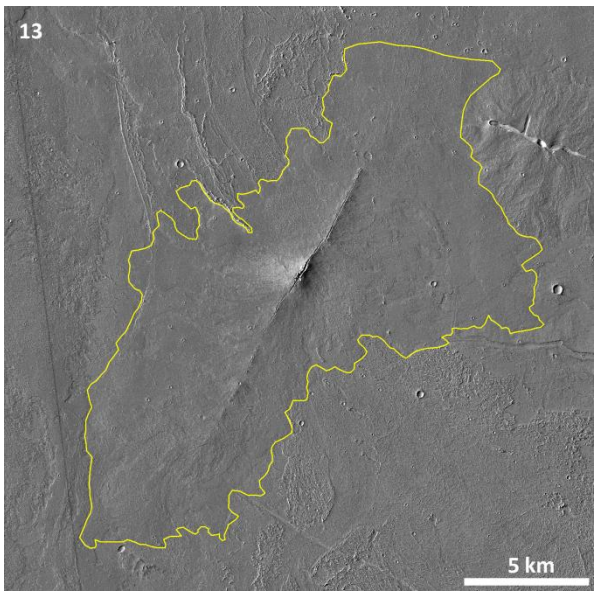

No. 13 (SE from Olympus Mons)

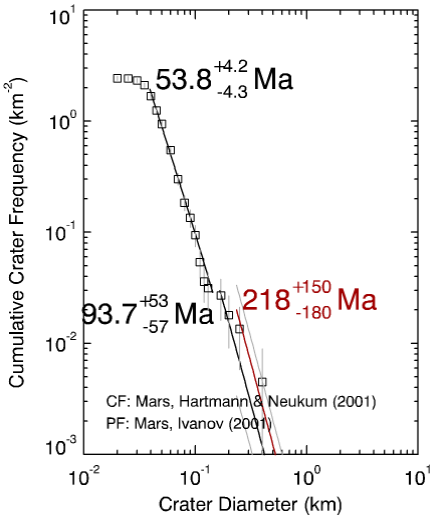

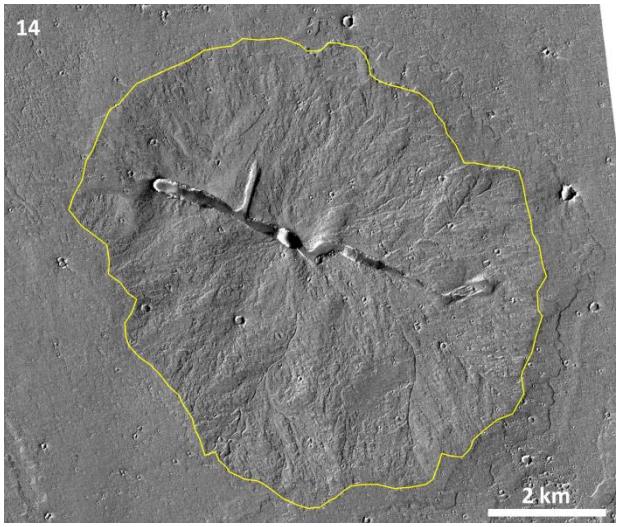

No. 14 (SE from Olympus Mons)

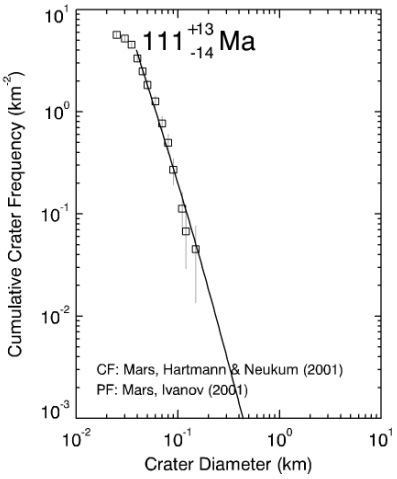

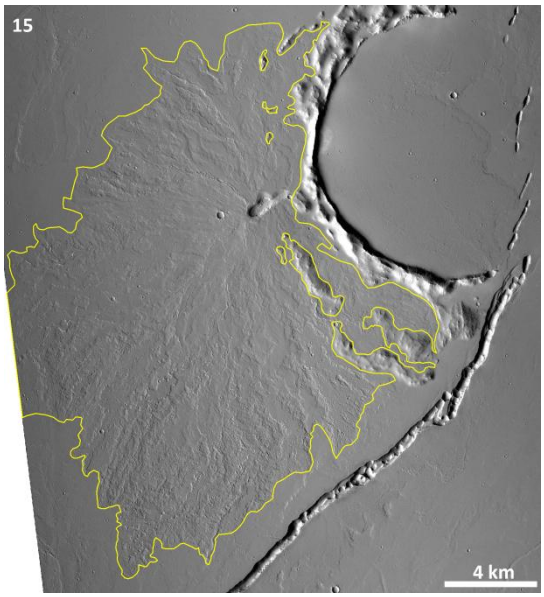

No. 15 (S from Ceraunius Fossae)

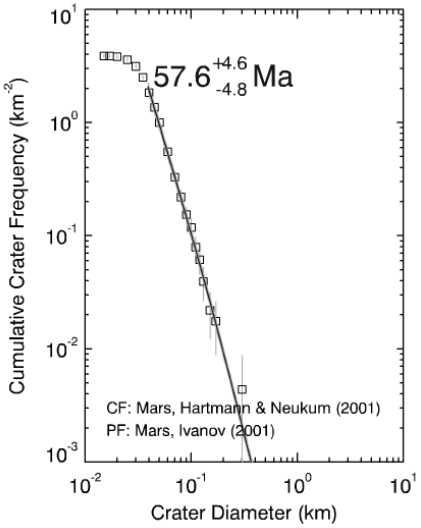

h

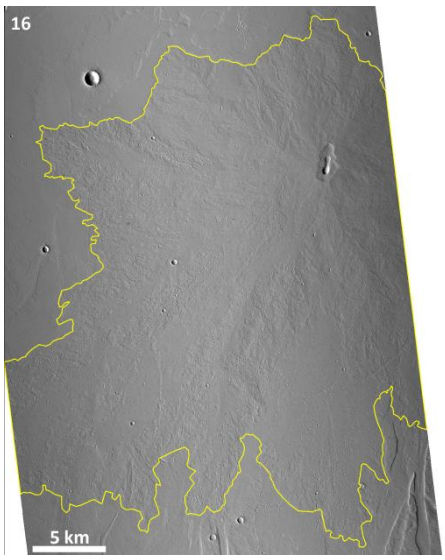

No. 16 (S from Ceraunius Fossae)

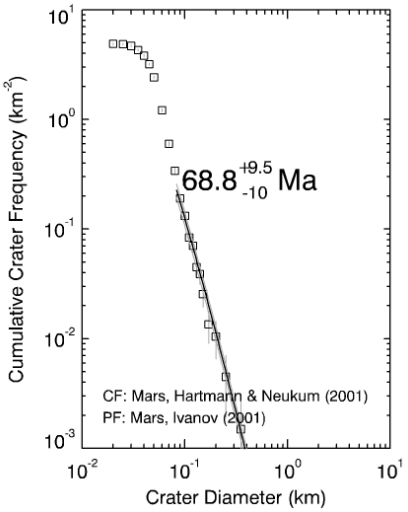

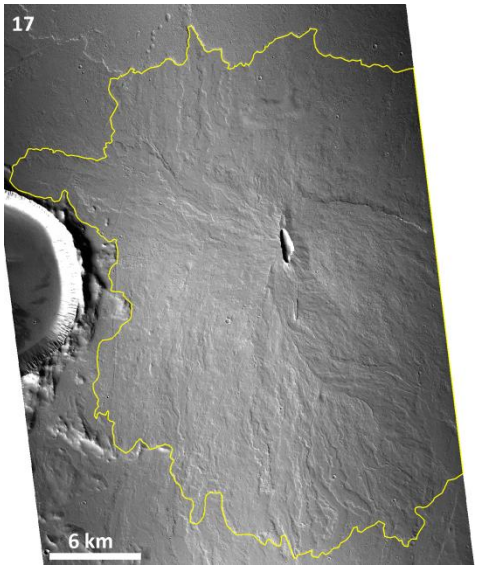

No. 17 (S from Ceraunius Fossae)

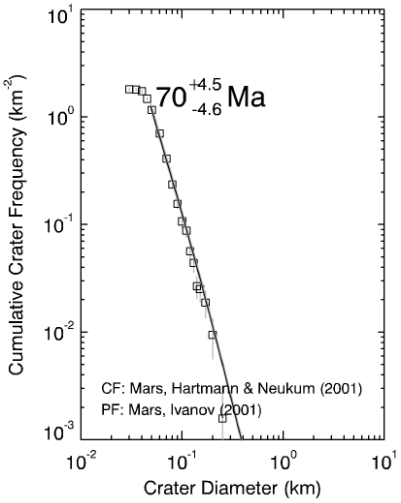

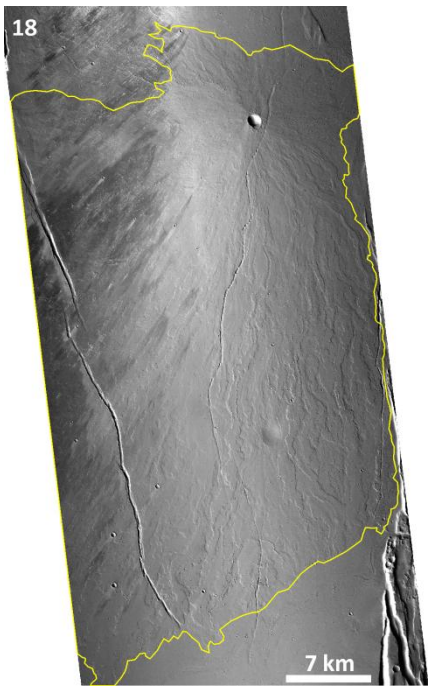

No. 18 (S from Ceraunius Fossae)

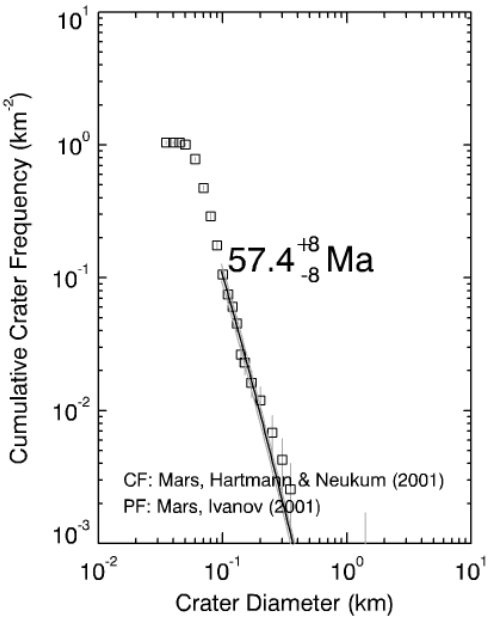

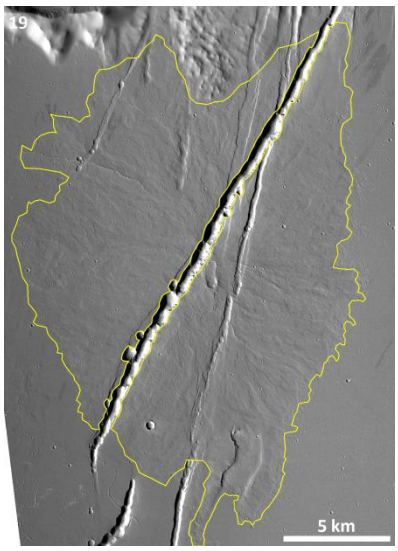

No. 19 (S from Ceraunius Fossae)

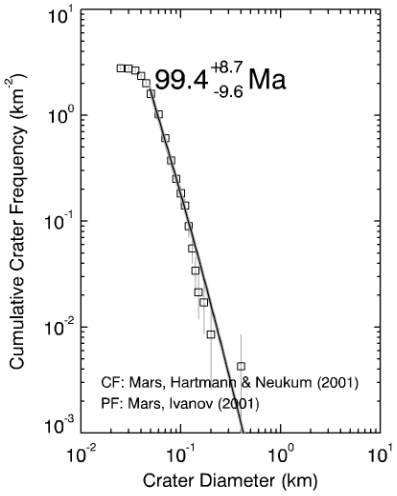

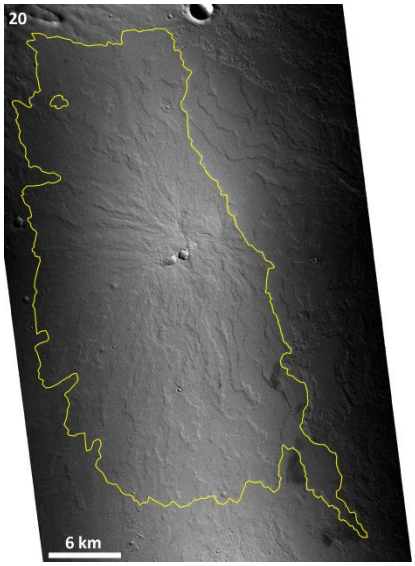

No. 20 (S from Ceraunius Fossae)

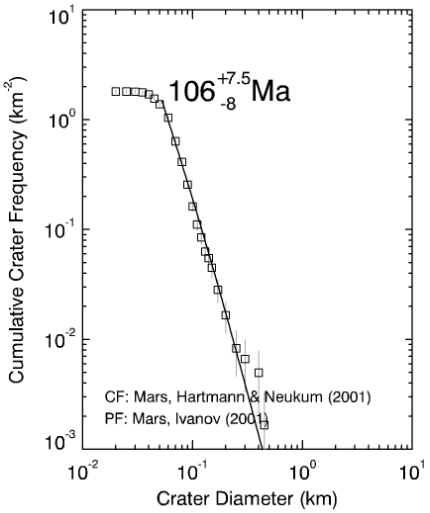

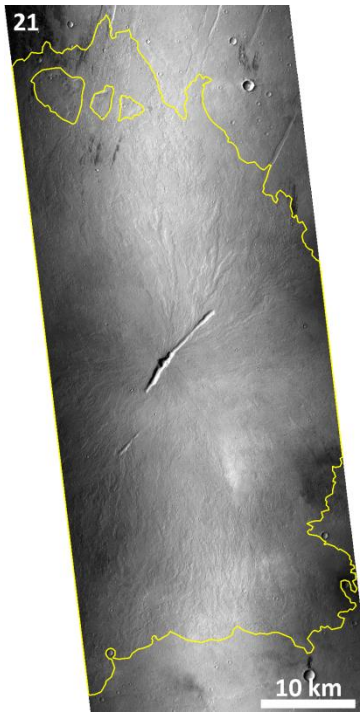

No. 21 (S from Ceraunius Fossae)

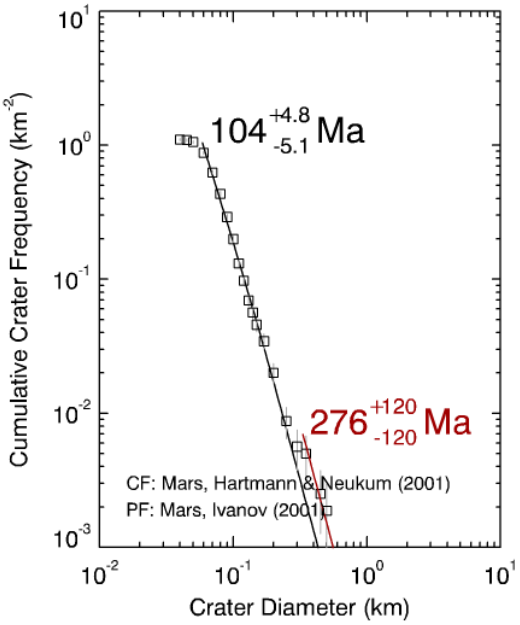

j

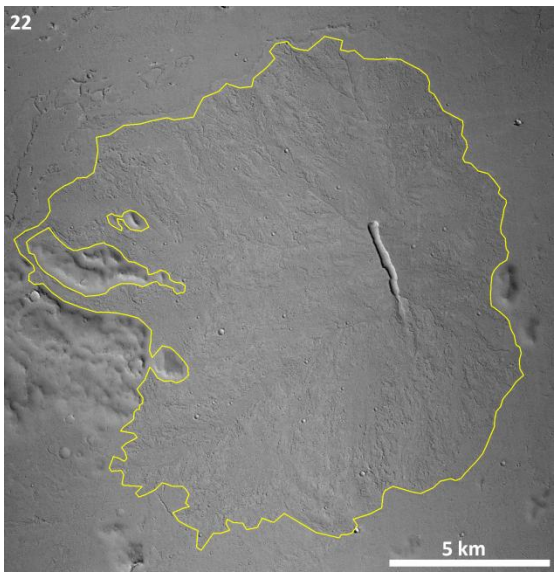

No. 22 (S from Ceraunius Fossae)

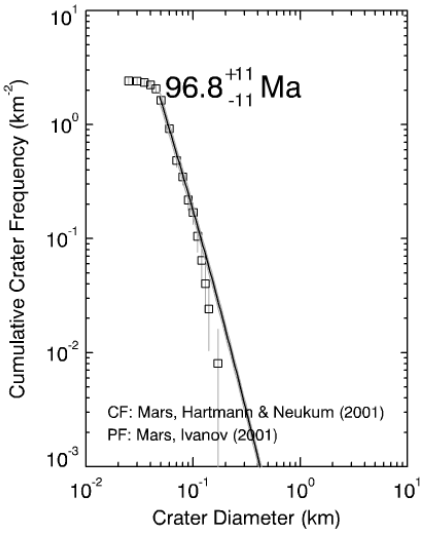

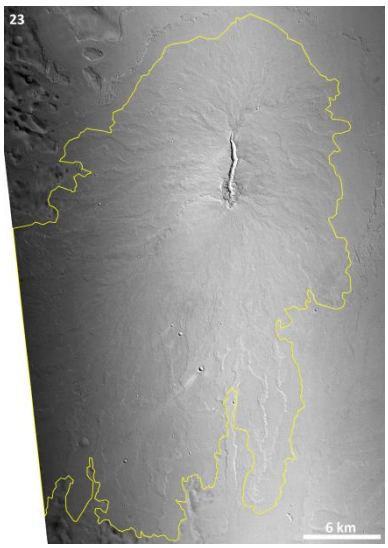

No. 23 (S from Ceraunius Fossae)

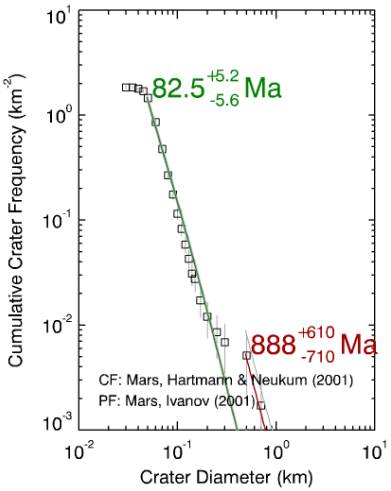

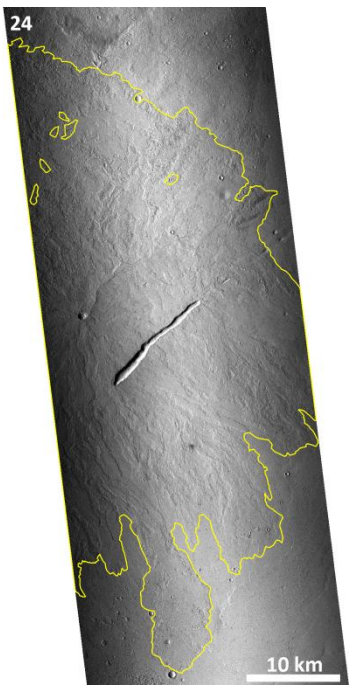

No. 24 (S from Ceraunius Fossae)

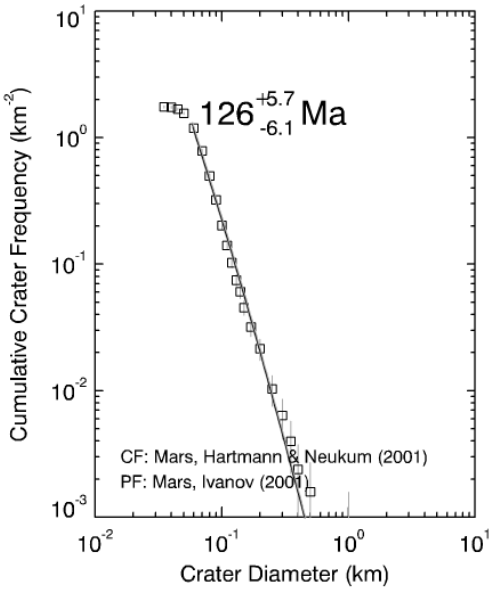

k

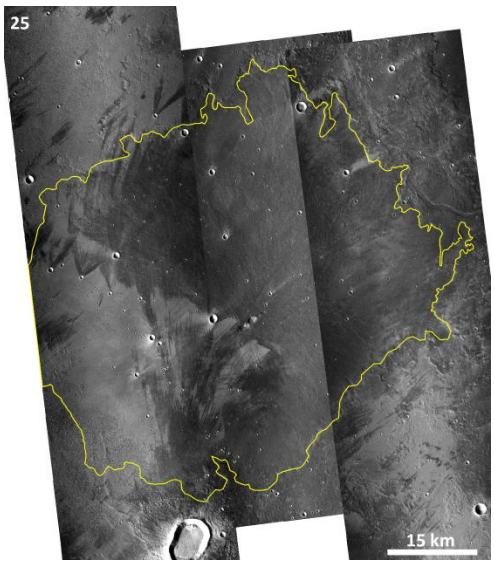

No. 25 (Tempe Terra)

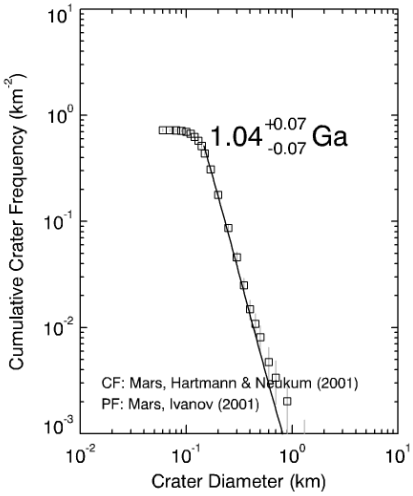

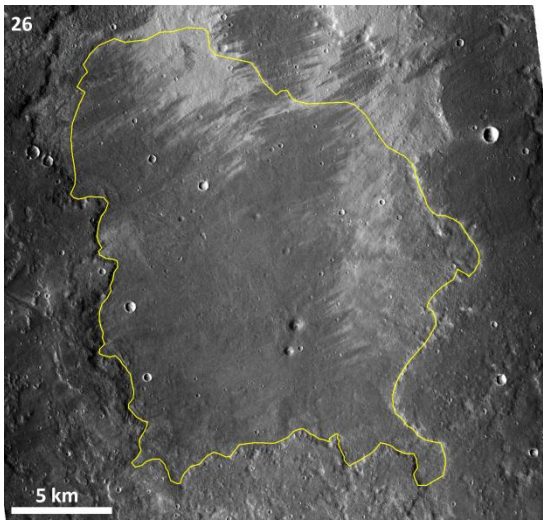

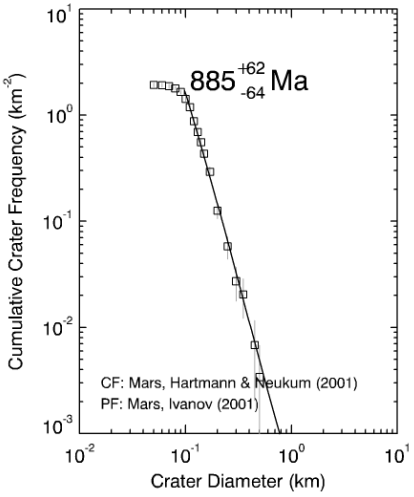

No. 26
(Tempe Terra)

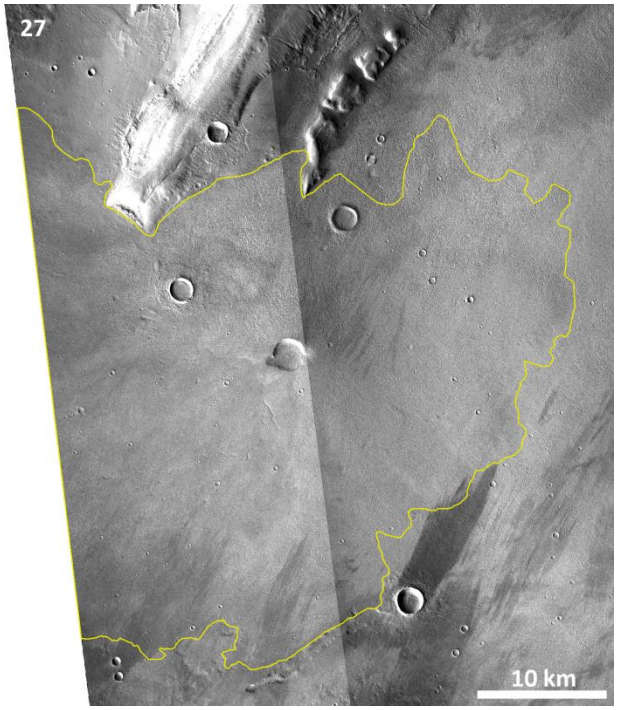

No. 27 (Tempe Terra)

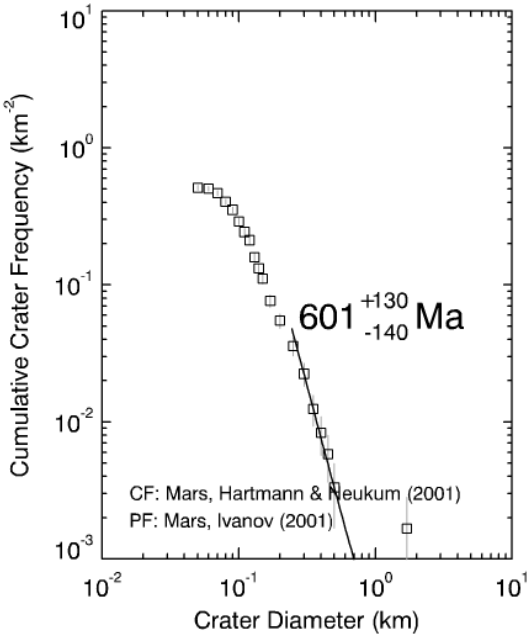

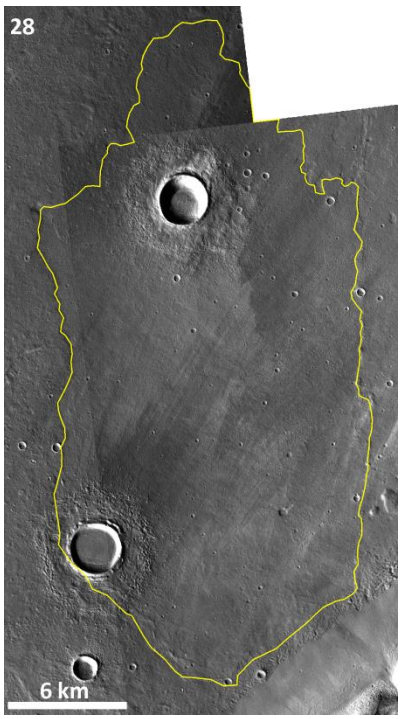

No. 28 (Tempe Terra)

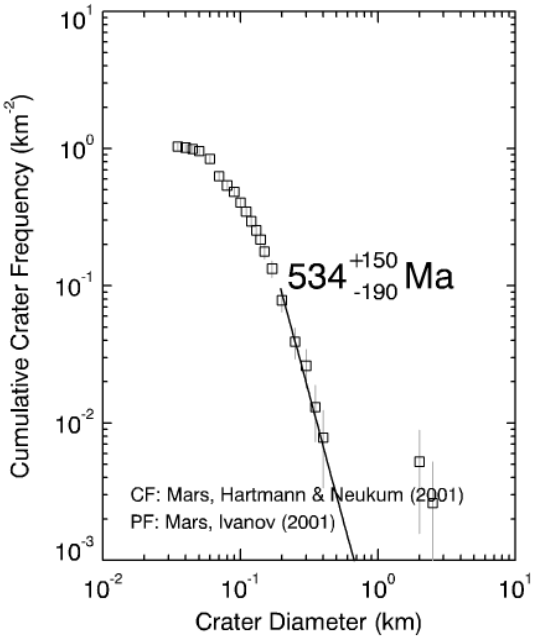

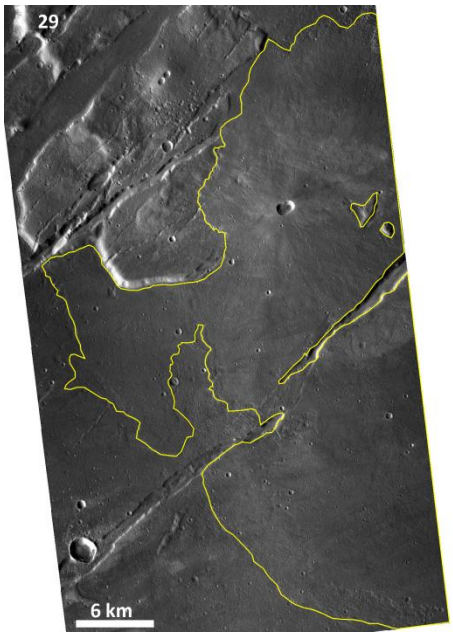

No. 29 (Tempe Terra)

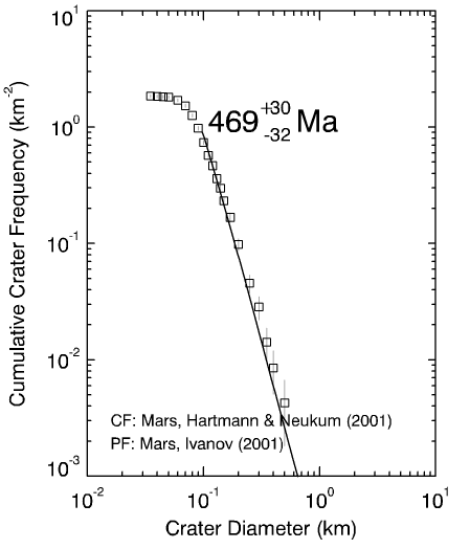

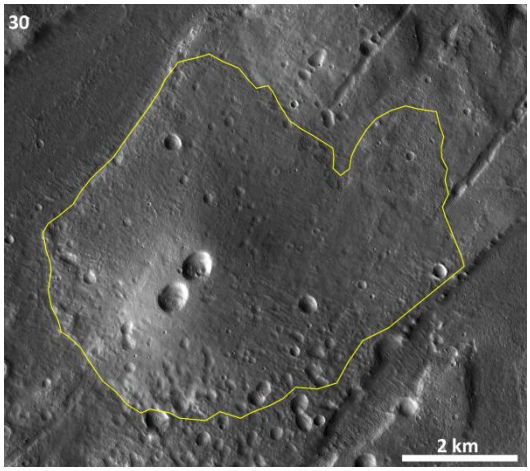

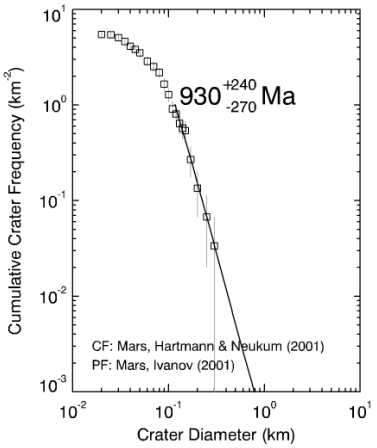

No. 30
(Tempe Terra)

m

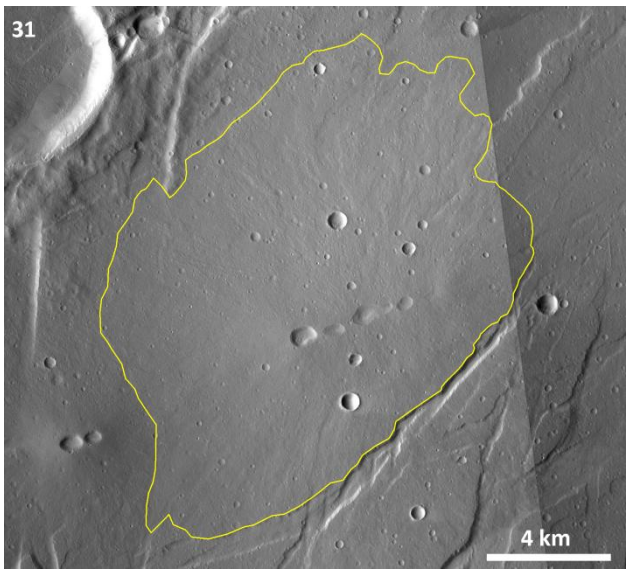

No. 31 (Tempe Terra)

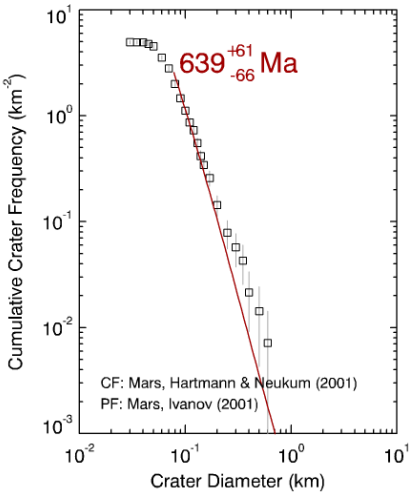

No. 32 (Tempe Terra)

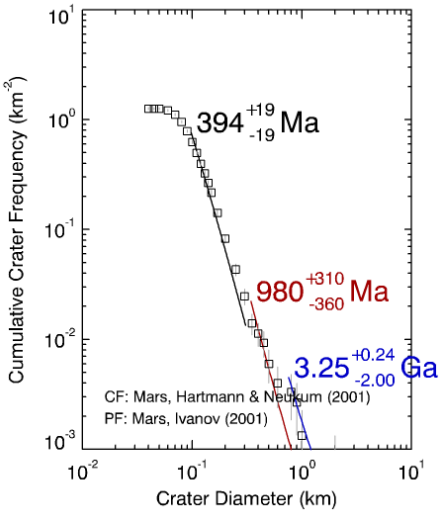

No. 33 (Tempe Terra)

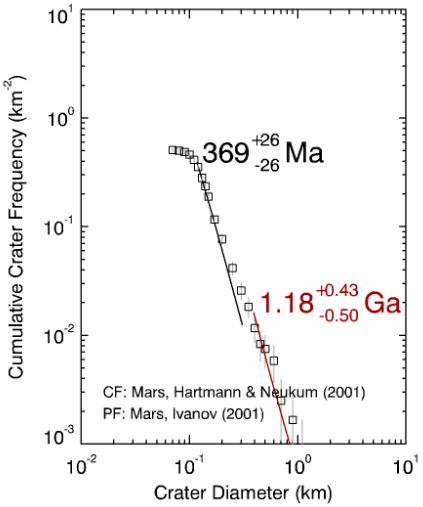

n

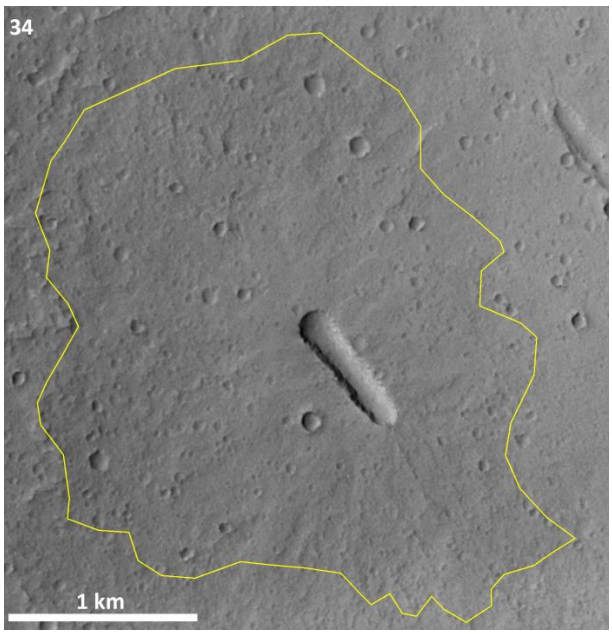

No. 34 (Caldera of Arsia Mons)

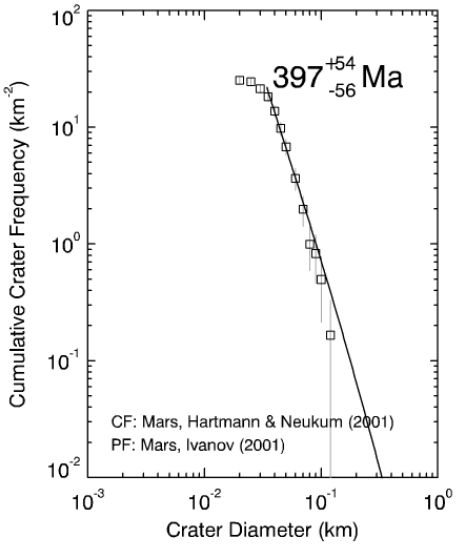

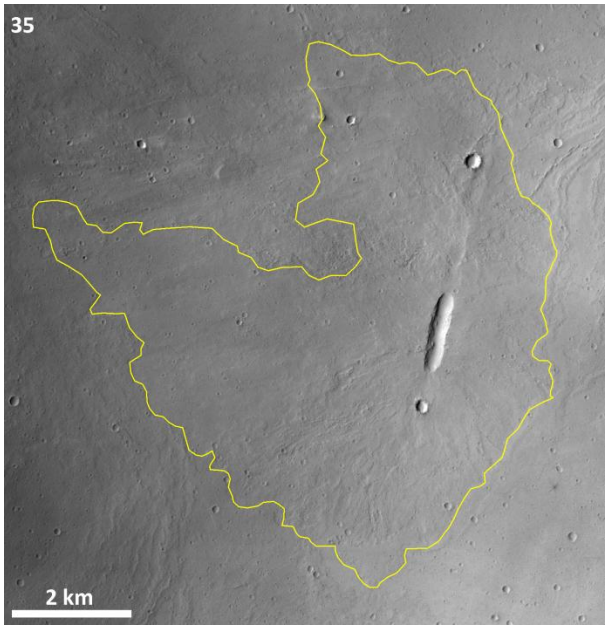

No. 35 (Caldera of Arsia Mons)

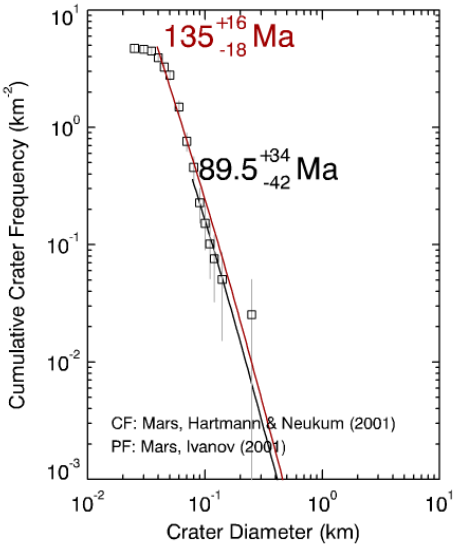

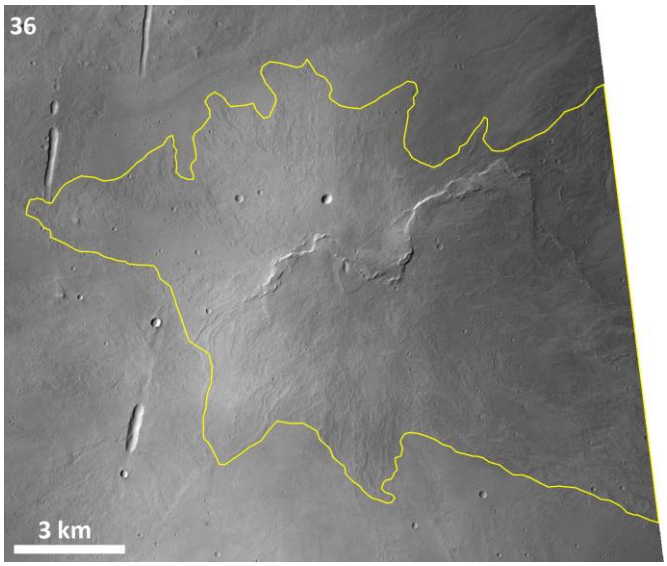

No. 36 (Caldera of Arsia Mons)

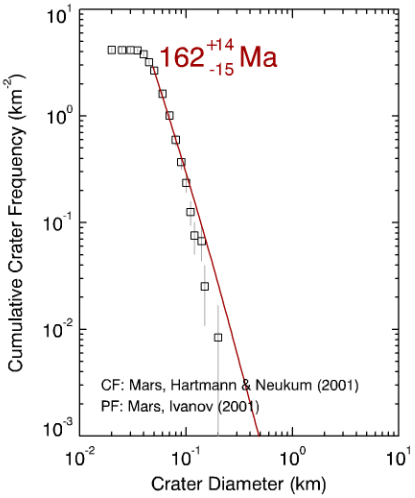

o

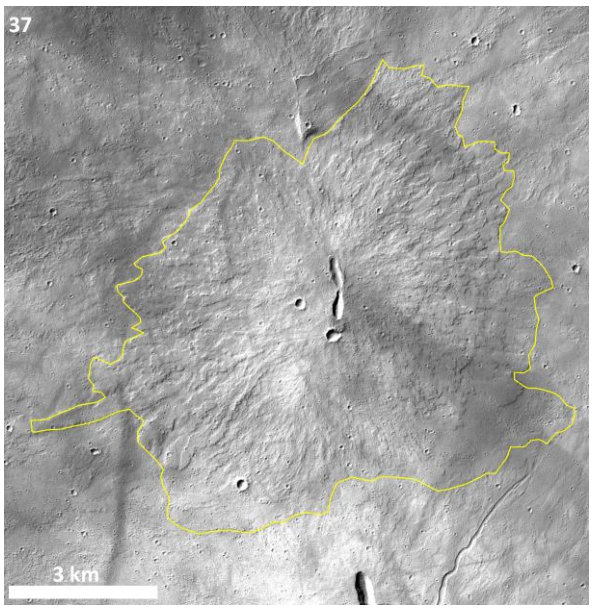

No. 37 (Caldera of Arsia Mons)

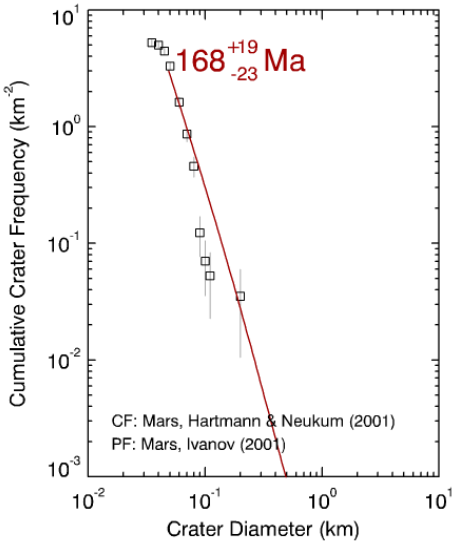

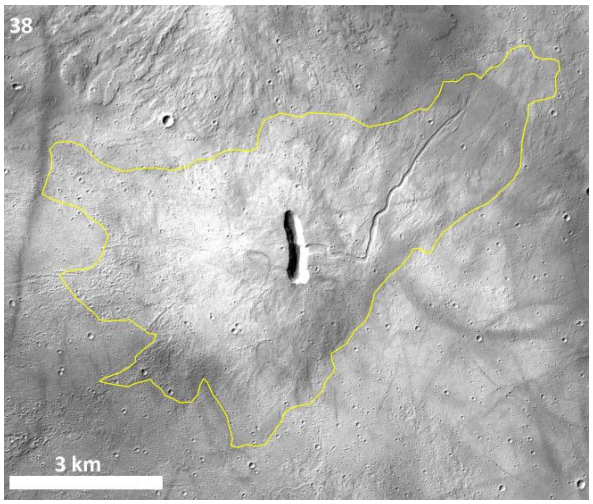

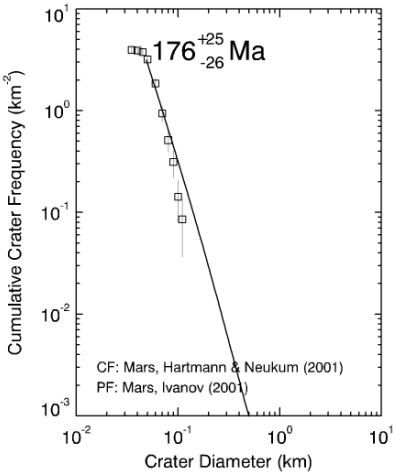

No. 38 (Caldera of Arsia Mons)

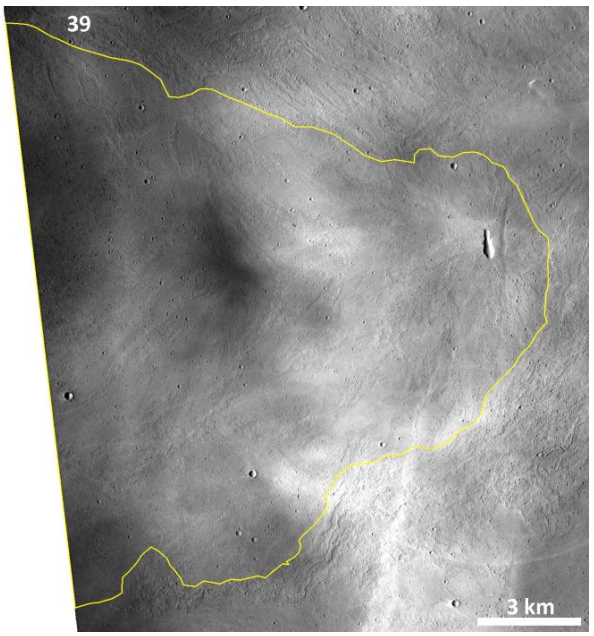

No. 39 (Caldera of Arsia Mons)

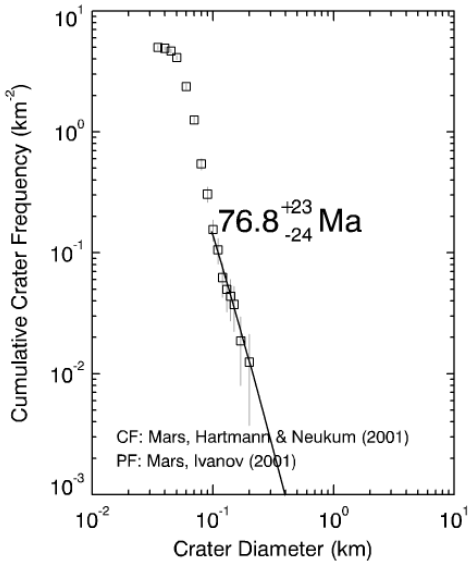

p

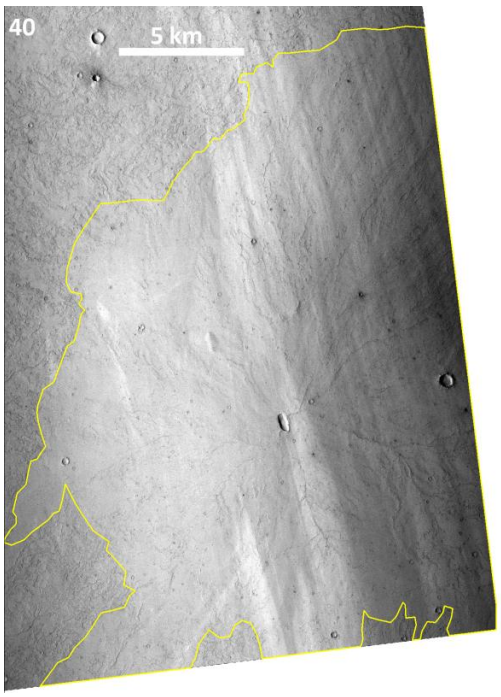

No. 40 (S from Pavonis Mons)

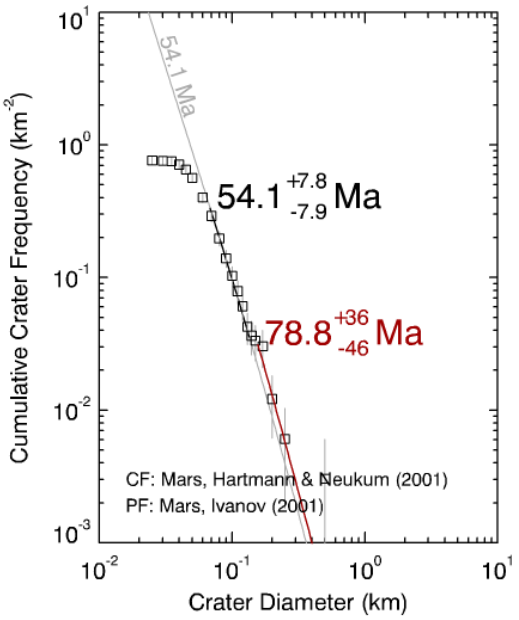

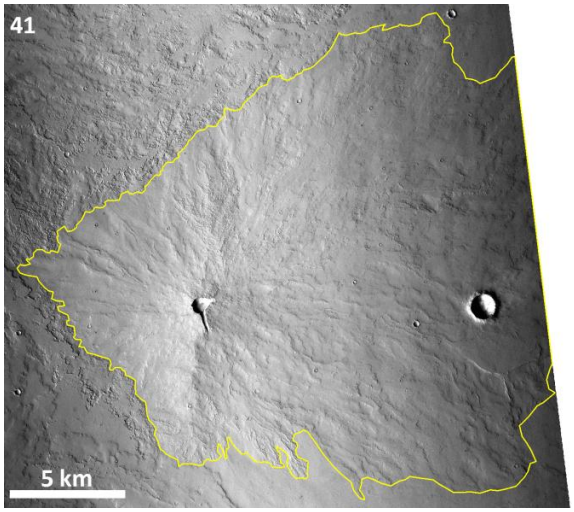

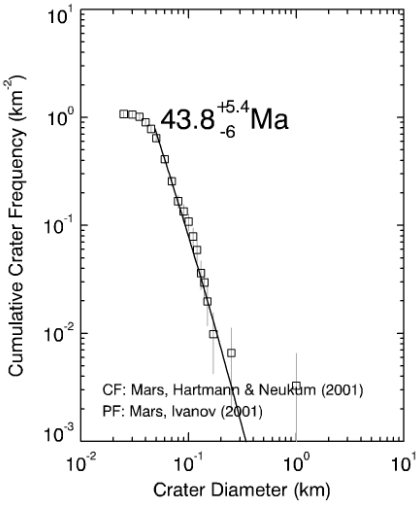

No. 41 (S from Pavonis Mons)

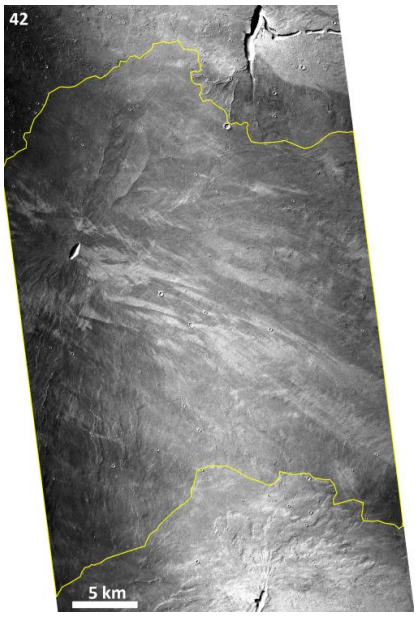

No. 42 (S from Pavonis Mons)

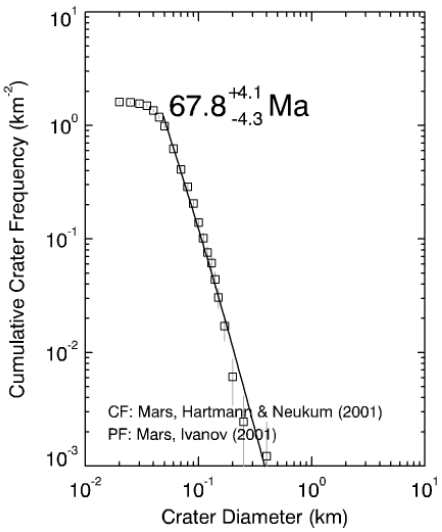

q

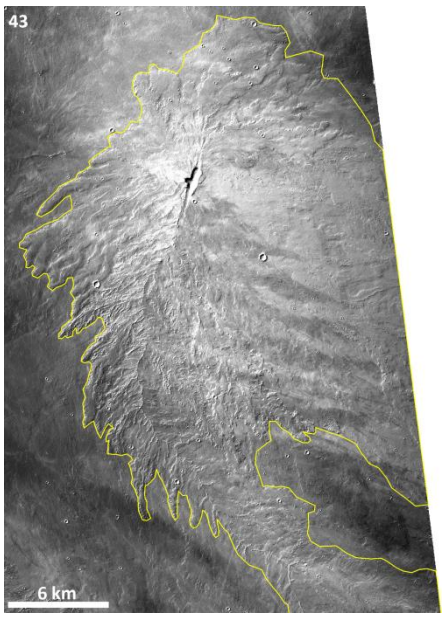

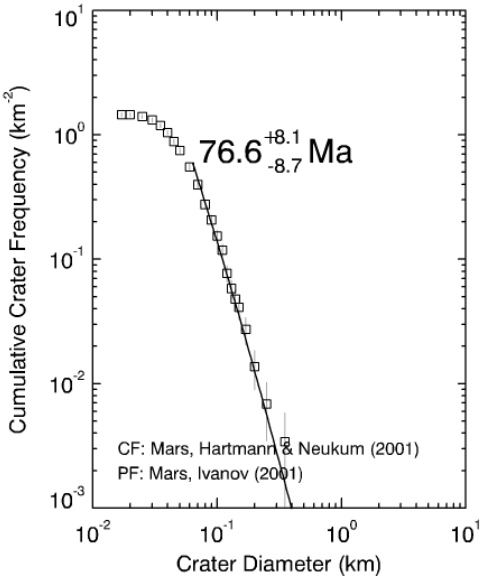

No. 43
(S from Pavonis Mons)

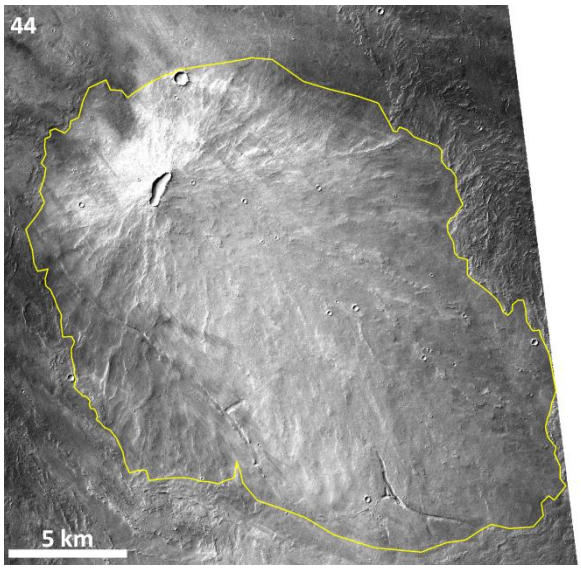

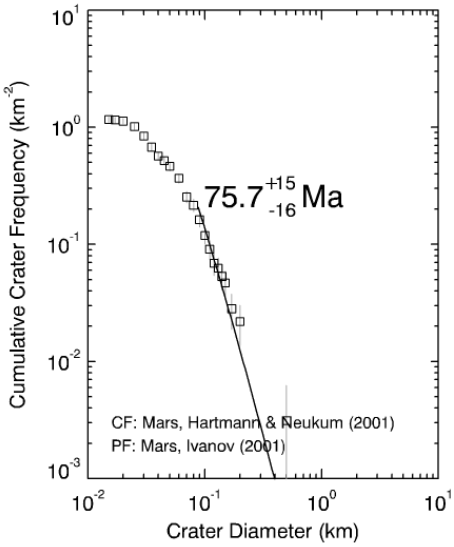

No. 44
(S from Pavonis Mons)

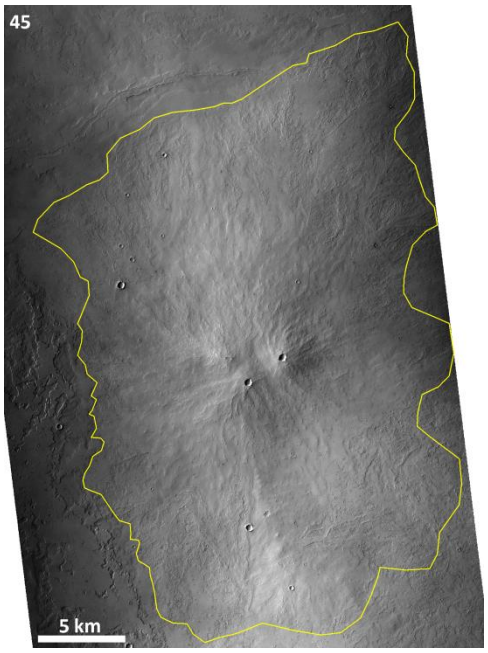

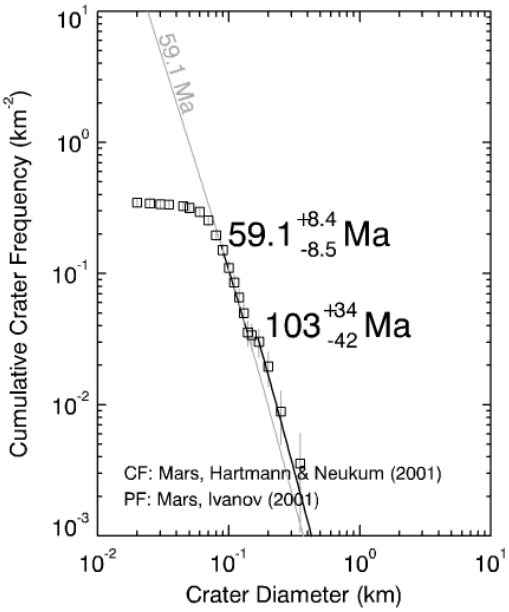

No. 45
(S from Pavonis Mons)

r

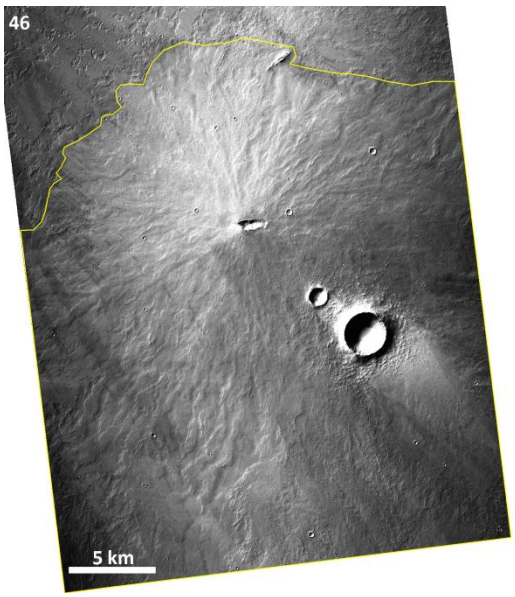

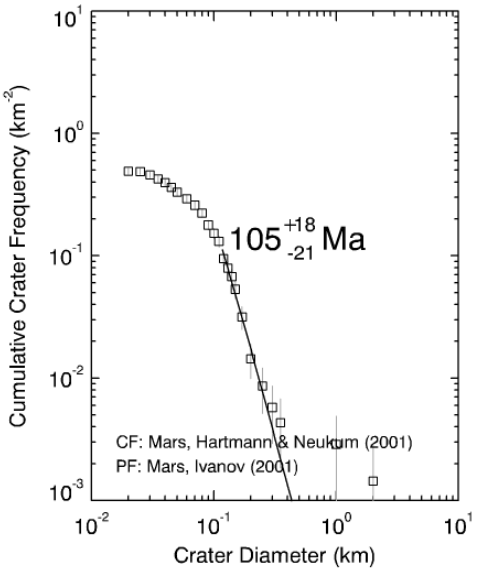

No. 46
(S from Pavonis Mons)

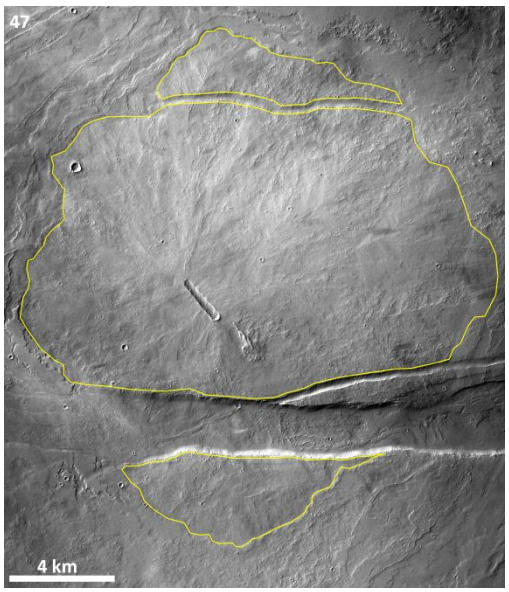

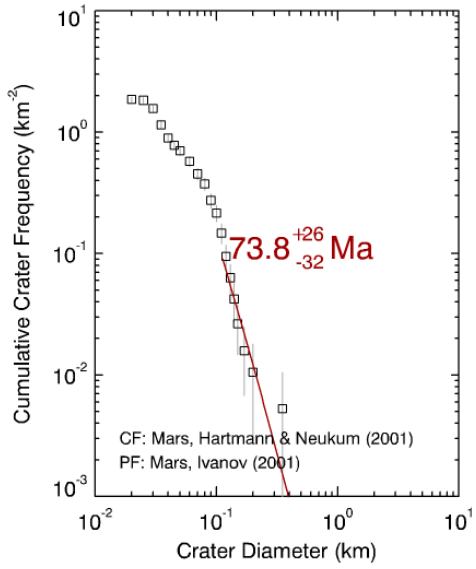

No. 47
(S from Pavonis Mons)

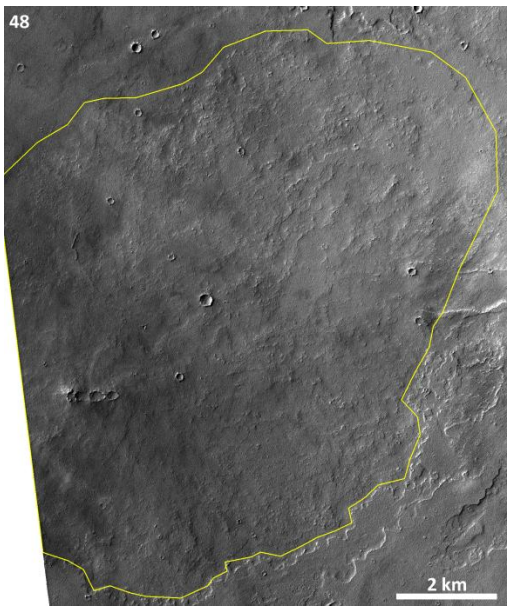

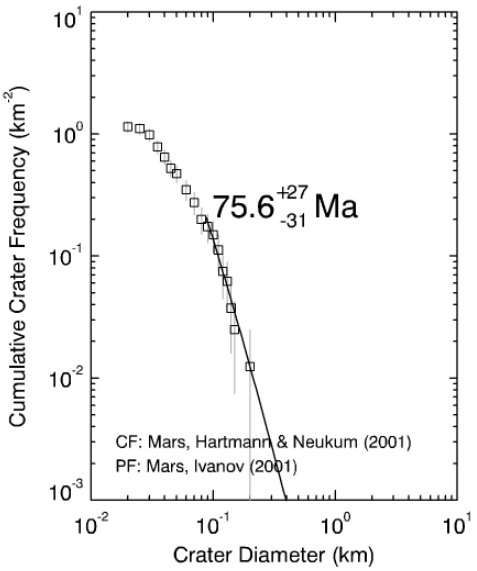

No. 48
(S from Pavonis Mons)

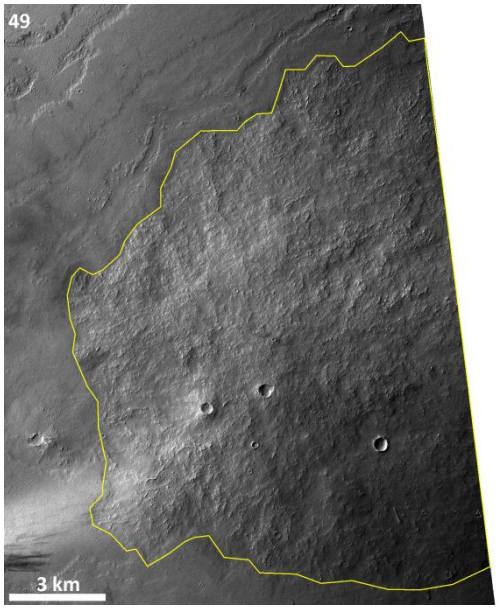

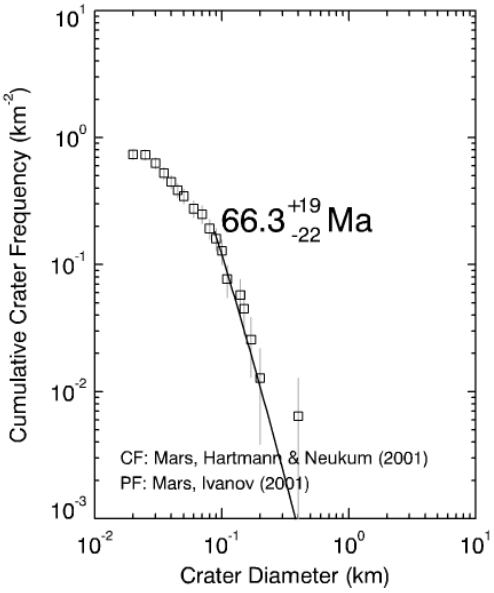

No. 49
(S from Pavonis Mons)

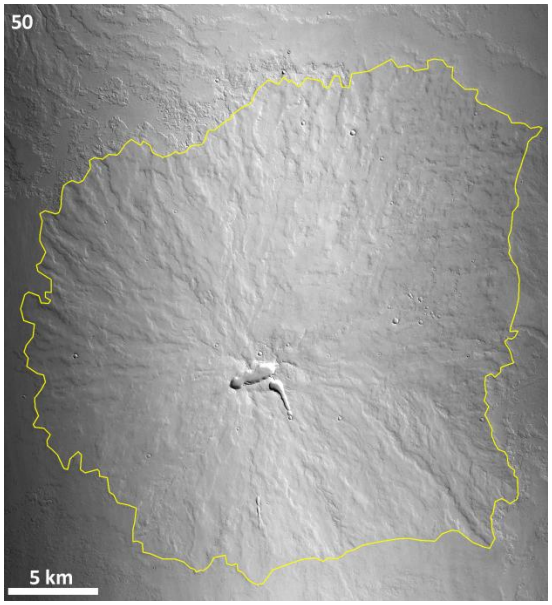

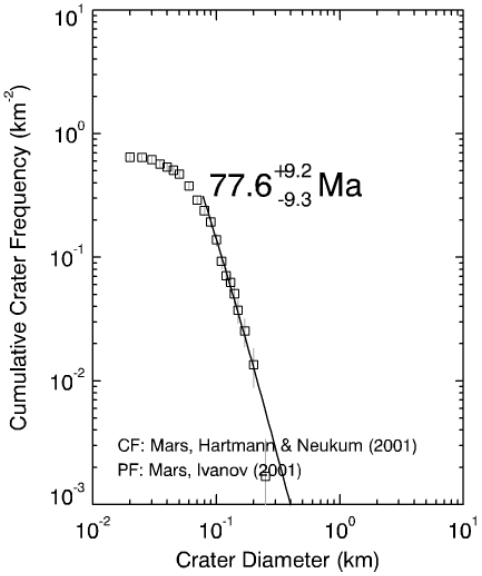

No. 50
(S from Pavonis Mons)

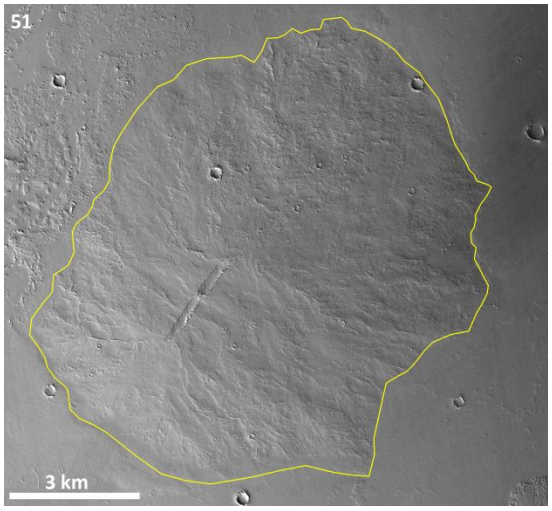

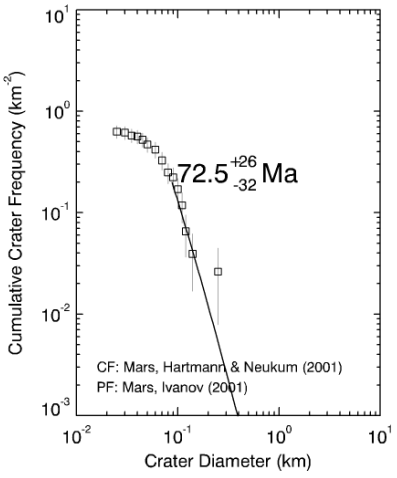

No. 51
(S from Pavonis Mons)

t

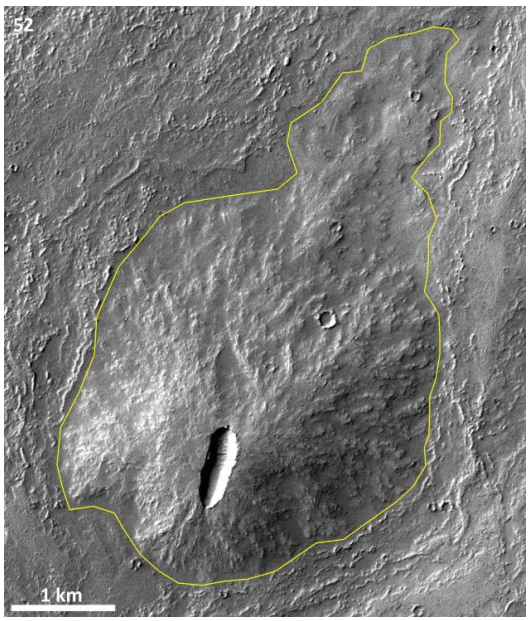

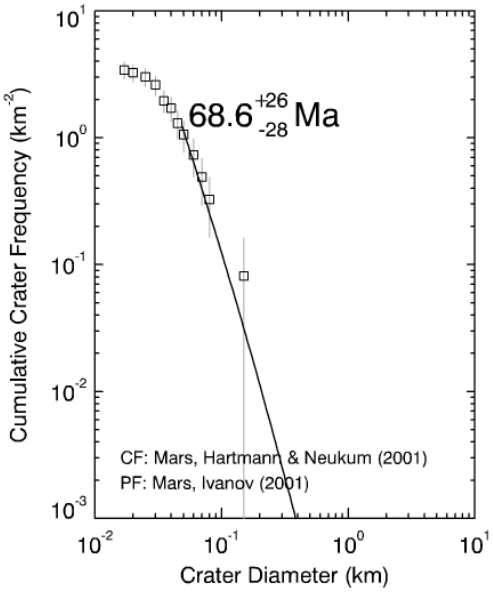

No. 52
(S from Pavonis Mons)

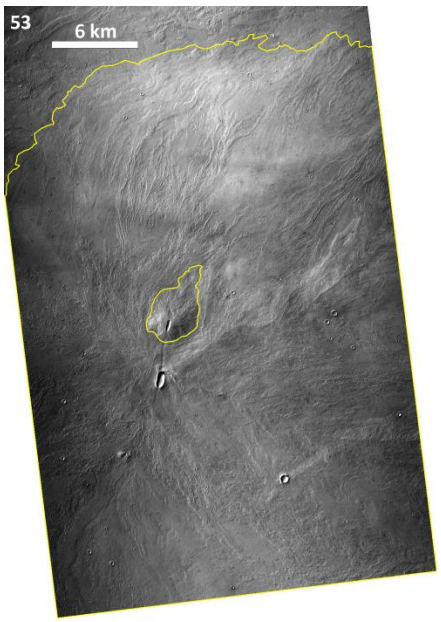

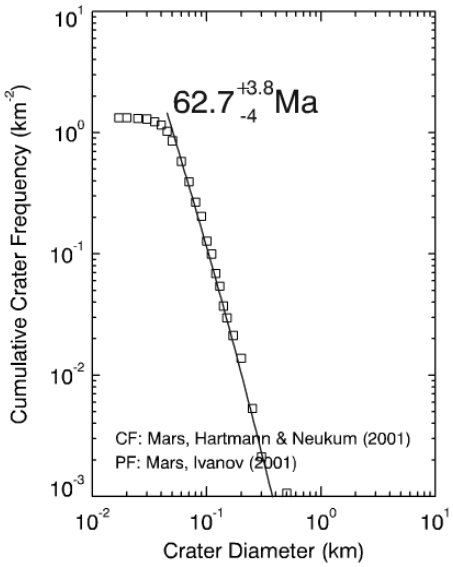

No. 53
(S from Pavonis Mons)

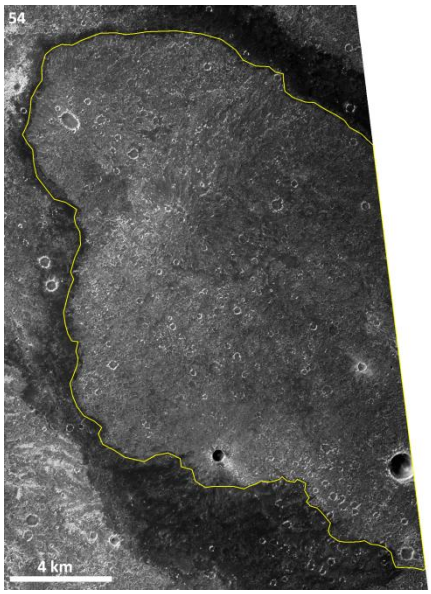

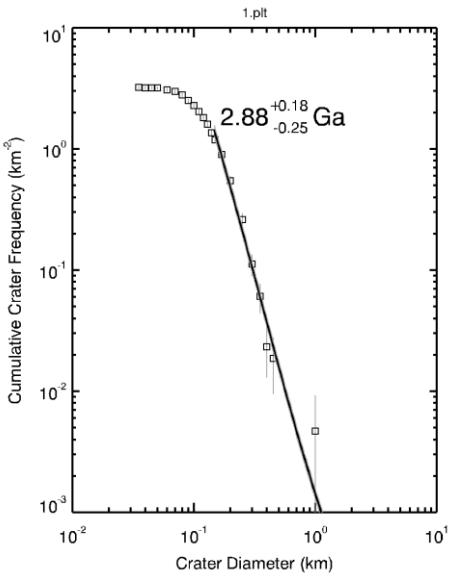

No. 54
(Syria Planum)

u

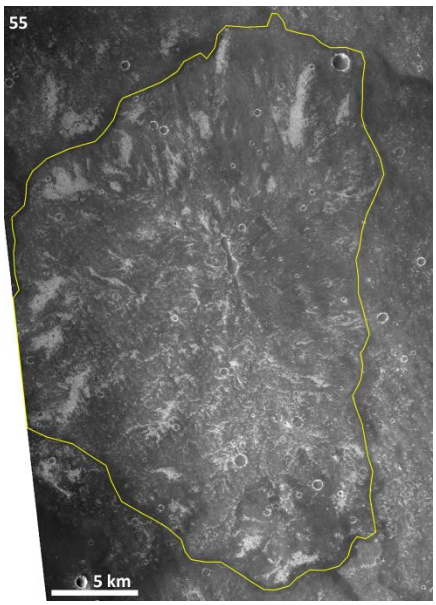

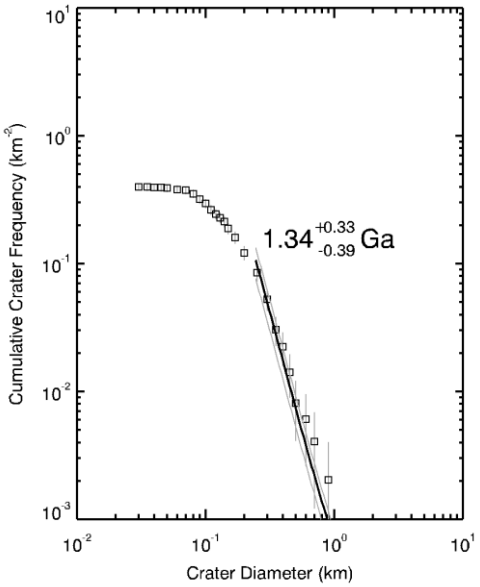

No. 55
(Syria Planum)

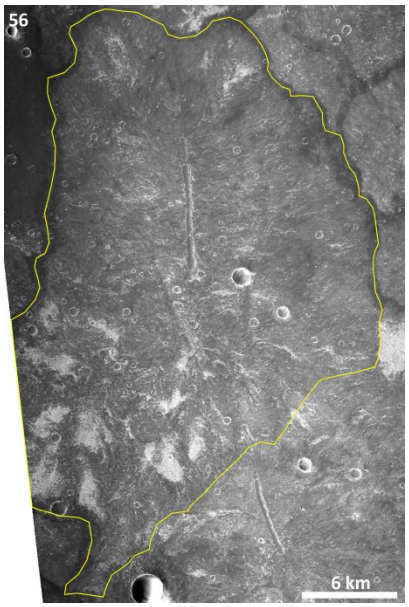

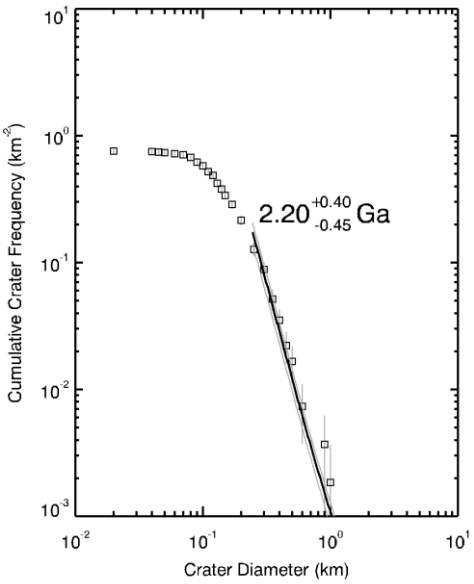

No. 56
(Syria Planum)

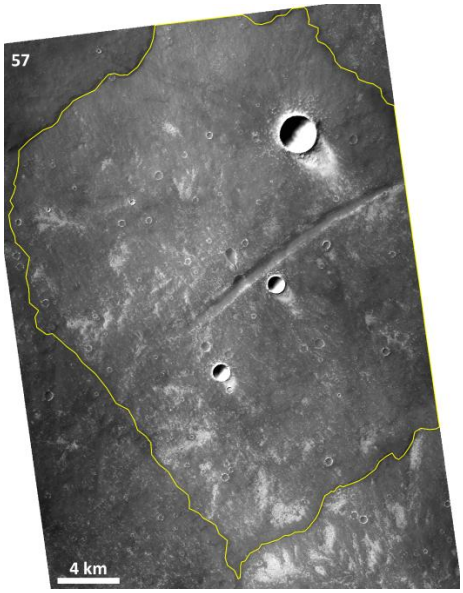

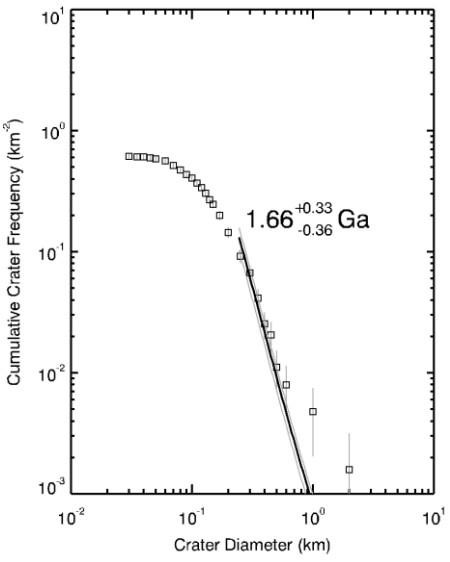

No. 57
(Syria Planum)

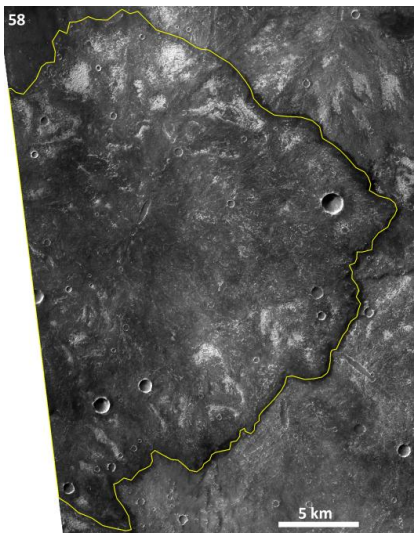

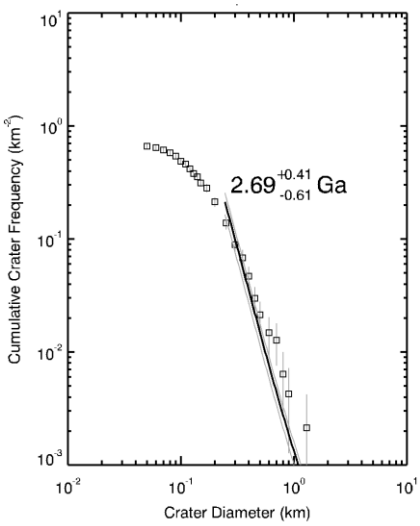

No. 58
(Syria Planum)

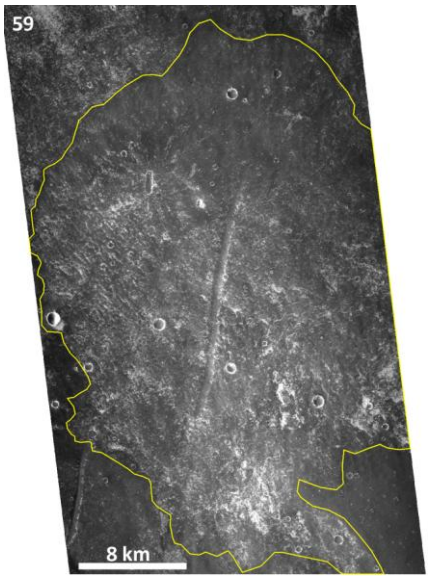

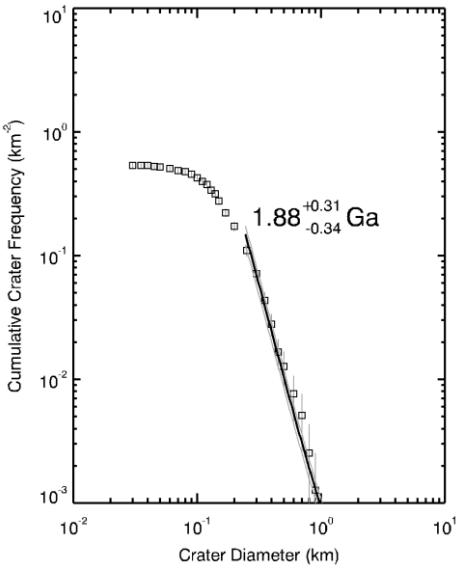

No. 59
(Syria Planum)

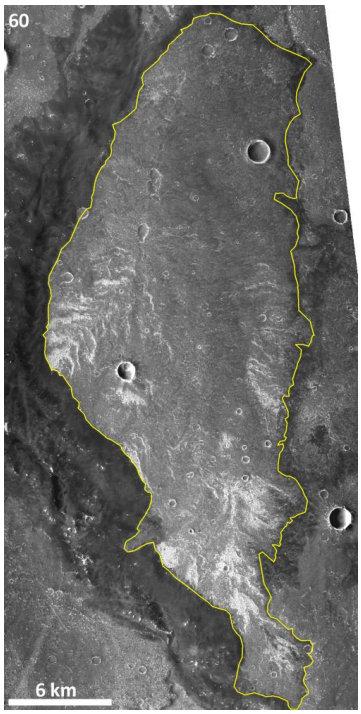

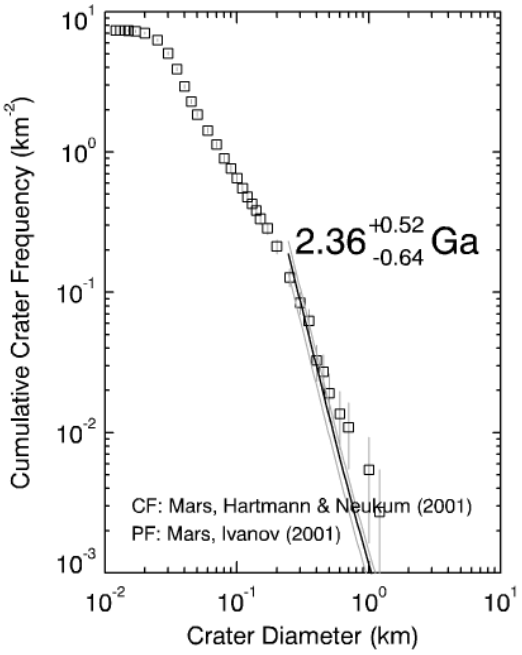

No. 60
(Syria Planum)

w

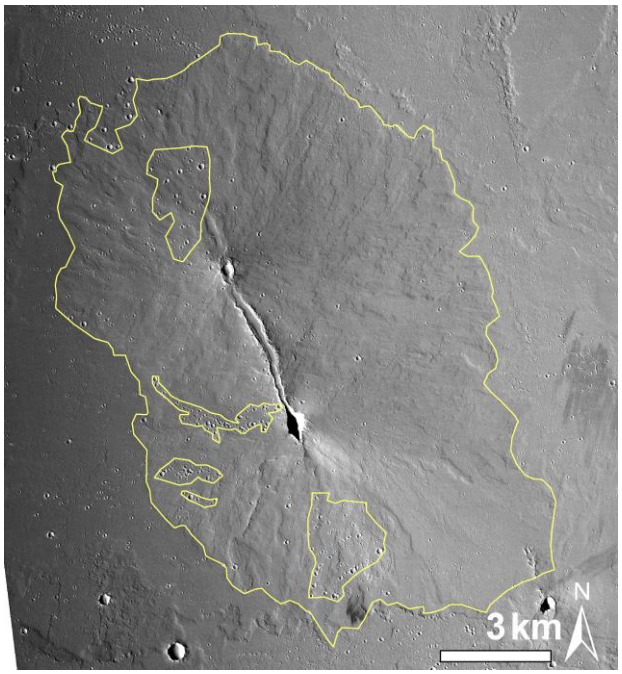

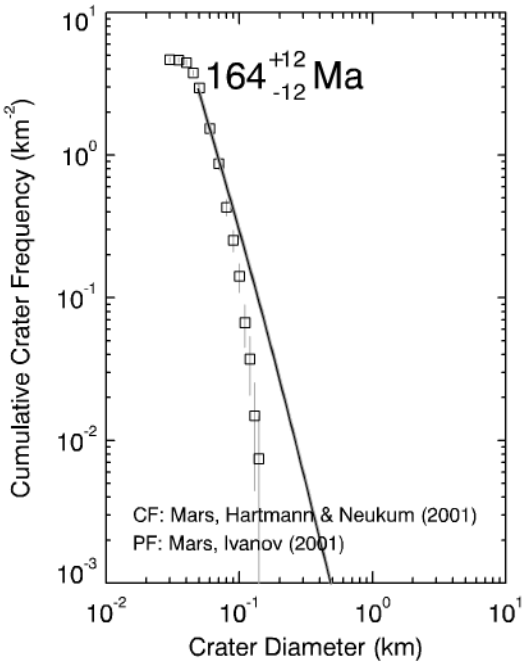

Low shield volcano in Ceraunius Fossae exluded from our investigation due to heavy contamination by secondary craters. Several clusters of secondaries are visible on CTX image. Secondary craters caused atypical steepness of CSFD curve and overestimate the real age of volcano.